Rensselaer

The MANE Journal for Student Research, Innovation, and Design

2017
Volume 2

Featuring:

Inventor's Studio Innovations

(Partially funded by VentureWell)

Published by:

Department of Mechanical, Aerospace & Nuclear Engineering
Rensselaer Polytechnic Institute
110 8th Street Troy, NY
Department of Mechanical, Aerospace, & Nuclear Engineering
Rensselaer Polytechnic Institute

ISBN 978-0-692-89505-4

The MANE Student Research, Innovation, and Design Journal is published annually by the Department of Mechanical, Aerospace, & Nuclear Engineering (MANE) Department at Rensselaer Polytechnic Institute (RPI) located at 110 8th St. Troy, NY 12180.

Research

Innovation and Design: Inventor's Studio at Rensselaer

June 2017

Dear RPI Community,

We are proud and pleased to present the second published issue of RPI's MANE Student Research, Innovation, and Design Journal. The Journal showcases some of the impactful research and innovative design work performed by undergraduate students within cutting-edge laboratories across The MANE Department at RPI.

This journal is completely student-run, and the large effort is significantly supported by The MANE Department's Student Advisory Council under the direction of the Department Head—Dr. Suvranu De—and Professor of Inventor's Studio—Dr. Asish Ghosh. The Journal is composed entirely of undergraduate students' contributions to research and innovative solutions to design problems developed by students. The editorial staff consists of graduate and undergraduate students in the MANE Department, who have experience publishing research in peer-reviewed technical journals. Thanks to Justin Clough, Brian Waite, Nicolas Thompson, Elisabeth Ryan, Youmans, and Nicholas Thompson for serving on the editorial staff and contributing to this publication.

I hope you enjoy this issue of the MANE Student Research, Innovation, and Design Journal, as it is the product of hard work and commitment from many talented students. We are very proud of the students who contribute to research at RPI, many of whom are on their way to becoming innovators, entrepreneurs, and prolific authors of impactful research publications.

Sincerely,

Adam Weltz
Editor-in-Chief

Modeling a Simplified Wind Turbine System to Ascertain Parameters for a Spring-Mass System

David Schwenker*, Michael Smith, Dan Goodman
Rensselaer Polytechnic Institute
Department of Mechanical, Aerospace, and Nuclear Engineering
In association with the RAMS lab at RPI
david.j.c.schwenker@gmail.com, smithm.mech@gmail.com, goodmd@rpi.edu
Winner of the 2017 Mechanical Engineering Weiss Award
**Winner of the 2017 Arthur M. Greene Prize*

The theoretical framework for a simplified wind turbine model is presented in order to ascertain the bending moments experienced by the blade's root. The aerodynamic loads are evaluated through the blade element momentum theory with the gravitational and inertial forces being evaluated through Lagrangian mechanics. The entire model is then implemented within MATLAB and Simulink to determine system behavior. From this modeling, parameters for a spring-mass system for fatigue reduction can be inferred by imposing a representative force and observing its effect on the overall system.

I. INTRODUCTION

Within a preceding article, a spring-mass system was outlined which would reduce the root bending fatigue of a wind turbine blade [1]. For the design process, the loading conditions and its corresponding frequencies must be ascertained to scale the mass and spring appropriately. As such, a method of modeling the wind turbine system is necessary to estimate these values – the most important aspect being the evaluation of the aerodynamic loads as this is the primary source of the periodic loading.

II. AERODYNAMIC LOADS

II.A. Blade Element Momentum Theory

In order to determine the forces and bending moments exerted on the blades of a wind turbine, the blade element momentum (BEM) theory was implemented to assist in determining these quantities.

The principle behind this method is that two approaches are utilized – (1) momentum theory and (2) blade element theory – with the necessary unknown solved by a simple guess-and-check method until both theories agree upon the same value.

The unknown being solved within this case is a parameter imposed upon the system called the axial flow induction factor (a) which is simply a measure of the deviation from the wind's free stream axial velocity. An additional parameter – the tangential flow induction factor (a') – is related as follows:

$$a' = \frac{a(1-a)}{\lambda_r^2} \tag{1}$$

where λ_r is the local tip speed ratio, which is the fraction of the rotational speed over the wind speed.

An exhaustive theoretical derivation is beyond the scope of this report though such analysis is readily available in literature [2,3]. That said, in general the momentum theory analyzes the forces at the blade through the conservation of linear and angular momentum [2], yielding the following expression for the thrust coefficient C_T (which is a non-dimensionalised form of the thrust):

$$C_{T,M} = 4a(1-a) \tag{2}$$

where the subscript M indicates the thrust coefficient is derived from momentum theory. However, if the induction factor proves to be higher than 0.4, an empirical model is used instead [4]:

$$C_{T,M} = \frac{1}{9}(8 - 4a + 14a^2) \tag{3}$$

The blade element theory analyzes the forces as a function of blade geometry [2], yielding:

$$C_{T,B} = \frac{c}{2\pi r}\sqrt{f}\,(C_d(1-a) + C_l\lambda_r(1-a') \tag{4}$$

$$f = (1-a)^2 + \lambda_r^2(1+a')^2 \tag{5}$$

where the subscript B indicates the thrust coefficient is derived from blade element theory, C_d is the drag coefficient, C_l is the lift coefficient, and f is the components of the velocity vector [4].

A residual equation R is established to check for convergence of the induction factors [4]:

$$R = C_{T,B} - C_{T,M} \tag{6}$$

When the residual equation approaches zero, the induction factors from both theories will then be in unison. An iterative process can then be established which begins with an initial "guess" for the axial induction factor (typically 0.3), solves for both forms of the thrust coefficients, checks for convergence, and modifies the axial induction factor appropriately to have the coefficients incrementally converge.

In order to modify the axial induction factor efficiently amongst iterations, the Newton-Raphson method is utilized [5]:

$$a_n = a_{n-1} - \left. \frac{R}{\partial R / \partial a} \right|_{a_{n-1}} \tag{7}$$

Once convergence is achieved, the induction factors will be known and direct evaluation of the components of the aerodynamic loading with respect to the rotor plane can be evaluated as follows:

$$F_{normal} = F_{tip}\left(\frac{1}{2}\rho_{air} U_{wind}^2 f c \Lambda_i C_f\right) \tag{8}$$

$$F_{tangential} = F_{tip}\left(\frac{1}{2}\rho_{air} U_{wind}^2 f c \Lambda_i C_m\right) \tag{9}$$

Where F_{tip} is the tip loss correction factor, ρ is the density of air, U is the wind speed vector, c is the chord length, Λ_i is a transformation matrix to achieve the normal and tangential components through the inflow angle, C_f contains the drag and lift coefficients while C_m is the moment coefficient for the airfoil.

II.B. Wind Shear Profile

Assuming steady wind speed but variation with height, the BEM model needs to be evaluated at various blade positions to ascertain the change in aerodynamic loading. Provided the wind speed at the hub is known, the mathematical model 'power law' can be utilized to determine the wind shear profile:

$$U_{wind} = U_{hub}\left(\frac{Z}{Z_{hub}}\right)^{0.14} \tag{10}$$

where U_{hub} is the wind speed at the hub, Z is the height of the point being evaluated, and Z_{hub} is the hub height. The 0.14 is the exponential value for offshore wind conditions given by the International Electrotechnical Commission (IEC) [6].

II.C. Root Bending

Once the aerodynamic loading has been evaluated, the root bending M of a blade can be calculated through the addition of the torque vector with the cross product of the radial displacement and thrust vector. Since the BEM model evaluates at discrete points, numerical integration by the Gaussian quadrature rule is necessary:

$$M = L\int_0^1 \left(\tilde{r} \times \Lambda_a \tilde{F}_{thrust} + \Lambda_a \tilde{F}_{torque}\right) d\xi \tag{11}$$

where L is the length of the blade, r is the non-dimensionalized radial position of the force vector, Λ_a is a transformation matrix from the aerodynamic reference frame to rotating frame at the blade root [4], and the symbol ~ indicates the vectors are the elemental values along the length of the blade.

II.D. Results

Utilizing MATLAB for the implementation of the BEM model in conjunction with the wind shear profile, the aerodynamic loading conditions were evaluated for a NREL 5MW blade assuming a wind speed of 11 m/s at the hub – this is just before the rated speed of 11.4 m/s so that a pitch angle of 0° can be utilized – and a rotational speed of 1.28 rad/sec.

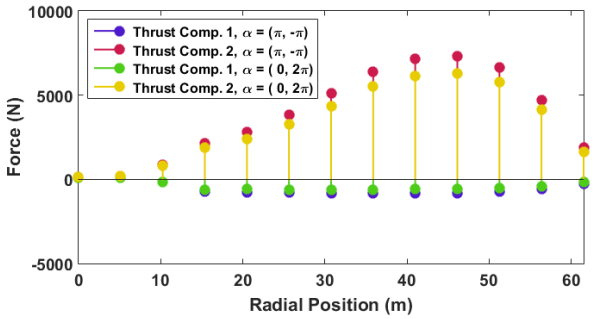

Figure 1. Thrust force at ψ = 0° & ψ =180°.

Figure 1 visualizes the components of the thrust force at an azimuth angle of 0° (red/blue) and 180° (yellow/green) where the azimuth angle ψ is defined as the angular position of the blade in reference to the peak of its rotation. Note that the thrust force is

at a noticeably larger magnitude at its peak position (0°) than at its lowest position (180°).

III. SYSTEM MODELING

The process of establishing a simplified wind turbine model for analysis was led by Dr. Etana Ferede within RPI's Rotorcraft, Adaptive, and Morphing Structures (RAMS) laboratory through the Undergraduate Research Program (URP). The theoretical derivation is too complicated and extensive to present here, but a brief overview is included to provide a basis for the system analysis.

III.A. Simplifications

In order to reduce complications within the analysis, the following simplifications were imposed upon the model parameters [7]:

- The tower is modeled as a rigid structure.
- The blade is modeled as a flexible beam with deflections represented by linear modal shapes.
- The blade is straight with no coning, and its reference axis is coincident with the elastic and pitch axes as well as the aerodynamic center while the center of gravity is at an offset.
- The Euler-Bernoulli model is used to simplify the blade, assuming a linear strain-displacement relationship exists.
- The aerodynamic loading is steady.
- The Coriolis effect from the blade's tip displacement is negligible.
- The drive train is modeled as two inertias connected with a rigid drive train.

III.B. Derivation Overview

A wind turbine blade can be modeled as a cantilevered beam, and, as such, the mode shapes associated with the natural frequencies of these cantilevered beams can be implemented [2].

The displacement and twist of the blade can therefore be parameterized in terms of modal shapes:

$$u = \Phi_u \eta \tag{12}$$

$$\theta = \Phi_\theta \eta \tag{13}$$

Where u is the displacement of the blade, θ is the twist of the blade, η is the scaling coefficient, and Φ is the corresponding modal shape [7].

From these definitions, substitutions can be made into strain and curvature equations given for a linear strain-displacement relationship from which the corresponding strain energy U for a deformed blade can be derived [7], which is given as:

$$U = \frac{1}{2}\eta^t K \eta \tag{14}$$

where K is the blade stiffness matrix.

The kinetic energy T can also be derived based upon evaluation of the blade's mass distribution in relation to its corresponding translational and rotational speeds [7], which is given as:

$$T = \frac{1}{2}\dot{\eta}^t M \dot{\eta} + \frac{1}{2}\dot{\psi}_r{}^2(\eta^t K_c + 2 f_c^t)\eta + \dot{\psi}_r(\eta^t K_{\dot{c}} + f_{\dot{c}}^t)\dot{\eta} \tag{15}$$

where M is the blade mass matrix, K_c is the centrifugal stiffness matrix, f_c is the centrifugal loading vector, and ψ_r is the rotor azimuth angle.

Utilizing the Euler-Lagrange analytical approach, a system of equations which describe the motion of the wind turbine model is obtained [7]:

$$M\ddot{\eta}_i + (K - \dot{\psi}^2 K_c)\eta_i = f_i + \dot{\psi}^2 f_c \tag{16}$$

$$(J_r - n_g^2 J_g)\ddot{\psi} = T_a - n_g T_g \tag{17}$$

where f_i is the combined aerodynamic and gravitational loading, J_r and J_g are the rotational inertias of the blade and generator respectively, T_a and T_g are the torques of the rotor and generator respectively, and n_g is the gear ratio.

Finally, these equations of motion can be collected together in a matrix form and converted to state space for analysis, where Simulink can then evaluate the behavior of the system over time.

III.C. The Coriolis Effect

Having a wind turbine model now established, a force which is representative of the Coriolis Effect from the spring-mass system can be imposed into the system with the corresponding reactions observed. To generate the necessary counter effect of the root bending moment, the force must assume the following form:

$$F_{cor} = F_0 \sin(\psi + \phi) \tag{18}$$

where ϕ would be the phase angle at which point the force responds appropriately to the frequency of in-plane bending moment.

The four parameters of this force which are controllable by the designer is the magnitude of the force F_0, the aforementioned phase angle ϕ, the radial position r at which the force is applied, as well as the eccentricity e of the mass given by the chordal position which offsets it from the reference axis. Varying all of these parameters as inputs to the Simulink model through an iterative process allows one to observe the effect that this combination of forces has on the root bending moment.

III.D. Results

Figure 2 demonstrates the effect of the phase angle on the peak-to-peak root bending moment of the *in-plane* (Z axis) orientation at varying magnitudes of force with a constant radial position of 70% of the blade length with no eccentricity. It is shown that the maximum reduction occurs at $\phi = 0°$ (or 360°). Similarly, varying the radial position while holding the magnitude of the force constant at 5kN with no eccentricity results in a nearly identical plot (*Figure 3*). Fortunately, root bending moments in the X and Y axes were negligibly affected with no eccentricity considered (*Figure A1*).

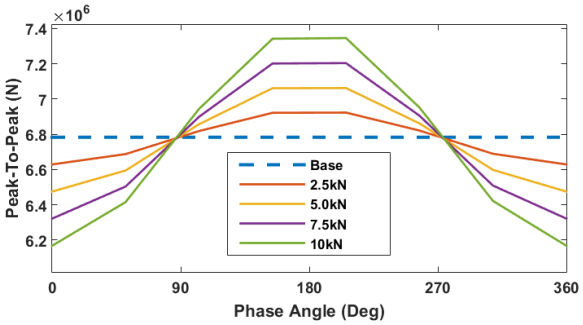

Figure 2. Phase angle effect at various magnitudes.

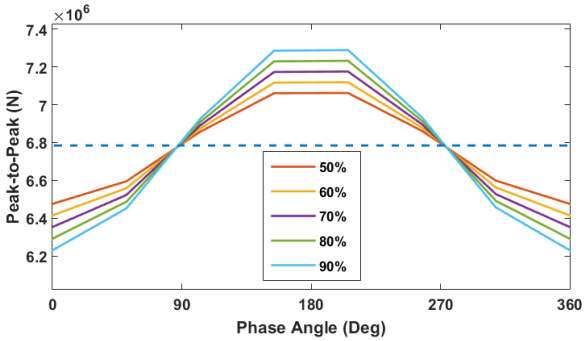

Figure 3. Phase angle effect at various radii.

Figure 4 shows the percent reduction in the peak-to-peak response of the root bending moment as a function of both the magnitude and radial position of the Coriolis force at the optimal phase angle of 0°.

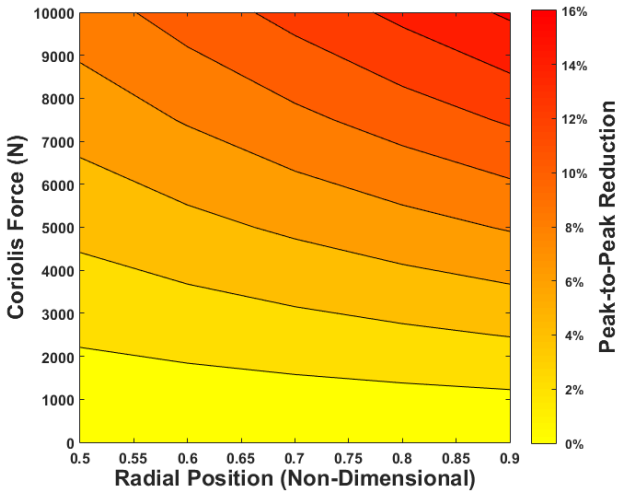

Figure 4. Peak-to-peak reduction as a function of both the magnitude F_0 and the radial position r.

Limiting the analysis to 10kN and 90% blade length as the upper limits of what is technically feasible, it is shown that a 16% reduction in peak-to-peak is theoretically possible, though in actuality it will be much less due to physical constraints [8].

Figure 5 demonstrates the effect of the eccentricity of the Coriolis force on the peak-to-peak root bending moment of the *out-of-plane* (Y axis) orientation as a function of the phase angle with a constant magnitude of 5kN and at a radial position of 70% of the blade length. Note that at $\phi = 0°$ the peak-to-peak is only marginally increased from the base case. Therefore, eccentricity has only a minor effect on out-of-plane bending while having a negligible effect on in-plane bending (*Figure A2*).

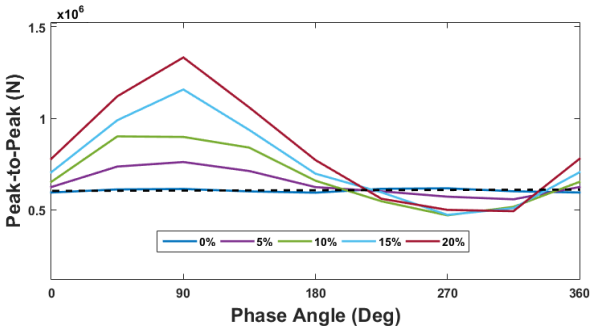

Figure 5. Phase angle at various eccentricities.

IV. CONCLUSIONS

Having successfully modeled the wind turbine system and implementing the hypothetical force which would be generated by a spring-mass system, it remains for the designer to take the results from this analysis and ascertain the corresponding spring stiffness and mass necessary to achieve a similar system response. This evaluation will be explored within a proceeding article which seeks to harmonize a model for the spring-mass system with the model of the wind turbine presented here [8].

ACKNOWLEDGMENTS

The authors would like to thank Dr. Etana Ferede (PhD) for his extensive contributions to the establishment of a wind turbine model, including the theoretical derivation of the said model, his expertise in MATLAB and Simulink programming to implement it, and the technical support he provided in applying this model to the spring-mass system project – much of this would not be possible without his help.

REFERENCES

[1] D. SCHWENKER and M. SMITH and D. GOODMAN, "Reduction in Root Bending Fatigue of Wind Turbine Blades by a Spring-Mass System," *The MANE Student Research and Design Journal*, pp. 19-23, Rensselaer Polytechnic Institute, Troy, NY, (2017).

[2] J. F. MANWELL and J. G. MCGOWAN and A. L. ROGERS, *Wind Energy Explained: Theory, Design, and Application*, pp. 257-265, John Wiley & Sons, Hoboken, NY (2009).

[3] T. BURTON and N. JENKINS and D. SHARPE and E. BOSSANYI, *Wind Energy Handbook*, pp. 4, John Wiley & Sons, Hoboken, NY (2011).

[4] E. FEREDE, *Static Aeroelastic Optimization of Composite Wind Turbine Blades Using Variable Stiffness Laminates*, pp. 12-16, Delft University of Technology, Delft, Netherlands (2016).

[5] R. L. BURDEN and J. D. FAIRES, *Numerical Analysis*, pp. 67, Cengage Learning, Boston, MA (2011).

[6] M. C. HOLTSLAG and W. A. A. M. BIERBOOMS and G. J. W. VAN BUSSEL, "Wind Turbine Fatigue Loads as a Function of Atmospheric Conditions Offshore," *Wind Energy* (2016).

[7] E. FEREDE, *Simplified Wind Turbine Model*, pp. 1-5, Rensselaer Polytechnic Institute, Troy, NY, (2017).

[8] M. SMITH and D. SCHWENKER and D. GOODMAN, "Modeling of a Spring-Mass Compensator System for a Wind Turbine Blade," *The MANE Student Research and Design Journal*, pp. 9-14, Rensselaer Polytechnic Institute, Troy, NY, (2017).

APPENDIX

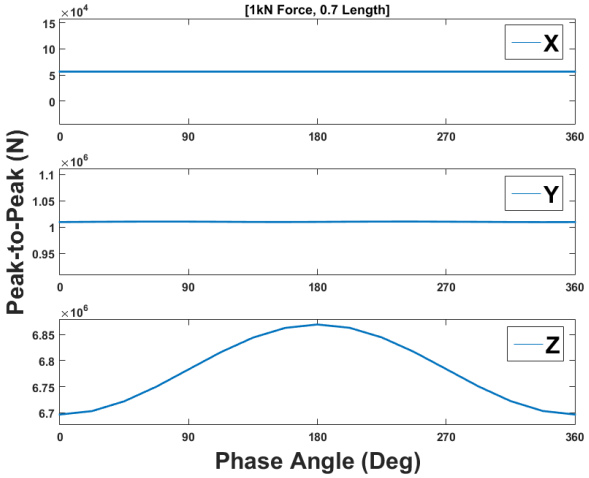

Figure A1. Effects of the Coriolis force on all three axes at a constant magnitude (1kN) and radial position (0.7L) with no eccentricity.

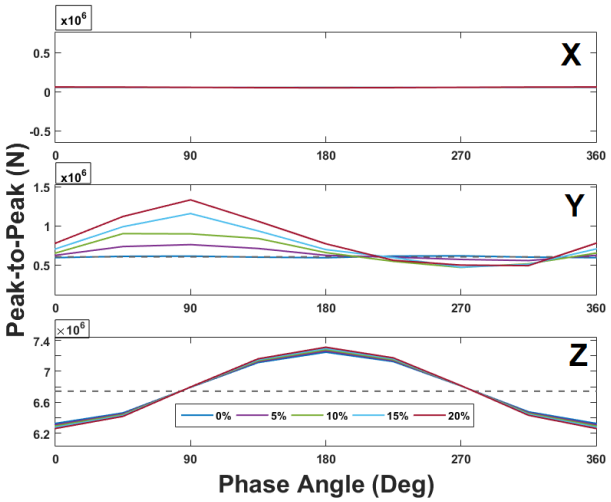

Figure A2. Effects of the Coriolis force on all three axes at a constant magnitude (5kN) and radial position (0.7L) with varying eccentricity.

Spring-Mass Compensator Model for a Wind Turbine Blade

Michael Smith, David Schwenker*, Dan Goodman
Rensselaer Polytechnic Institute
Department of Mechanical, Aerospace, and Nuclear Engineering
In association with the RAMS lab at RPI
smithm.mech@gmail.com, david.j.c.schwenker@gmail.com, goodmd@rpi.edu
Winner of the 2017 Mechanical Engineering Weiss Award
**Winner of the 2017 Arthur M. Greene Prize*

The theoretical framework for the modeling of a spring-mass compensator is presented along with its corresponding implementation within MATLAB and Simulink. This analytical process enables the tuning of a spring-mass-damper assembly which is necessary to counteract the torsional loading at the root of a wind turbine blade.

I. INTRODUCTION

Within a preceding article [1], a model of a wind turbine system experiencing the effects of aerodynamic loading was presented. The model ascertained the necessary phase, magnitude, and radial position of the Coriolis force to minimize the peak-to-peak of the in-plane root bending moment.

However, it was also necessary to ascertain the physical limitations of a spring-mass system as well as the magnitudes of the Coriolis force achieved by such a device. Comparisons have been made to the corresponding wind turbine model from these results. The effects that a spring-mass system has on the overall wind turbine were determined.

II. ASSUMPTIONS

II.A. Physical Conditions

The compensator model is a guided spring-mass assembly mounted to the shear web within the turbine blade [1]. The following assumptions were made:

1. The motion of the spring-mass assembly was one dimensional along the radius of the wind turbine blade.
2. The mass of both the spring and mounting apparatus were negligible in comparison to the oscillating mass.
3. Out-of-plane bending was negligible to the compensator performance and thus the blade was assumed rigid.

An additional damper was included in the model of the assembly in order to account for inherent damping within the spring and the assembly.

The point of operation was also constrained. The spring-mass apparatus should ideally engage only at the rated rotational velocity of the wind turbine of 1.288 rad/s. Oscillation in the unrated region of operation would result in an irregular period and increase root bending on the blade. The model considered nonlinear spring operation, in the form of a pre-compression, which regulated the active period of the mass oscillation.

II.B. Loading Conditions

The in-plane loads considered in the one dimensional motion of the assembly were the gravitational, centrifugal, and centripetal loads. Out-of-plane forces, such as loads due to air pressure, were assumed to have negligible effects on the operation of the spring-mass assembly. This assumption was made in part because the assembly was mounted within the sealed turbine blade.

III. ANALYTICAL MODELING

III.A. Mass Equation of Motion

The equation of motion of the spring-mass assembly with an assumed frictional damping is shown in Equation (1):

$$f(t) = m\ddot{x}(t) + b\dot{x}(t) + kx(t) \qquad (1)$$

where f is the force exerted on the mass, x is the position of the mass relative to the rest-equilibrium position, m is the mass of the mass, b is the damping

coefficient of the assembly, k is the tuned spring constant, and t is time [2]. The transfer function relating the position of the mass to the force exerted on the mass is derived using the Laplace transform of Equation (1). The result is shown in Equation (2):

$$\frac{X(s)}{F(s)} = \frac{1}{ms^2 + bs + k} \tag{2}$$

where $X(s)$ and $F(s)$ are the Laplace transforms of $x(t)$ and $f(t)$, respectively, while s is the Laplace domain variable used in this analysis.

III.B. Parallel Loading Equations

The loading considered in the motion of the spring-mass system were the centrifugal and gravitational loads on the mass. The Coriolis force exerted on the mass was assumed negligible in the linear displacement of the spring; it was instead included in the modeling of the torque exerted on the root of the blade. The forces exerted on the mass in the direction of the radial axis of the blade are shown in Equations (3) and (4):

$$f_{g\parallel}(t) = -mg\cos(\psi) \tag{3}$$

$$f_c(t) = m\dot{\psi}^2(x(t) + r) \tag{4}$$

where $f_{g\parallel}$ and f_c are respectively the gravitational and centrifugal forces, r is the radial position of the mass at rest from the center of the wind turbine, and ψ is the azimuth angle which is the angle of the wind turbine blade relative to the vertical axis. *Figure 1* shows the loading diagram of the one-dimensional parallel analysis.

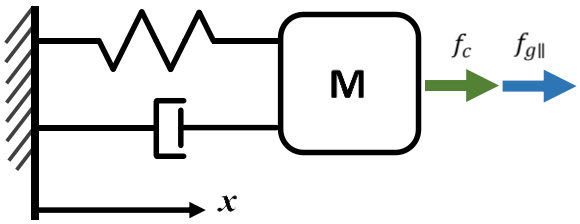

Figure 1. Loading diagram of the one-dimensional parallel analysis.

Note that the damper included in the diagram is representative of assumed frictional forces exerted on the mass during loading.

III.C. Perpendicular Loading Equations

The equations used to calculate the net force exerted by the spring-mass assembly on the blade were provided through Equation (5) and Equation (6). Equation (5) is the Coriolis force due to the radial velocity of the mass $\dot{\rho}$ and the angular velocity of the blade $\dot{\psi}$ [3]. Note that the negative sign of Equation (5) indicates that the Coriolis force operates in the direction opposite the motion of the blade. Equation (6) is the perpendicular component of the force, complementary to the force in Equation (3).

$$f_{cor} = -2m\dot{\rho}\dot{\psi} \tag{5}$$

$$f_{g\perp} = mgsin(\psi) \tag{6}$$

The root moment exerted on the blade through these forces, M_{ms}, was calculated through Equation (7). A loading diagram of the induced forces contributing to the bending moment at the root of the wind turbine blade is provided in *Figure 2*.

$$M_{ms} = \rho(f_{cor} + f_{g\perp}) \tag{7}$$

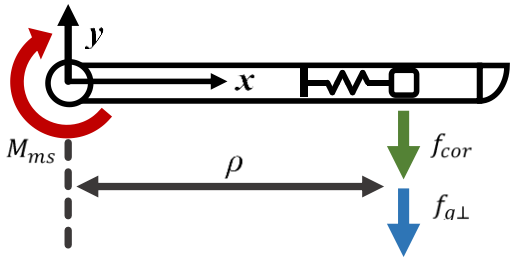

Figure 2. Loading diagram for bending moment calculation at the root.

The magnitude of the Coriolis force in *Figure 2* is normal to the blade and opposite to the direction of angular motion. The perpendicular component is always perpendicular to the blade, however the sign and magnitude alter with the azimuth angle according to Equation (6).

III.D. Model Assembly

The equations modelling the gravitational and centrifugal forces shown in Equation (3) and Equation (4) cannot linearize from the input azimuth angle to the output force, which would be desirable.

This nonlinearity prevented the linear combination of the input force equations and the spring-mass transfer function. Therefore, the linear combination was made possible by additionally assuming a constant angular velocity $\dot{\psi}$ at the rated operational speed. The process of linearization and discretization used MATLAB and Simulink [4].

The Simulink diagram for the spring-mass compensator system is provided in Appendix A. The input to the system was the angular velocity of the wind turbine blade. The outputs of the system were the displacement of the mass and the torque induced on the root of the blade by the mass. The angular position of the turbine blade was calculated through integration of the input velocity signal [4].

The precompression of the spring was implemented in the Simulink model by subtracting the precompression force from the input force and saturating the resulting signal at zero. Similarly, the limits of displacement were ensured using saturation of the displacement between zero and the span of the assembly.

IV. MODEL RESULTS

The simulation ran through 648 iterations of 9 mass values between 0 and 250 kg, 9 spring constant values between 1 and 4 kN/m, and through 8 initial positions between 50% and 80% of the blade length. The maximum displacement response in meters of the system for a maximized radial position corresponding to 80% of the blade length is provided in *Figure 3*. The simulation was run in each case for a 120 second period with a step size of 5 milliseconds. The maximum stroke length of the device oscillation for this simulation is taken to be 10 meters.

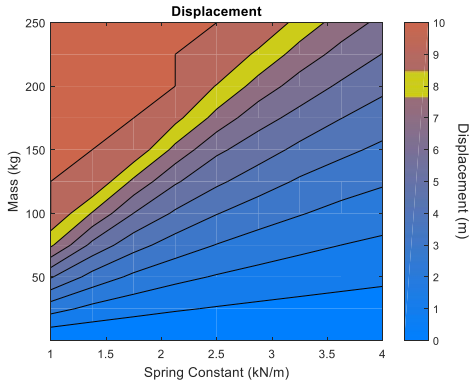

Figure 3. Displacement (m) compared to mass and spring constant

The yellow bar in each plot demonstrates the design case for the mass-spring system, with the displacement maximized but safely away from the maximum stroke length. The chosen region for safe operation is approximately 80% of the spring-mass stroke length.

The simulation allows for the determination of the mass-to-spring constant ratio for optimal performance, such that there is maximal oscillation of the mass without exceeding the reasonable stroke length of 10 meters. The root bending on the root of the blade due to the implemented device was also calculated.

The calculated moment was compared to the baseline bending moment experienced by the unmodified wind turbine blade, determined in the preceding article [5]. *Figure 4* displays the reduction in peak-to-peak bending moment experienced at the root of the blade in Newton-meters at the same 80% position as used in *Figure 3*.

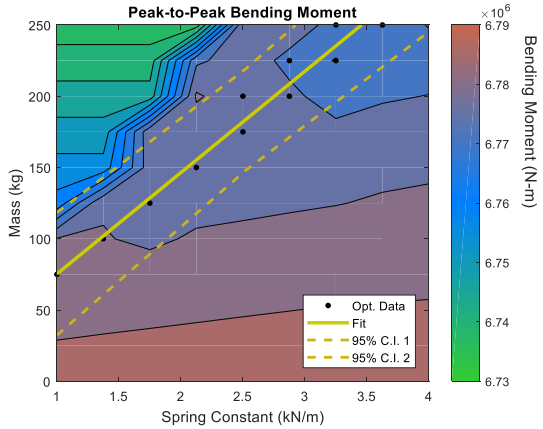

Figure 4. Peak-to-Peak Bending Moment (N-m) at root of blade, optimal region highlighted

The yellow lines in *Figure 4* correspond to the 80% idealized operation region highlighted in *Figure 3*. The dashed lines correspond to 95% confidence interval which defines the optimal operational region. The equation for the optimal spring stiffness from a given mass was approximated using a linear fit of the indicated optimal region in *Figure 3*, resulting in Equation (8). The adjusted R-squared value for this fit is 0.9622, indicating that the curve is a strong fit of the designed optimal region.

$$m = 71.13 \frac{\text{kg} \cdot \text{m}}{\text{kN}} \left(k + 0.05836 \frac{\text{kN}}{\text{m}} \right) \qquad (8)$$

The baseline uncompensated model is represented in *Figure 4* by the response at zero mass. An exemplary plot of the bending moment time response is shown in *Figure 5* for a mass of 175 kg and a spring constant of 2.5 kN/m.

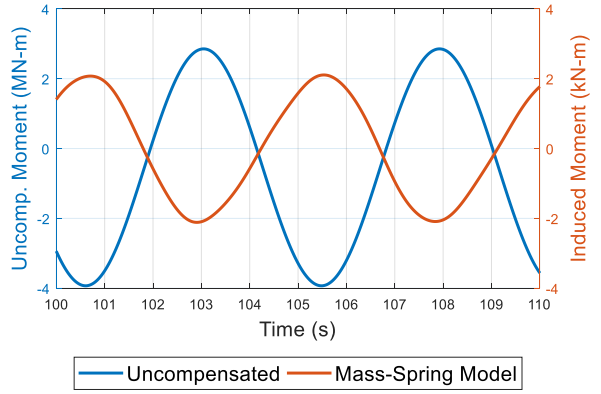

Figure 5. Baseline and implemented root bending moment.

Figure 6 illustrates the change in net bending moment that results from the combination of the two bending moment time response plots from *Figure 5*.

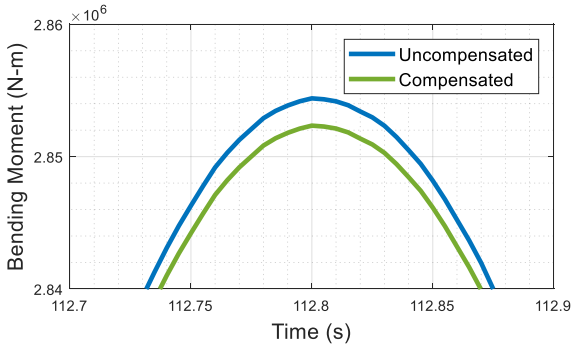

Figure 6. Net bending moment comparison

The difference between the compensated and uncompensated bending moment time responses shown in *Figure 6* is minimal; however, the model does verify that the spring-mass compensator is reducing the magnitude of the oscillation.

III. CONCLUSIONS

The simulation of the mass-spring compensator system within the wind turbine blade modeled the curvilinear motion of the system within the blade. It also calculated the effect such a mass and motion would have on the bending moment at the root of the blade.

The results of the curvilinear motion simulation determined the ratio of mass to spring-constant which was required in order for the model to oscillate safely within the predefined stroke length of 10 meters.

The root bending moment comparison revealed that the bending moment induced by the mass-spring compensator system due to gravitational and Coriolis force loading does reduce the net bending moment oscillation magnitude, albeit minimally. The response is in phase with the idealized model discussed in the previous article [5]. Further design considerations regarding the out-of-plane bending and feasible span of device oscillation are required in order to increase the reduction of the response to affect the lifespan of the blade.

ACKNOWLEDGMENTS

The authors thank Dr. Farhan Gandhi (PhD) for his feedback on the modeling of the spring-mass system and Dr. Etana Ferede (PhD) for his tremendous help in modeling the wind turbine system which provided the necessary benchmarks to measure the success of the results.

REFERENCES

[1] D. SCHWENKER and M. SMITH and D. GOODMAN, "Reduction in Root Bending Fatigue of Wind Turbine Blades by a Spring-Mass System," *The MANE Student Research and Design Journal*, pp. 19-23, Rensselaer Polytechnic Institute, Troy, NY, (2017).

[2] F. FRANKOVSKY and D. HRONCOVA and I. DELYOVA and I. VIRGALA, "Solutions to Free Undamped and Free Damped Motion Problems in Mass-Spring Systems," *American Journal of Mechanical Engineering*, pp. 282-288, Science and Education Publishing, Newark, DE (2013).

[3] E. HERRERA and SIGRID MORETT, "On the Direction of Coriolis Force and the Angular Momentum Conservation," *Revista Brasileira de Ensino de Física*, pp.1-7, Sociedade Brasileira de Fisica, 2016.

[4] J. SUNDAY and A.A. JAMES and M.R. ODEKUNLE and A.O. ADESANYA, "Solutions to Free Undamped and Free Damped Motion Problems in Mass-Spring Systems," *American Journal of Computational and Applied Mathematics*, pp. 82-91,

Scientific & Academic Publishing, Rosemead, CA (2016).

[5] D. SCHWENKER and M. SMITH and D. GOODMAN, "Modeling a Simplified Wind Turbine System to Ascertain Parameters for a Spring-Mass System," *The MANE Student Research and Design Journal*, pp. 3-8, Rensselaer Polytechnic Institute, Troy, NY, (2017).

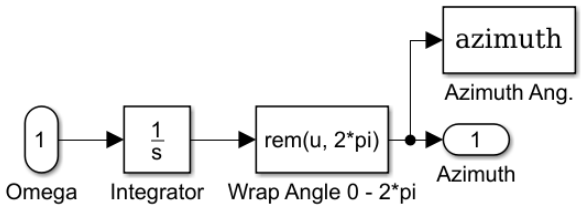

APPENDIX A: SIMULINK MODEL

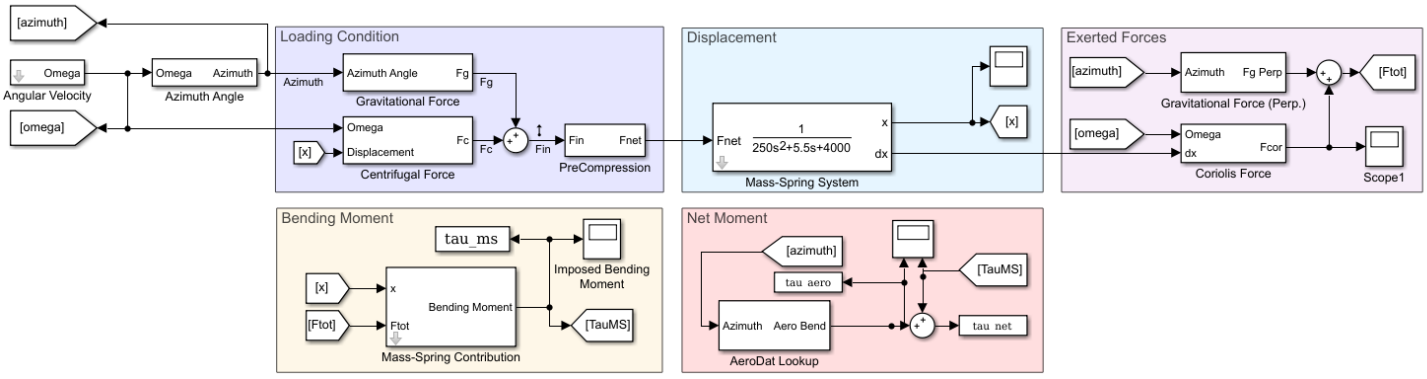

Angular Velocity Calculation

A first-order transfer function of the form $\frac{1}{\tau s+1}$ was used in order to reduce unuseful noise in the data.

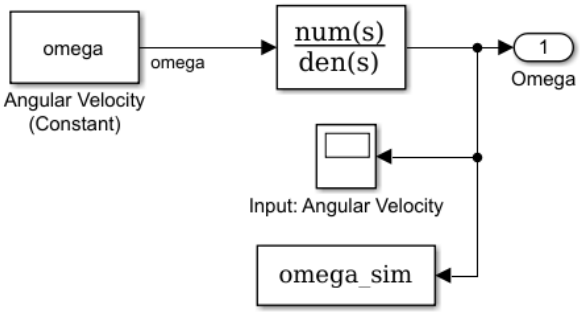

Azimuth Angle

Gravitational Force (Perp.)

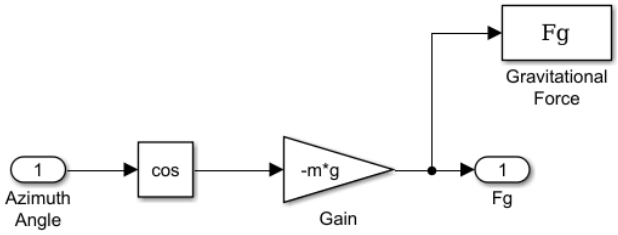

Centrifugal Force

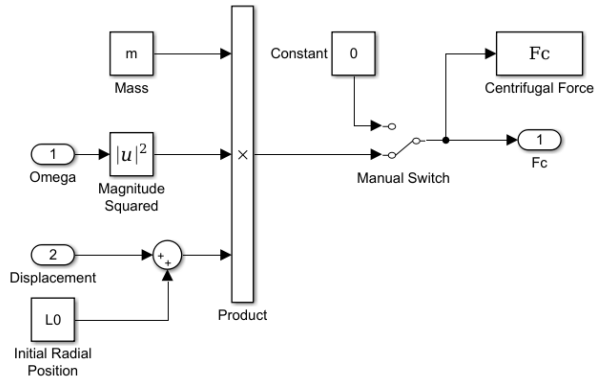

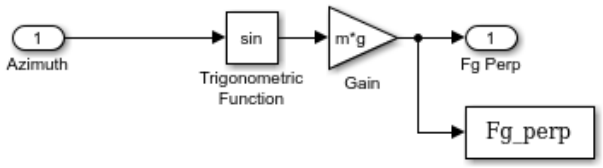

Mass-Spring Contribution

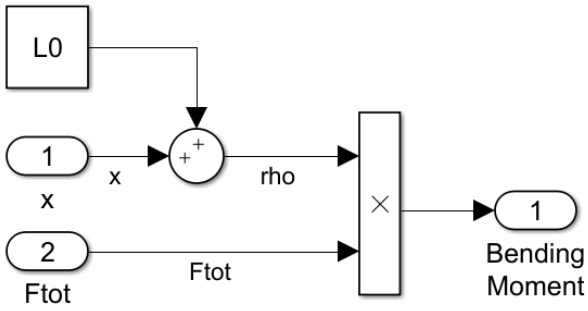

Precompression

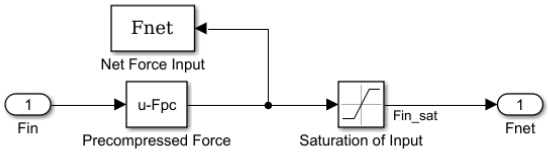

Mass-Spring System

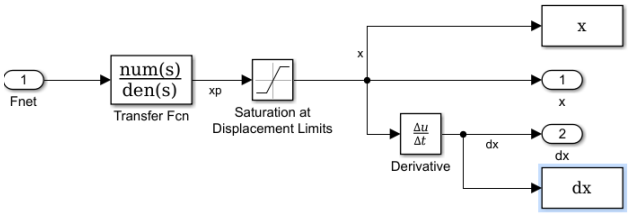

Coriolis Force

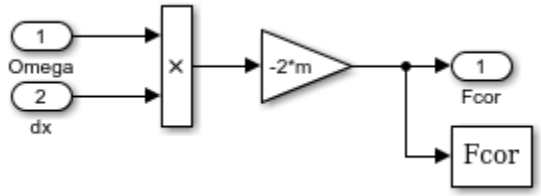

Gravitational Force (Perp.)

AeroDat Lookup

Uses data calculated in [5] in order to approximate the uncompensated bending moment at a given azimuth angle assuming constant rotational velocity.

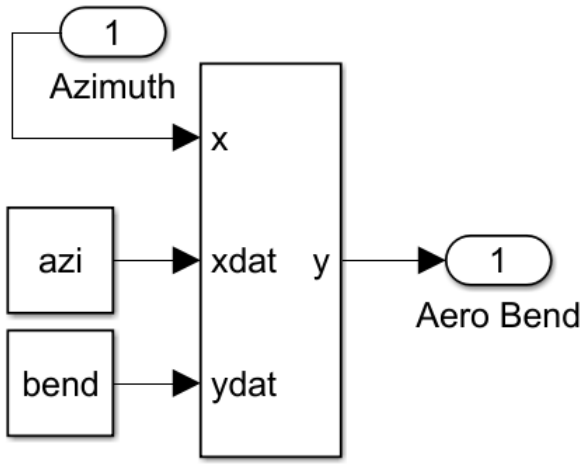

Designing a Simplified Wind Turbine Mounting System to Ascertain Device Performance

Dan Goodman, David Schwenker*, Michael Smith
Rensselaer Polytechnic Institute
Department of Mechanical, Aerospace, and Nuclear Engineering
In association with the RAMS lab at RPI
goodmd@rpi.edu, david.j.c.schwenker@gmail.com, smithm.mech@gmail.com
Winner of the 2017 Mechanical Engineering Weiss Award
**Winner of the 2017 Arthur M. Greene Prize*

The design process for the physical components of a spring-mass system mounted within a wind turbine blade is presented. It is necessary to resolve previously discussed theory and analytics with the physical constraints imposed by the blade design, industry standards, and the spring-mass system itself. To verify the success of the developed code and design, a prototype was constructed to ascertain the feasibility of the solution concept.

I. INTRODUCTION

Within preceding articles, the theoretical framework for a spring-mass system was presented [1] along with the associated analysis for ascertaining loading [2] and modeling [3] parameters. From this set of results, the physical components can be designed. The design involves an iterative process to determine the most feasible and practical solution. Beginning with the delineation of constraints, followed by CAD modeling and finally scaled prototyping, the practicality of the spring-mass system can be determined.

II. CONSTRAINTS

II.A. Geometric Constraints

The geometric constraints of the device and its corresponding mounting structure are governed predominately by the available build volume within the blade itself. By modeling the spring-mass system, it was determined that the most effective location for the device was approximately 75% of the blade length [2,3]. However, at this position the blade has already tapered considerably and, consequently, the build volume on either side of the main shear web has reduced to a cross-section of approximately 1 meter wide by ½ meters tall.

A typical blade is composed of three main components: the shell, the shear web, and the spar caps. The spar caps and shear web provide much of the structural support of the blade [4] and, as such, the mounting structure for the spring-mass system should attach to these components.

II.B. Material Constraints

In addition to the geometric constraints, the material composition of the blade itself necessitates the device to be composed of similar elements.

For explanatory purposes, it may be useful to summarize the composition of the blade. First, its shell and shear web are typically constructed from balsa wood (or foam) wrapped in a biax (or triax) cloth which is then encapsulated in resin. Second, the spar caps are constructed from multiple layers of unidirectional glass fibers which are also encapsulated in the same resin [4].

It is critical for both the shear web and spar caps to be uniform and devoid of any air pockets or contaminants when they are molded as such stress concentrations would compromise the required strength and rigidity needed to sustain the external loading conditions [4]. Consequently, the mounting structure should be molded into the blade upon construction to avoid the aforementioned stress that other fastening methods may introduce.

In the event of a lightning strike, highly conductive material within the blade has the potential of interfering with the blade's embedded grounding rod, causing complications [4]. Therefore, such materials should be avoided in the device.

III. MOUNTING STRUCTURE DESIGN

III.A. Geometry

Utilizing the actual blade dimensions for the NREL 5MW blade, a five-meter-long blade segment at about 75% of the overall blade length was chosen to serve as the initial confinements of the device

mounting structure. Referencing this cross-section constantly throughout the design process, one could ensure the mounting structure would be appropriately constrained and a tight fit could be achieved.

The mounting structure exactly conforms to the cross-section of the blade near the shear web and is 5 meters long by ½ meters tall.

III.B. Attachment Methods

Three attachment methods were scrutinized for the device structure: (1) fasteners, (2) adhesives, and (3) direct molding to the blade structure (*Figure 1*).

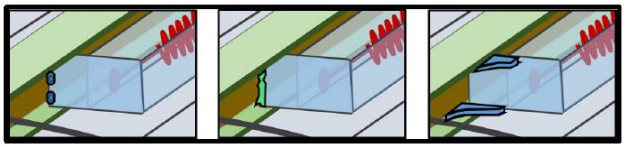

Figure 1. Concept art for fasteners, adhesives, and direct modeling attachment methods.

Each condition was analyzed using finite element analysis (FEA) by constraining the end points of the mounting structure as fixed, setting the appropriate contact type between two surfaces based upon the attachment method being studied (bolted, glued, molded), and applying the calculated Coriolis force from previous analysis [2] to mounting points of the spring-mass system (*Figure 2*).

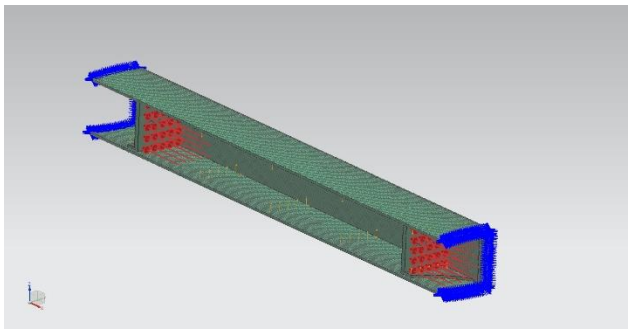

Figure 2. Constraints, contacts, and loading conditions for the mounting structure.

Results demonstrated that the fasteners were not a reliable solution whereas the "direct molding" approach proved to be the optimal case as it experienced the least amount of stress and displacement (*Figure 3*).

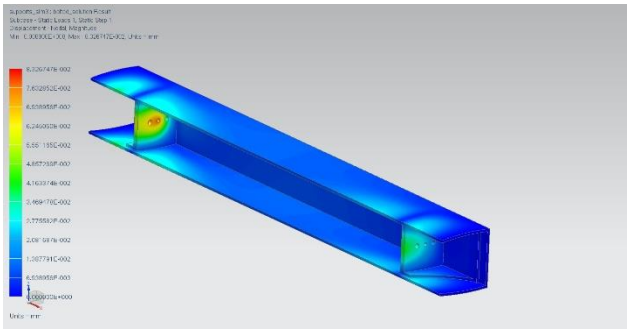

Figure 3. FEA results for maximum displacement of the direct molding case.

IV. DEVICE DESIGN

IV.A. Guide Rail System

In developing a guide rail system for the initial design, sealed linear ball bearings and polished steel shafts borrowed from a 3D printer were situated on either side of the mass with a pre-compression rod running down its axial center.

IV.B. Spring Pre-Compression System

In order to ensure the device remains inactive at regions of operation below the rated speed of the wind turbine, a pre-compression mechanism was implemented. To achieve pre-compression, a threaded rod was inserted in the center of the spring with an adjustment nut that allows for the pre-compression to be adjusted.

IV.C. Mass Carriage Assembly

Although the necessary mass and spring constants can be chosen from analytical approach, it is beneficial to have adjustability of the mass for finer-tuning in real-world applications. To achieve this, a series of calibrated masses were implemented that can be bolted onto the device in a uniform pattern. Given geometry constraints, the mass was designed to encapsulate the aforementioned linear bearings while maintaining a void which allows for the pre-tension assembly to pass through its center.

IV.D. Results

The final design of the device is visualized within *Figure 5.* The design provides for limited adjustment in the engagement point by utilizing the

pre-compression assembly, as well as limited adjustments in the operating frequency and magnitude of the Coriolis force through the addition or subtraction of the configurable masses.

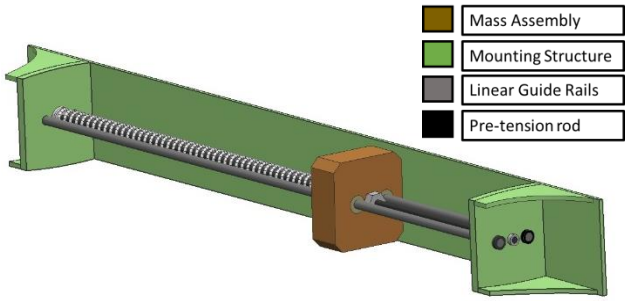

Figure 5. CAD model of the spring-mass system with its mounting structure.

V. PROTOTYPE

Given budgetary and time constraints, the design for this system was simplified in order to achieve an operable prototype by the conclusion of the semester. Both geometric and material constraints were considered but not prioritized to allow the flexibility of construction and usage of readily available tools and supplies.

V.A. Design

To ensure the prototype was manageable, the design was scaled down to an approximate ratio of 1:100 so that its overall length was about 0.5 meters. At this scale, it was necessary for the width and thickness to be exaggerated so that the device can be easily fabricated by hand.

Similarly, the wind turbine hub and drivetrain were also reduced in size to create a rotating test fixture. Again, this component did not adhere to a true scale nor was it built using the same material and geometric constraints.

The hub was simplified to a triangular design to reduce production time. It was constructed of three 8x8” square plates with two 8” triangle plates at its ends. A ½” aluminum wheel spacer taper is welded to the center of the hub so the drive shaft may be attached.

The blades were also simplified, consisting of only a 6” circular base plate, a 2’ long by 4” wide shear web, and a 3” triangular gusset (*Figure 6*).

Figure 6. CAD model of the scale wind turbine test fixture

V.B. Production

The hub of the device as well as the blade sections were constructed from ¼” thick 6061 aluminum. These parts were designed within a CAD program, cut on a waterjet machine, and then welded together to form a complete assembly.

The bedplate – or main frame of the wind turbine power train – were assembled using 2x6” and 2x12” dimensional lumber. The main bearing support on this frame was formed by laminating two 2x6” boards and drilling a 1” hole through the center to allow the drive shaft to pass through. Additionally, two ½” pillow block bearings were bolted onto either side of this support structure to carry the load of the hub assembly. This allowed for the usage of a small, high torque electric motor for rotation as the motor’s shaft was not subjected to the main hub loads.

The tower of the prototype was constructed from a 3’ long piece of 4” schedule 40 PVC pipe which was screwed to the top bedplate and bottom base to allow for ease of transportation and disassembly.

Lastly, the base of the model was constructed similarly to the bedplate using 2x6” and 2x12” dimensional lumber. It too was also screwed together to allow for transportability.

V.C. Results

In *Figure 7* and *Figure 8*, the measured response of the prototype system is compared to the Simulink model developed previously [3]. The Simulink model is shown to be at most 8.2% greater than the measured response, and at the least 5.8% less than the measured response. Given the approximations used in both the development of the model and the scaling of the prototype, this type of error is passable and indicates that the model is functioning well as an approximation of the prototype performance.

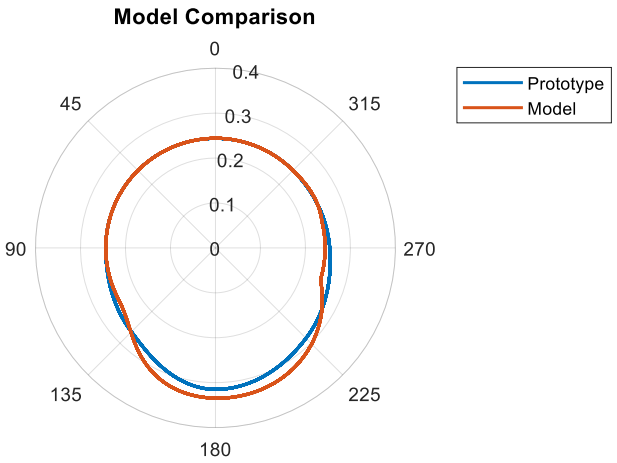

Figure 7. Displacement comparison between the prototype and Simulink model.

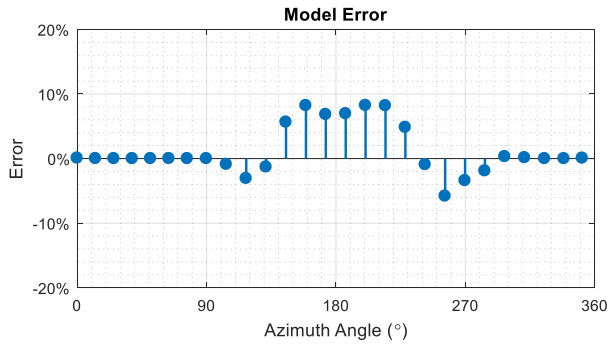

Figure 8. Prototype's deviation from Simulink model.

However, given the loose adherence to the scaling and constraints of the wind turbine model, the system should not be used to extrapolate meaningful data aside from verifying the success of operation and the system's reliance on gravity as the driving force for the generation of the Coriolis force.

VI. CONCLUSIONS

Having ascertained the aerodynamic loading [2], modeled the behavior of the wind turbine given certain parameters [2] and the response of the spring-mass system to a given stiffness and mass [3], and constructed a physical prototype to act as proof of concept, it has been shown that the design is a valid solution and warrants more intense scrutiny and experimental exploration in the future.

ACKNOWLEDGMENTS

The authors thank Dr. Bharat Bagepalli (PhD) for his knowledge on the materials and manufacturing of wind turbine blades as well as the fabrication resources RPI has offered in support of this project.

REFERENCES

[1] D. SCHWENKER and M. SMITH and D. GOODMAN, "Reduction in Root Bending Fatigue of Wind Turbine Blades by a Spring-Mass System," *The MANE Student Research and Design Journal*, pp. 19-23, Rensselaer Polytechnic Institute, Troy, NY, (2017).

[2] D. SCHWENKER and M. SMITH and D. GOODMAN, "Modeling a Simplified Wind Turbine System to Ascertain Parameters for a Spring-Mass System," *The MANE Student Research and Design Journal*, pp. 3-8, Rensselaer Polytechnic Institute, Troy, NY, (2017).

[3] M. SMITH and D. SCHWENKER and D. GOODMAN, "Modeling of a Spring-Mass Compensator System for a Wind Turbine Blade," *The MANE Student Research and Design Journal*, pp. 9-14, Rensselaer Polytechnic Institute, Troy, NY, (2017).

[4] B. BAGEPALLI, *Wind Turbine Rotor Blade Design and Manufacture* [Power Point Presentation]. Rensselaer Polytechnic Institute, Troy, NY, 2016.

Reduction in Root Bending Fatigue of Wind Turbine Blades by a Spring-Mass System

David Schwenker*, Michael Smith, Dan Goodman
Rensselaer Polytechnic Institute
Department of Mechanical, Aerospace, and Nuclear Engineering
In association with the RAMS lab at RPI
david.j.c.schwenker@gmail.com, smithm.mech@gmail.com, goodmd@rpi.edu
Winner of the 2017 Mechanical Engineering Weiss Award
**Winner of the 2017 Arthur M. Greene Prize*

The theoretical framework and necessary design parameters for a proposed system which reduces the root bending fatigue of a wind turbine blade is outlined. A spring-mass system, tuned to a certain frequency and positioned along the length of the blade, would generate an inertial force that counteracts the in-plane periodic loading generated by wind shear. Such a change would extend the fatigue life of the blade, thereby allowing wind turbines to more readily scaled to larger proportions and constructed in more turbulent regions to increase power generation.

I. INTRODUCTION

At its current state, the wind energy industry is not capable of sustaining the current societal energy demands as it accounts for only 2.1% of the total US energy consumption [1]. To increase its energy production, the industry has been steadily increasing the size of its wind turbines and placing them offshore to capture higher wind speeds, thereby allowing them to generate more power [2]. The power generated by a wind turbine is indicated by *Equation 1*, where P is power, C_p is the power coefficient, ρ is the air density, A is the rotor swept area, and U is the wind speed [3]:

$$P = \frac{1}{2} C_p \rho A U^2 \qquad (1)$$

As the size of the wind turbine increases, the fatigue life of the blades diminishes due to higher magnitudes in bending moments produced by periodic and stochastic loading conditions.

I.A. Loading Conditions

Stochastic loading comes from the unpredictable nature of the wind and is therefore random. Periodic loading comes from the wind shear profile and is easier to anticipate (*Figure 1*).

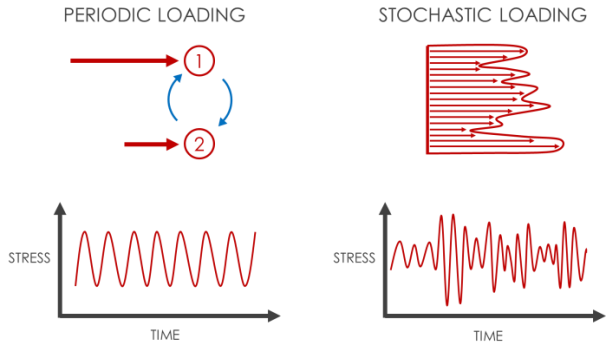

Figure 1. Comparison of loading conditions.

Typically, wind speed increases with height, so as a blade rotates it will experience a higher load at the apex of its rotation and a smaller load at the base of its rotation [3].

I.B. Bending Conditions

This periodic loading manifests itself in two dimensions: out-of-plane bending and in-plane bending. The plane is defined as being coincident with the rotation of the blades (*Figure 2*).

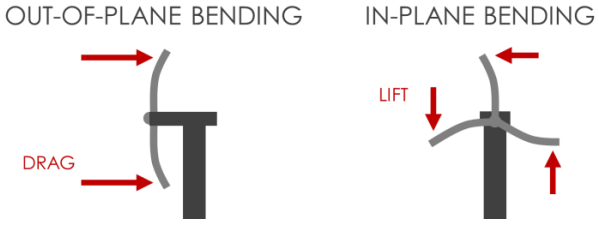

Figure 2. Comparison of bending conditions.

Out-of-plane bending is predominately due to the drag forces generated by the wind and already has several aerodynamic solutions which reduces the

fatigue bending in this orientation, including active cambering, blade twist, and trailing edge flaps [3].

In-plane bending, on the other hand, is predominately due to the lift forces generated by the wind. Current solutions are typically material-based in nature where the blade is made stronger at its root through steel connectors [3]; no system currently exists that actively seeks to reduce this periodic load.

I.C. Operating Conditions

Figure 3 delineates the operation of a wind turbine based upon the wind speed.

Figure 3. Regions of operation for a wind turbine.

At low wind speeds (Region I), the wind turbine does not operate and therefore in-plane bending is not a concern. At intermediate wind speeds (Region II), the wind turbine turns on at a prescribed cut-in speed and will ramp up to its rated speed, varying its rotational speed accordingly during this transition. Here, the wind turbine functions for the majority of its operational time. At higher wind speeds (Region III), motorized pitch control causes the rotational velocity to become constant. Here, the loading conditions are at their maximum and therefore the project's focus was limited to this region for initial development.

I.D. Problem Statement

The periodic loads within the in-plane orientation of the wind turbine during Region III operation need to be minimized. This allows for increased fatigue life of the blades. In turn, this also allows for scaling of wind turbines to increase power generation in more turbulent environments.

II. THE SPRING-MASS SYSTEM

A spring-mass system was developed in conjunction with the faculty and research associates within RPI's Rotorcraft, Adaptive, and Morphing Structures (RAMS) laboratory. The concept for this system, shown in *Figure 4*, involved a spring operating parallel to the main shear web of the blade with a mass fixed to one end and a support structure encapsulating the system.

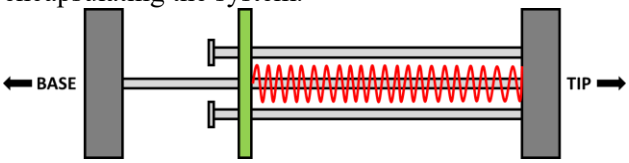

Figure 4. Simplified spring-mass system. The spring is indicated by red, the mass by green.

Conceptually, the centrifugal force generated by the rotation of the blade would push the mass radially outwards, causing a displacement of the spring. The gravitational force, however, is periodic and would cause the mass to oscillate in response.

II.A. Coriolis Effect

The operating principle as to how a spring-mass system would reduce the in-plane periodic loading is through the exploitation of an inertial force known as the Coriolis Effect. This effect refers to an apparent force which is generated by altering a particle's radial position within a rotating reference frame. Technically due to being a perceived force of planar motion relative to a rotating frame, it has real effects on the overall system [2].

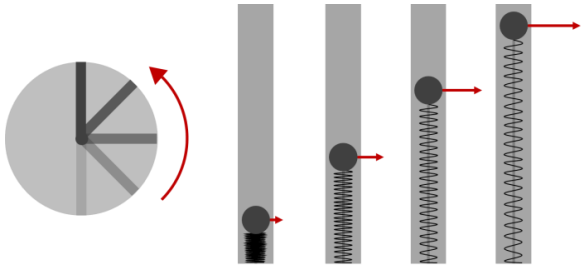

Figure 5. The "Coriolis Effect" visualized.

Therefore, as gravity and the centrifugal force push the mass radially out towards the blade's tip, its resultant inertia will exert a force tangentially opposing the direction of rotation, thereby counteracting a portion of the periodic load due to the lift force (*Figure 5*).

II.B. Frequency Response

In order to diminish only the periodic component of the lift force, it is necessary for the system to oscillate at a frequency that matched the periodic load (*Figure 6*). If the correct offset phase difference is not achieved, there is the opportunity for amplification of the periodic load.

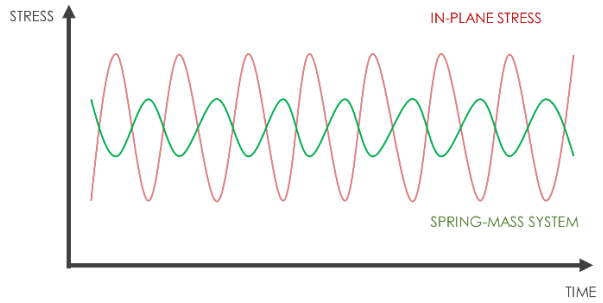

Figure 6. Simplified alternating stress model. The in-plane stress is red, the spring-mass is green.

Assuming simple harmonic motion, the in-plane load alternates regularly during Region III operation due to the constant rotational speed of the turbine. The spring-mass system, therefore, has to match its angular frequency ω_n to the driving frequency ω of the periodic load. This angular frequency is dependent on the ratio of the spring stiffness and the mass. If the correct phase offset can be achieved between the stiffness-mass ratio and the frequency of the external load, the resultant alternating stress experienced by the blade should be reduced due to the opposing force vectors of the spring-mass system and the periodic loading [4].

II.C. Spring Stiffness

Given that the project's focus was limited to only the periodic loading generated within Region III of the wind turbine's operation, it was necessary for the spring-mass system to be inoperable within Regions I and II to avoid unintentional oscillations. To achieve this behavior, a two-stage spring system was developed where no displacement of the mass occurs until the rated speed was achieved. At this point in time, the spring would then exhibit standard linear behavior (*Figure 7*).

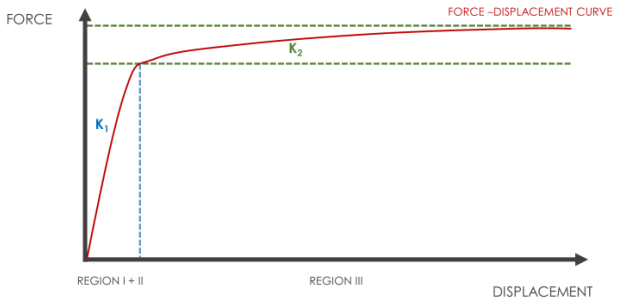

Figure 7. The required two-stage spring system.

This two-stage system can be accomplished by either utilizing (1) non-linear springs or (2) pre-compressed springs. Non-linear springs – including conical, barrel, and dual pitch springs – may potentially work but pre-compressed springs have the distinct advantage of preventing any displacement whatsoever within Region I and II operation, provided that the pre-compression is accurately applied. Given these options, the pre-compressed spring model was chosen.

II.D. Pre-Compressed Springs

This model featured a plate (the mass of the system) pressed against a spring and tightened through the use of bolts. The spring began at a pre-compressed state where it exerted a force against the plate while a reaction force from the bolts kept the system static.

As an external force increased in magnitude, the corresponding reaction forces from the bolts would decrease until they became zero. In the case of a wind turbine blade, this external force was a combination of the centrifugal and gravitational forces. At this point in time, the external force would then achieve a magnitude that exceeds the initial spring force at its pre-compression state and therefore cause the plate to displace. While external force exceeds the initial spring force, the mass-spring system would then exhibit typical linear behavior (*Figure 8*).

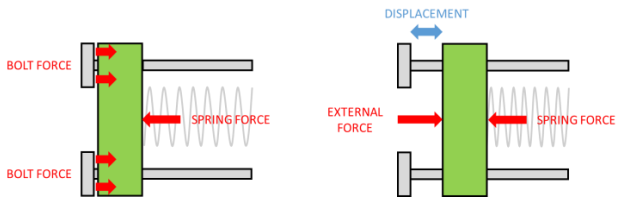

Figure 8. Pre-compressed spring operation.

The external force in Region III operation must be determined in order to calculate the spring force needed at the pre-compressed state. Once determined, the spring can then be tightened to exert a corresponding force on the opposing end of the plate.

II.E. Fatigue Analysis

To quantify how a reduction in the periodic loading could change the system, fatigue analysis will be necessary. A typical S-N curve which characterizes the fatigue life of a given material by plotting experimental data of failure points against their corresponding stress and cycle values is presented in *Figure 9* [5]. For a wind turbine blade, the fatigue failure line would be more linear due its composition of glass reinforced plastics but generally conforms to the line shown [6]. It becomes visually apparent that a reduction in the equivalent stress of the system would prolong the intersection with material's fatigue failure line, thereby increasing the number of cycles to failure [7]. This metric will determine the success of our technical analysis.

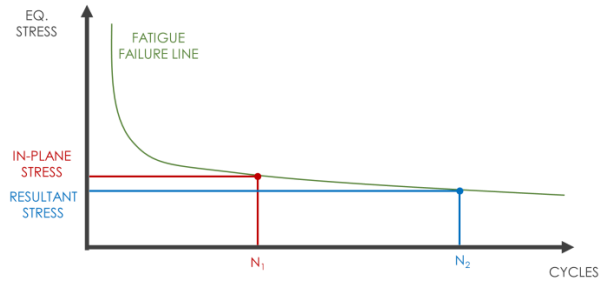

Figure 9. Simplified S-N curve. The in-plane stress is red, the reduced stress is blue.

III. CONCLUSIONS

Pivoting from fossil fuels to renewable resources is a necessity and this process would be facilitated if one could extend the fatigue life of wind turbines so that greater scalability can be achieved for increased power output. The general theoretical framework for a spring-mass system to solve this problem appears sensible by general analytical benchmarks.

With the necessary design parameters and metrics now established, technical analysis – presented in a series of proceeding articles – will be used to model the aerodynamic loading [8], wind turbine behavior [8], spring-mass tuning [9], and physical response of the overall system [10] to effectively design the apparatus. Results of this technical analysis will show the theoretical framework presented is valid and warrants more intense scrutiny in the future.

ACKNOWLEDGMENTS

The authors thank Dr. Farhan Gandhi (PhD) for his many contributions to the design of the spring-mass system including the definition of the pre-compressed spring and the general design procedure, Dr. Etana Ferede (PhD) for his contributions to the effective modeling of the wind turbine system to accurately anticipate loading conditions, Dr. Bharat Bagepalli (PhD) for his knowledge on the materials and manufacturing of wind turbine blades, and the many resources RPI has offered in support of this project.

REFERENCES

[1] U.S. EIA, *The Monthly Energy Review (MER)*, pp.5, April 2017.

[2] U.S. DOE, *Wind Vision: A New Era for Wind Power in the United States*, April 2015.

[3] T. BURTON and N. JENKINS and D. SHARPE and E. BOSSANYI, *Wind Energy Handbook*, pp. 4, 16, 413, 418, John Wiley & Sons, Hoboken, NY (2011).

[4] J. L. MERIAM and L.G. KRAIGE, *Engineering Mechanics: Dynamics*, pp. 581-590, 600-606, John Wiley & Sons, Hoboken, NY (2012).

[5] J. F. MANWELL and J. G. MCGOWAN and A. L. ROGERS, *Wind Energy Explained: Theory, Design, and Application*, pp. 257-265, John Wiley & Sons, Hoboken, NY (2009).

[6] M. M. SHOKRIEH and R. RAFIEE, "Simulation of Fatigue Failure in a Full Composite Wind Turbine Blade," *Composite Structures*, Vol. 74, Issue 3, (2006).

[7] B. BAGEPALLI, *Wind Turbine Rotor Blade Design and Manufacture* [Power Point Presentation]. Rensselaer Polytechnic Institute, Troy, NY, 2016.

[8] D. SCHWENKER and M. SMITH and D. GOODMAN, "Modeling a Simplified Wind Turbine System to Ascertain Parameters for a Spring-Mass System," *The MANE Student*

Research and Design Journal, pp. 3-8, Rensselaer Polytechnic Institute, Troy, NY, (2017).

[9] M. SMITH and D. SCHWENKER and D. GOODMAN, "Modeling of a Spring-Mass Compensator System for a Wind Turbine Blade," *The MANE Student Research and Design Journal*, pp. 9-14, Rensselaer Polytechnic Institute, Troy, NY, (2017).

[10] D. GOODMAN and D. SCHWENKER and M. SMITH, "Designing a Simplified Wind Turbine Mounting System to Ascertain Device Performance," *The MANE Student Research and Design Journal*, pp. 15-18, Rensselaer Polytechnic Institute, Troy, NY, (2017).

The following section represents student design projects developed within Inventor's Studio at Rensselaer; Innovations are partially funded by VentureWell.

Novel Device and Method for the Treatment of Raynaud's Phenomenon

Frank Charbonier
Rensselaer Polytechnic Institute
Department of Mechanical, Aerospace and Nuclear Engineering
frank.charbonier13@gmail.com
Winner of the 2017 Clarence E. Davies Award and 2017 Stanley I. Weiss Capstone Design Award

A novel device and method for treatment of Raynaud's phenomenon is presented. Raynaud's is a condition characterized by an exaggerated vasoconstrictive response to cold or emotional stress. Sufferers experience excessive narrowing of blood vessels, most commonly in the fingers, which can lead to permanent tissue damage and loss of digits in severe cases. The proposed device enables precise local delivery of a vasodilating drug via a microneedle array to counter or prevent these symptoms. Local release rather than systemic delivery aims to maximize the impact and reduce side effects common to current treatments. The device may be easily combined with a continuous monitoring system to enable unprecedented personalization of Raynaud's treatment. If successfully validated, the proposed device and method have the potential to impact the lives of millions of Raynaud's sufferers.

I. INTRODUCTION

Raynaud's phenomenon (RP) – also known as Raynaud's or Raynaud's disease – is a condition affecting roughly five percent of the population. In patients suffering from Raynaud's, the blood vessels of the digits constrict excessively in response to cold or stress [1]. While RP can affect the toes, nose, ears, and even tongue, the condition is primarily limited to the fingers. Typically, fingers will turn white as blood flow cuts off (digital ischemia), blue as blood becomes deoxygenated (anoxia), and then bright red as blood rushes back in (reperfusion) [2].

It is important to distinguish between the two types of Raynaud's. Primary Raynaud's is not linked with any other pre-existing conditions and affects 80-90% of Raynaud's sufferers. The exact causes remain unclear, although vascular and neural abnormalities appear to play a role in the hyperactive vasoconstrictive response [3]. Secondary Raynaud's, meanwhile, is associated with another underlying medical condition. This is commonly a connective tissue disorder such as scleroderma or rheumatoid arthritis [4]. While primary Raynaud's is often relatively benign, secondary Raynaud's is usually more serious and can lead to permanent tissue damage. This includes ulcers, gangrene, and even amputation of the digits in severe cases [2].

In most cases, primary Raynaud's phenomenon can be treated with lifestyle changes and does not require drug treatments. Minimizing cold exposure is the most effective therapy, while supportive measures like avoiding smoking and exercising regularly may also be helpful. Given the greater severity and distinct mechanisms of secondary Raynaud's, this form often demands pharmacologic treatment in addition to cold avoidance [2].

I.A. Limitations of the State-of-the-Art

A definitive cause for primary Raynaud's has yet to be determined, and much is still not understood about how both forms of the condition work on a physiological level. Furthermore, treatments developed to date have not been universally successful in mitigating or altogether eliminating the effects of RP. If self-treatment by lifestyle adjustments is insufficient, medications aim to reduce the frequency, severity, and duration of attacks as well as prevent tissue damage. Many drugs currently used for RP (e.g., calcium channel blockers (CCBs), phosphodiesterase inhibitors, angiotensin II receptor blockers, topical nitroglycerin) are commonly accompanied by side effects such as headaches, flushing, dizziness, nausea, and low blood pressure [2]. Current treatments show mixed efficacy among patient populations, and many newer therapies remain underexplored and insufficiently characterized [3].

II. PROPOSED SOLUTION

The proposed solution is a device enabling local release of a vasodilator agent to prevent or counter a Raynaud's attack. Maximization of local impact and

reduction of systemic side effects are crucial features. One key enabling component is the novel use of microneedles in treatment of RP.

The thin outermost layer of skin (i.e., the stratum corneum) provides the body's greatest barrier to external substances such as drugs and vaccines. By reversibly disrupting the stratum corneum with micropores or bypassing the layer altogether, microneedles ranging in height from 25-2000 µm enable effective transport of a wide range of pharmaceuticals [5]. As they avoid the nerve fibers and blood vessels of the dermis, microneedles may also improve patient compliance by providing pain-free delivery [6].

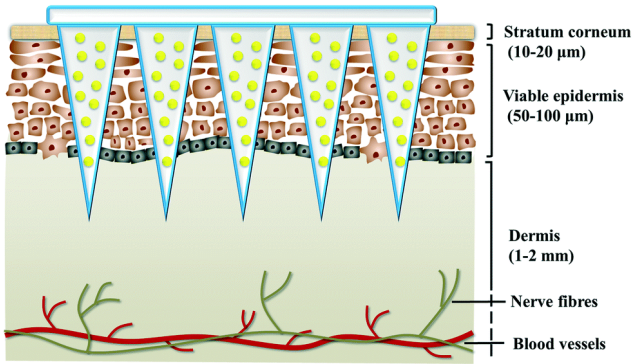

Figure 1: Schematic illustration of transdermal drug delivery with a microneedle array. Microneedles bypass the stratum corneum without stimulation of dermal nerves or puncture of dermal blood vessels. Reproduced from Ref. [7] with permission of The Royal Society of Chemistry.

In one configuration of the proposed device, the user presses a button to deliver a precise drug dosage to the affected body parts via a plurality of microneedles (Figure 2). The device may be applied directly to the finger or wrist or incorporated into a wristband, ring, glove, or similar apparatus. While some microneedle systems rely on passive transport, pressure-driven and other active methods are capable of delivering large amounts of drug through hollow microneedles as a single, bolus injection or as a time-dependent or continuous infusion [8]. In this particular configuration, the mechanical motion of the button drives rapid dose metering and transport. Mepham et al. (2017) demonstrated a similar power-free manipulation of picoliter droplets, although further work is required to make their design robust and commercially viable [9].

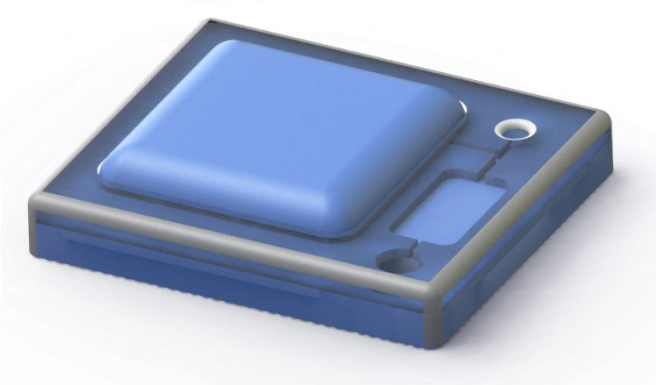

Figure 2: One configuration of the envisioned device. A simple button press precisely aliquots and delivers the drug locally. Device dimensions are 32 x 28 x 7mm.

Some candidates for medication include calcium channel blockers such as nifedipine, perhaps the most common current drug treatment currently used for RP [3]. Microneedle-assisted delivery of two types of CCBs has been recently explored [10]. Prostacyclin analogs such as treprostinil and iloprost also show promise for reducing frequency and severity of attacks as well as preventing or healing digital ulcers [3]. Clinical studies noted that many patients were unable to tolerate subcutaneous infusions of treprostinil despite improvement of ischemia and ulceration, suggesting that treatment with this class of drugs may benefit from transdermal delivery [11].

III. DISCUSSION

One key benefit of the proposed device is the reduction or elimination of side effects accompanying current vasoactive drugs by delivering the drug locally rather than systemically. The user is able to self-medicate daily with regular doses, preventatively when at risk (e.g., going for hike in the winter), or reactively when symptoms are self-observed. Automation of the mechanism provides more control for both patients and caregivers by permitting scheduled dosing with high accuracy and minimal manual intervention.

During informal interviews, several Raynaud's patients expressed interest in a wearable device

capable of monitoring for drops in local skin temperature and providing an alert to take preventative measures. Such a device would not only benefit the significant RP population relying on non-drug self-treatment, but also facilitate the use of diagnostic feedback to tailor doses for individuals and enable an advanced degree of personalized medicine. Oxygen saturation, heart rate, and levels of relevant biomarkers (e.g., nitric oxide) are just some of the additional measurements which could be incorporated into a complementary continuous monitoring system.

Rigorous clinical and nonclinical testing will be required to validate the device and treatment strategy. More work is needed to fine tune the delivery system and address the challenges involved with large-scale fabrication of microneedles and repeatable insertion into the skin. Once successfully demonstrated, the device has the potential to enable future studies of drug efficacy in Raynaud's patients and perhaps even lead to much-needed treatment breakthroughs.

IV. CONCLUSIONS

Two key ideas are presented: a new approach for treatment of Raynaud's phenomenon, and a device enabling this approach. To the best of the author's knowledge, highly localized drug delivery via microneedles has not yet been demonstrated for the treatment of RP. The proposed device aims to empower Raynaud's patients by minimizing the side effects of current drugs, maximizing the positive impact on symptoms, and reducing the time spent worrying about when the next attack might happen. Whether implemented as a standalone drug delivery platform or combined with a diagnostic monitoring system, this device and method could have a significant impact on the way Raynaud's phenomenon and other vascular conditions such as critical limb ischemia and pulmonary hypertension are treated.

ACKNOWLEDGMENTS

The author would like to thank Professor Asish Ghosh for his guidance and support, as well as Carol Maxwell and Paul Pagnozzi for mentoring and advice.

REFERENCES

[1] F. M. Wigley and N. A. Flavahan, "Raynaud's Phenomenon," *The New England Journal of Medicine,* vol. 375, no. 6, pp. 556-565, 11 August 2016.

[2] F. M. Wigley, A. L. Herrick and N. A. Flavahan, Raynaud's Phenomenon, A Guide to Pathogenesis and Treatment, New York: Springer, 2015.

[3] T. L. Levien, "Advances in the treatment of Raynaud's phenomenon," *Vascular Health and Risk Management,* vol. 6, pp. 167-177, 2010.

[4] J. P. Cooke and J. A. Marshall, "Mechanisms of Raynaud's disease," *Vascular Medicine,* vol. 10, pp. 293-307, 2005.

[5] R. F. Donnelly, T. R. R. S. Singh and A. D. Woolfson, "Microneedle-based drug delivery systems: Microfabrication, drug delivery, and safety," *Drug delivery,* vol. 17, no. 4, pp. 187-207, 2010.

[6] E. Larraneta, R. E. M. Lutton, A. D. Woolfson and R. F. Donnelly, "Microneedle arrays as transdermal and intradermal drug delivery systems: Materials science, manufacture and commercial development," *Materials Science and Engineering: R: Reports,* vol. 104, pp. 1-32, 2016.

[7] M. Wang, L. Hu and C. Xu, "Recent Advances in the design of polymeric microneedles for transdermal drug delivery and biosensing," *Lab Chip,* no. 17, pp. 1373-1387, 2017.

[8] Y.-C. Kim, J.-H. Park and M. R. Prausnitz, "Microneedles for drug and vaccine delivery," *Advanced drug delivery reviews,* vol. 64, no. 14, pp. 1547-1568, 2012.

[9] A. Mepham, J. D. Besant, A. W. Weinstein, I. B. Burgess, E. H. Sargent and S. O. Kelley, "Power-free, digital and programmable dispensing of picoliter droplets using a Digit Chip," *Lab Chip,* vol. 17, pp. 1505-1514, 2017.

[10] M. Kaura, K. B. Itaa, I. E. Popovab, S. J. Parikhb and D. A. Bair, "Microneedle-assisted delivery of verapamil hydrochloride and amlodipine besylate," *European Journal of Pharmaceutics and Biopharmaceutics,* vol. 86, no. 2, p. 284–291, 2014.

[11] G. Engel and S. G. Rockson, "Treprostinil for the treatment of severe digital necrosis in systemic sclerosis," *Vascular Medicine,* vol. 10, pp. 29-32, 2005.

Automated 360-Degree Gamma-Ray Imaging System

Hyung-Jin Choun
Rensselaer Polytechnic Institute
Department of Mechanical, Aerospace, and Nuclear Engineering
chounh@rpi.edu

There are occasions where human intervention is inevitable in radioactively contaminated facilities. The exposure rate threatens the workers and limits their activities. One of the reasons for the limitation is that it is difficult and time consuming to locate and quantify the radioactive sources. The proposed solution, the Automated 360-degree Gamma-Ray Imaging System, implements 360-degree camera and a virtual reality machine to the gamma imaging system with an array of detectors. Having a virtual view with a radiation intensity map will shorten the time for data acquisition and also gives a clear view where actual the contamination is located. The automation feature will allow the gamma imaging system to move around to perform data acquisition and provide the radiation intensity map even more efficiently. The future plans of the work and how it is set apart from currently issued patents is discussed.

I. Introduction

Workers who work in facilities where radioactive contamination exist are threatened by the radiation exposure in various occasions including emergency situations (Fukushima Accident), during decommissioning, and dismantling process, or even during standard operations. It is crucial to locate and quantify the radioactive sources present in contaminated facilities, before preparing an intervention or defining a decommissioning strategy in order to keep the radiation exposure as low as reasonably achievable. However, the knowledge of position, identification and radiological characteristics of the contamination is often difficult to obtain due to uncertainties such as high background caused by high activity. In addition, acquisition of necessary data for defining contamination is usually a time consuming process. Workers who work at the contaminated facilities are threatened by the exposure as it is difficult to locate and quantify the radioactive sources.

I.A. Existing Technology

There are commercially available gamma imaging systems in the market, which can map a radioactive area present in contaminated facilities [1]. A gamma imager, iPIX, as shown in Figure 1, is the system that identifies low-level radioactive sources from a distance while estimating the dose rate at the measurement point. It is capable of drastically decreasing the radiation exposure by mapping the radioactivity before human intervention. However, mapping the radioactive contamination still requires quite a long time when it comes to large facilities.

Figure 1: iPIX mounted on motorized tripod.

As shown on the Figure 2, the iPIX can only show the contamination information of one side. In order to map the radioactive contamination of the whole facility, which can be everywhere, it is necessary to manually adjust the angle and the distance between the object and the system numerous times for a good estimation. Figure 3 shows the radioactivity of a pipe that runs on the ceiling.

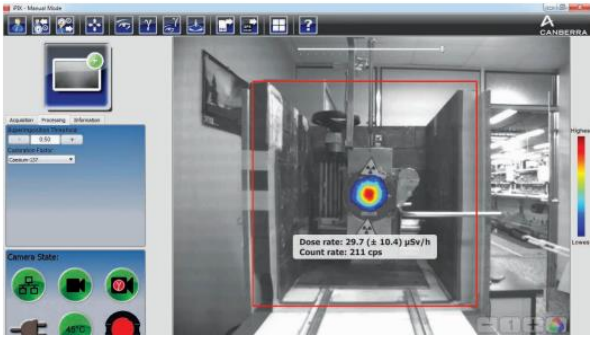

Figure 2: Resultant image of iPIX.

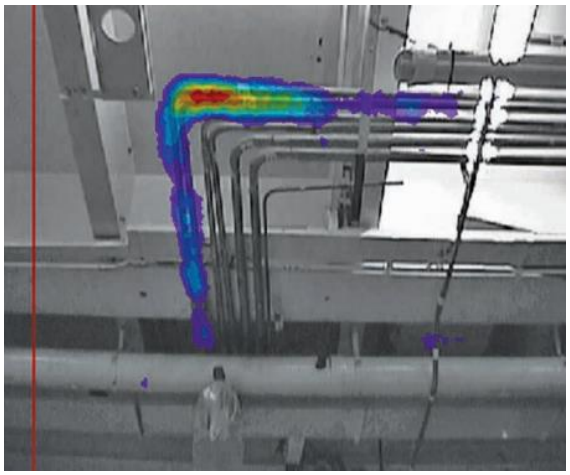

Figure 3: Contamination on a pipe mapped with iPIX

In addition, since the resultant image is two dimensional, the location of the contamination could be inaccurate and it would require additional takes at different location. For example, when it is necessary to find the radiation intensity of hole A with two identical gamma imaging system at two different locations as shown in Figure 4 the result could be different as shown in Figure 5. It shows that the resultant image and the spectra of the same location are not identical. The mapping of radioactive contamination could be very time consuming with the present method and it could be more problematic if it's a time sensitive situation such as during or after an accident.

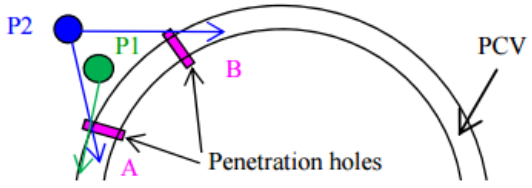

Figure 4: The gamma cameras are set at location point1 (P1) and point2 (P2).

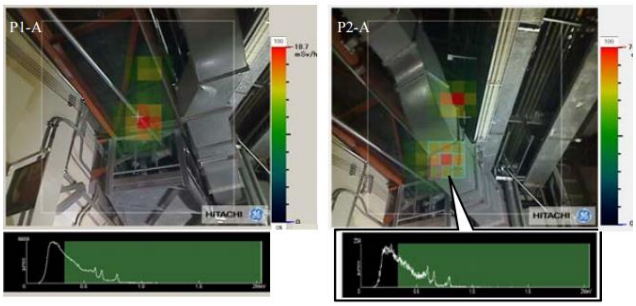

Figure 5: Visualization results. P1-A and P2-A are images of the same penetration holes observed from different locations with the gamma camera.

Also when the system is to be used in a situation where everything must be controlled remotely a camera will not provide enough vision. For example, in accident situations there could be a lot of obstacles on the floor and obstacles falling from the ceiling that could damage the system. Even if the camera can rotate 360 degrees, it would not be efficient to check every single side before moving forward.

II. Product Description

In order to have a full vision and shorten the time to map the radioactive contamination, a 360-degree camera and virtual reality will be added to the gamma imaging system. An array of detectors will be added to cover 360-degrees. Figure 6 shows a CAD mock-up of the product.

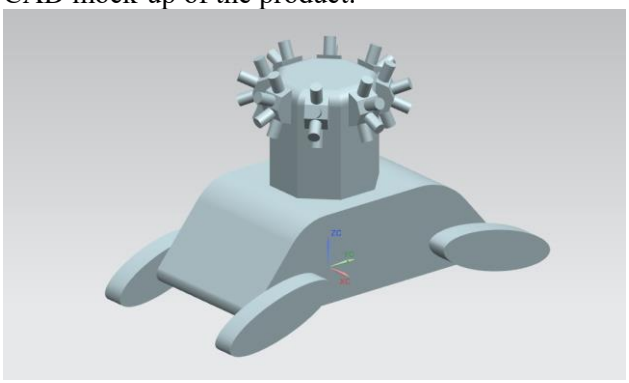

Figure 6: CAD mock-up of the product. Small cylinders represent detectors.

Having a virtual view with radiation intensity map shortens the time for data acquisition and also gives a clear view where actual the contamination is located. In addition, a feature that could allow the gamma imaging system to automatically move around to perform data acquisition is added. It

senses the radioactivity and gets close to the location to measure the intensity. Moreover, it senses other environmental factors such as high temperature that could damage the system or obstacles that could trip the system. This way an individual would not have to control the system to measure the whole facility.

III. CONCLUSIONS

Workers at the contaminated facilities are threatened by the radiation exposure because it is difficult and time consuming to locate and quantify the radioactive sources. To solve this problem a solution that could improve the defects of the existing system is proposed. For the proposed solution a 360-degree camera and virtual reality are added to the gamma imaging system. Having a virtual view with radiation intensity map shortens the time for data acquisition and gives a clear view where actual the contamination is located. In addition, a feature that could allow the gamma imaging system to automatically move around to perform data acquisition is added and multiple sensors is added on the system. Future work would include improvement on the accuracy of sensors, developing the array of detectors so that it is economically feasible.

REFERENCES

[1] "iPIX Ultra Portable Gamma-Ray," Canberra, 2015. [Online]. Available: http://www.canberra.com/products/insitu_systems/pdf/iPIX-SS_C47705.pdf. [Access: 1 11 2016].

Unlocking Control with Directional Gestures

Leying Hu, Yue Fang
Rensselaer Polytechnic Institute
Department of Mechanical, Aerospace and Nuclear Engineering
huleying6@gmail.com, evefangy@gmail.com

This paper addresses the problems caused by opening doors with keys. After interviewing current unlocking techniques' users and going through patent searches, loopholes of prior arts are found and referenced to improve the unlocking systems. The proposed approach is unlocking with gesture sensors, which reads and verifies inputs as passcodes, as an alternative method. The unlocking control with directional gestures should be traceless, keyless, and secure.

I. INTRODUCTION

People form the habit of carrying keys around for centuries. However, it is inevitable that they lose their keys, forget to bring their keys, lend out keys, or don't have functional keys. More seriously, people who don't have hands cannot use a key. So the traditional method turns out to be very inconvenient. It is reasonable to envision recognition techniques to take place of the keys.

Recognition based locks can be classified into three categories including: facial recognition based locks, voice recognition based locks, and gesture touchpad-input recognition based locks. From user feedbacks of the above methods, critiques are as follows.

For facial recognition based locks [3], the problems include an inability to distinguish faces with similar looks and an inability to detect faces with sunglasses or hats. For voice recognition based locks [6], the problems include an inability to distinguish similar voices and an inability to detect a voice after vocal changes due to physical condition. For touchpad-input recognition based locks [5], the problems include a lack of landscape mode compatibility, a short battery life due to erroneous detections, a lack of support for running parallel applications, and a tendency to leave fingerprint traces on the screen. In addition, if the users do not have hands, the unlocker will not be useful.

The objectives of the unlocking control with directional gestures are traceless, keyless, secure, convenient, and avoiding similarities with passcodes. The remaining sections of the paper covers the product overview, detailed system level design and concerns.

II. PRODUCT DESIGN

The goal of the gesture lock is to unlock the doors without a key. The Gesture Lock is an add-on to any physical locks. It reads hand gestures as passcode inputs and unlocks the door once the passcode is correct. In this section, details of the implementations will be covered.

II.A. Product Overview

Gesture Lock consists of three units: a gesture recognition unit, a servo unit, and an administration unit. The administration unit and the gesture recognition unit work together to check the input passcode. The servo unit is in charge of unlocking the door. Prior to use, the users can set up a sequence of hand gestures as a passcode. Whenever they need to unlock the door, they repeat that sequence in front of the gesture sensor. If the sequence matches with the one that preset, the door will be unlocked. A few safety features are added to the design. Limited number of incorrect input attempts are set. Once 5 attempts are reached an alert message will be sent to the users. Users can later reactivate the system through passcode reset at the administration level. The detailed system level design is shown in the figure below.

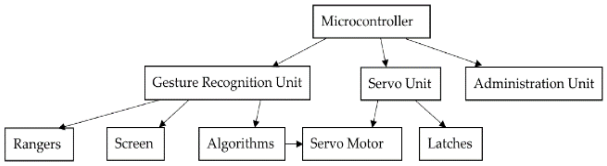

Figure 1. System level design diagram

II.B. System Level Design

Three units of the Gesture Lock communicate with each other via a microcontroller to set and verify input hand gestures and trigger the servo motor to unlock the door.

II.B.1 Gesture Recognition Unit

The gesture recognition unit consists of a microcontroller, a gesture sensor, a liquid crystal display (LCD), a pushbutton, a Bluetooth receiver, and a power supply. The unit's functions are to read and verify hand gestures given by the users.

A gesture sensor, which can be purchased from the market, can detect the 3D position of the object placed near it. One usual way to determine the hand position is to sense the reflected IR light with four directional photodiodes [1]. Locations of the hand will be constantly monitored and the changes in distances along the three axis during a finite time interval are interpreted as different gestures (e.g., up, down). Different combinations of the six gestures can be used as passcode for unlocking the door. Users will be allowed to set or reset the passcode by enable passcode setting mode through the administration unit. Details about administration unit will be covered at the end of this section. Once the passcode setting mode is activated, the gesture sensor will detect and record the gestures. The gesture sequence detected will be shown on the administration page simultaneously for the users to verify the inputs. A new sequence is saved in the microcontroller's internal memory system so data can be retrieved and compared later on. For this design, new gestures are saved in a microcontroller (Arduino Uno) by calling the eeprom function. The figure below displays the process of passcode initialization.

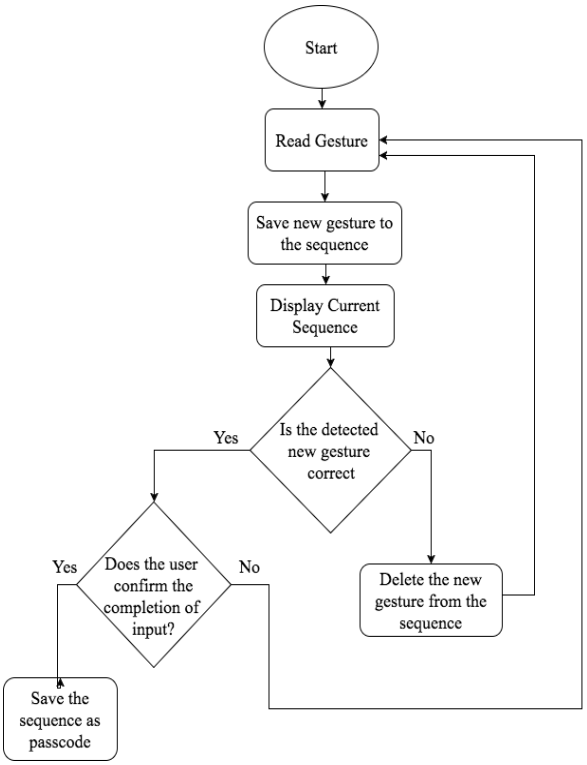

Figure 2. Logic diagram for passcode initialization

After the passcode is set, users can swipe above the gesture sensor to input a sequence. A pushbutton should be pressed to confirm the completion of inputting. If the sequence matches with the one preset, servo motor will be activated to unlock the door. A security feature is embedded in the gesture recognition unit: after 5 incorrect attempts, the system will shut down. This feature is implemented by counting the number of attempts before a correct input is received. Once number of wrong attempts is over the limit, gesture sensor will go into locked mode. Users can regain access by resetting gestures through administration unit.

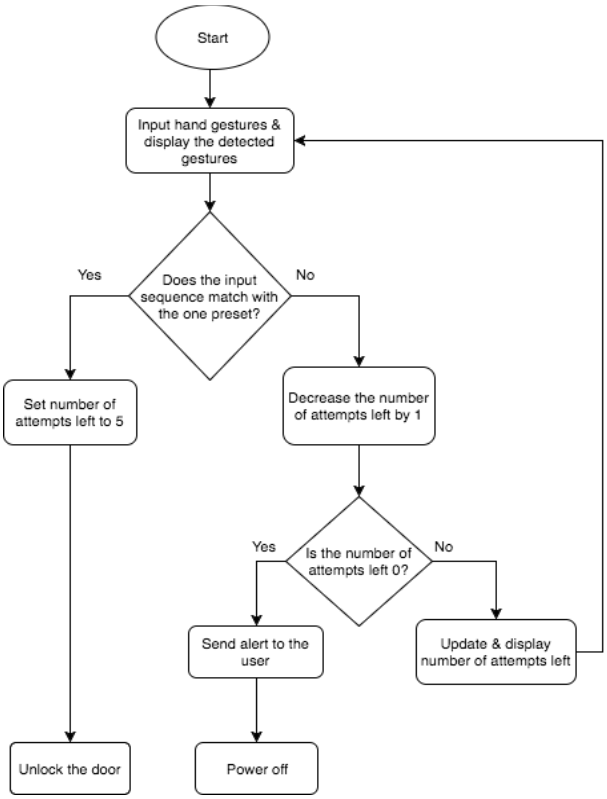

Figure 3. Logic diagram for door unlocking system

The LCD screen is for displaying recognized gestures and input attempts left. The LCD requires power, ground lines, and I2C connections. It displays the detected gestures from the gesture sensor and the match results from the microcontroller.

II.B.2 Servo Unit

The device for unlocking the door utilizes a servo motor. However, customized digital locks, DC motors, and linear actuators can also be used to work with gesture lock system. In this section, the description will focus on only servo motors since they offer the designers more controls on the degrees of freedom for turning the lock.

Servo motors are driven by magnetism. The control systems of motors can be explained by the simple DC motor circuit diagrams. The schematic of a DC motor includes DC voltages *Vdc*, resistors *R*, inductors *L*, and rotors in series. The relationship between the voltage drop is,

$$V_{dc} = IR + L\frac{dI}{dt} + V_{emf} \qquad (1)$$

where I is series current in circuits, and V_{emf} is electromotive force voltage. The torque τ on rotors is,

$$\tau = K_t I = J\alpha + B\omega \qquad (2)$$

where K_t is torque constant, J is moment of inertia, α is angular acceleration, B is viscous friction coefficient and ω is angular velocity. The V_{emf} generated can be expressed by,

$$V_{emf} = K_i\omega \qquad (3)$$

where K_i is electric constant. From Eqs. (II.B.2.1), (II.B.2.2), and (II.B.2.3), the substitution function is,

$$V_{dc} = \frac{(J\alpha + B\omega)R}{K_t} + L\frac{d}{dt}\left(\frac{J\alpha + B\omega}{K_t}\right) + K_i\omega \qquad (4)$$

The corresponding transfer function between the DC voltage input and motor angular velocity is,

$$\frac{\Omega(s)}{V(s)} = \frac{K_t}{(Js + B)(R + sL) + K_iK_t} \qquad (5)$$

From Eq. (II.B.2.5), the ideal output servo motor should depend on the voltage and the property constants of the servos.

II.B.3 Administration

The function of administration unit is to manage the security settings. The administration unit is an Arduino-software interface. Important codes can be saved in the Arduino-software phone application and uploaded to the Arduino via Bluetooth (or wifi) connection. For example, when setting gesture passcodes, the gesture detection and storage code is uploaded to the Arduino through Bluetooth to restart the

Arduino. Users will be allowed to input a new sequence that overwrites the old sequence. The same code will be uploaded if the users want to reactivate the gesture lock from power off mode. Since reload code will restart Arduino, gesture lock will exit the power off mode and function normally. The users can thus open the door with the new sequence set. A few notifications about the system status can be sent to the users' phones through Short Message Service. A General Packet Radio Service shield and a subscriber identity module card are utilized to send out messages. For example, when 5 wrong attempts of inputting passcodes are detected, a warning message will be sent to the users.

III. CONCLUSIONS

The common ways to unlock the doors are with a key or a keypad. However, these methods can be inconvenient and unsafe as the users can lose the keys or leave fingerprints on the keypad. A touchless gesture lock is designed to allow users to unlock the door with hand gestures as passcode. Since the doors are opened with only hand gestures, a security feature is also taken into consideration. A limited amount of attempts is enforced and any potential intrusion event will be sent out to notify the owner. Therefore, users can still open the doors without the presence of physical keys. Since inputting hand gestures doesn't require users to physically contact with the devices, fingerprints will not be left on the lock. Explanations about the implementation of the devices show the feasibility of the method. Therefore, the gesture lock can effectively solve the problems regarding losing keys and leaving fingerprints.

ACKNOWLEDGMENTS

This project is originally a design project for MANE 4220 Inventor's Studio 2 at Rensselaer Polytechnic Institute that aims to develop new and better methods for existing needs. Special thanks to Gesture Lock Project Teams at Design for America at Rensselaer for assisting the prototyping process and giving out insightful comments for the early design.

REFERENCES

[1] Avago Technologies. 2013 November 8. Digital Proximity, Ambient Light, RGB and Gesture Sensor. [accessed 2016 October 29]; https://cdn.sparkfun.com/datasheets/Sensors/Proximity/apds9960.pdf

[2] Arduino. c 2016. [accessed 2016]. https://www.arduino.cc/en/Reference/EEPROM

[3] Gary Mazo, Jul. 24, 2012. Androidcentrol. How to Set Up Face Unlock on Your Android Phone. [accessed December, 2016]. http://www.androidcentral.com/how-set-face-unlock-your-htc-one-x-or-evo-4g-lte

[4] G. F. Franklin, J. D. Powell, and A. Emami-Naeini. 2015. Feedback Control of Dynamic Systems. 7th Edition. Upper Saddle River, NJ: Pearson Higher Education, Inc

[5] Google Play Gesture Lock Screen. 2016. Google; [accessed December, 2016]. https://play.google.com/store/apps/details?id=qlocker.gesture

[6] Voice Lock Screen. 2016. Google; [accessed December 2016]. https://play.google.com/store/apps/details?id=cx.makaveli.voicelockscreenhd&hl=en

Learning Python from Your Loved Ones

Aditi Nataraj, Qijun Liu
Department of Electrical, Computer & Systems Engineering
adtnataraj@gmail.com, qijunliu5@gmail.com
*Winner of the 2017 Inventor's Studio Innovation Award

With the rise in popularity of technology, programming languages are being increasingly embraced. However, the material is not easily accessible for individuals who want to learn a programming language as well as how to program. The overall purpose of Pyathlon is to educate the public in programming language; PyAthlon is a web tutorial application with two main features. The first feature allows the user to learn Python through an interactive, fun, and informative tutorial set up by other users. The second feature makes the user feel as though they are connected with the person of their choice through the application. Whoever wants to learn about new technology should be able to do so, and with the use of this application, they will learn how to do it.

I. INTRODUCTION

As time passes, with ever changing trends in technology, people not only age, but their knowledge slowly becomes outdated. As this occurs, the older generation turns to their families, such as their children and grandchildren, to provide them with emotional stimulation and entertainment. A significant majority of older adults say they need assistance when it comes to using new digital devices. Just 18% would feel comfortable learning to use a new technology device such as a smartphone or tablet on their own, while 77% indicate they would need someone to help walk them through the process. Among seniors who go online but do not currently use social networking sites such as Facebook or Twitter, 56% would need assistance if they wanted to use these sites to connect with friends or family members [1]. Meanwhile, their children and grandchildren also act as a window to the outside world of new technologies, yet children and grandchildren may not have time between work and school to spend as much time with them. There is a a need for a method that the older generation can use to learn about new technologies that will keep them entertained, while also have them feel like they are connecting with their families.

In prior years, grandparents would live with their children as they aged. It was common for their children to take care of them in their homes, while also attending to their own lives. With this setup, the grandparents were able to interact with both their kids and their grandkids. However, recently, grandparents do not live with their children. In 1980, grandparents maintained 32.7% of families [2]. However, by 2014, a mere 10% of grandparents lived with their children [3]. The problem of grandparents' disconnections from their families did not exist about 40 years ago, but it is a growing problem as the number of grandparents connected with their families is rapidly decreasing.

Grandparents often want to spend time with their families, and having their families to teach them about new technology is one of the methods that makes the grandparents feel connected to their families. Providing grandparents with an interactive method of learning new technologies that is emulated the same emotional connection that their families fills the gap between the grandparents' disconnection and desire to learn.

Programming is one of the new technologies that helps connect older generation with the ever-changing world of technology. Furthermore, after completing introductory courses in programming, older adults were significantly more comfortable with and knowledgeable about computers and the Internet, and more likely to use them [4].

PyAthlon is such a web application that provides a solution that helps the older generation to learn about programming, specifically coding in Python, while feeling as though they are connecting with their grandchildren or children.

I.A. Existing Technology

There are a few methods of learning new technologies, which grandparents can use today. These methods include using Google to learn new information, using school notes from their children and grandchildren, or taking a class. However, there

are some flaws associated with all of these methods: Using Google or school notes to learn new material are not interactive, and most individuals prefer to use interactive methods of learning.

1. Taking a class may not be feasible. If a grandparent is not able to drive or has limited mobility, going to school to take a class will be hard. Furthermore, if a grandparent has arthritis, it will be difficult to write and take notes.
2. Using Google may procure results that are too advanced for a beginner to begin with. If the grandparent is not well versed with technology, it may be hard to find a different search result or narrow search results in general.
3. School notes often assume that the student learning the material has some sort of basic knowledge, or at least, in the case of a beginner course, which the student is comfortable using different kinds of technology. This may not be the case for elderly individuals, as something that seems simple to a student such as "download a Python interpreter" will leave the elderly stumped.

In terms of computer science, there have been a lot of recent inventions that are marketed towards beginners who are trying to learn the subject. For example, there are many interactive tools that help young children to learn how to code [5]. Nonetheless, even though these tools are interactive, they are marketed towards kids. Although most grandparents love cartoons, which the interactive tools often utilize, the reason they love cartoons is that it reminds them of their grandkids. There is no interactive tool that allows grandparents to learn a programming language, while also sustains the emotional connection with their grandkid as though the grandkid is teaching them.

II. PRODUCT DESCRIPTION

PyAthlon is an interactive web application that allows users to learn Python interactively. The application will have three main interfaces: front-end student view, front-end teacher view, and back-end. Both front-end interfaces are implemented with HTML and Java script. The backend is created using Python.

II.A. Product Sketch and Description

The front-end student view is the main view that the user will interact with. These interfaces (Figure 1 and 2) will contain all of the user's completed and unfinished lessons, as well as the different voices and avatars that the user can service. The user will also have access to a 'Settings' page, as shown in Figure 3, where they can set any preloaded voice as their default. The user will also use this view in order to work through and complete the tutorial. Since this interface is the primary interactive view that the user will see, this is the most detailed.

II.A.1. Front-end Student View

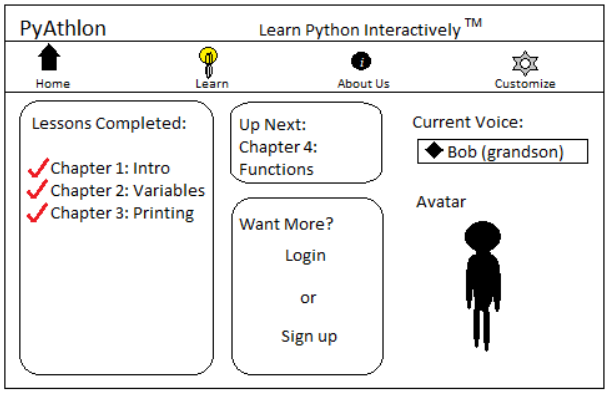

Figure 1. Home Page for Student Interface

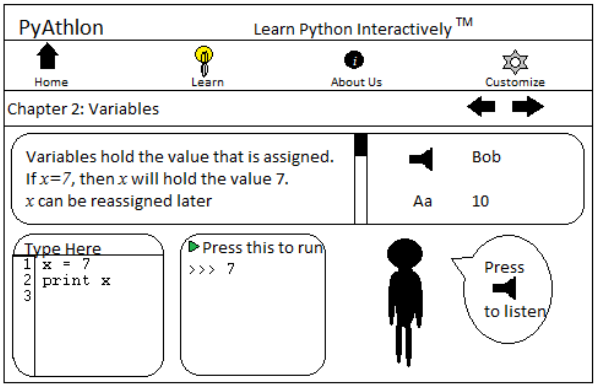

Figure 2. Learn (Tutorial) View

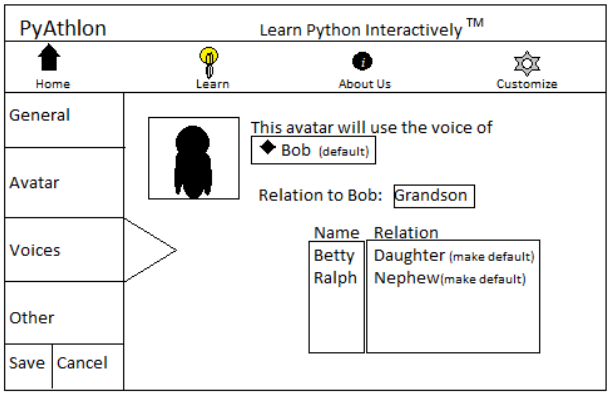

Figure 3. User Setting Page

II.A.2. Front-end Teacher View

The front-end teacher view (Figure 4) is a portal where the teacher, or voice of the different tutorials, uploads new files. The teacher will also be able to track the progress of the student, and see which lesson they are on right now. With this system, the teacher can upload lessons on an as-needed basis, depending on the student's progress.

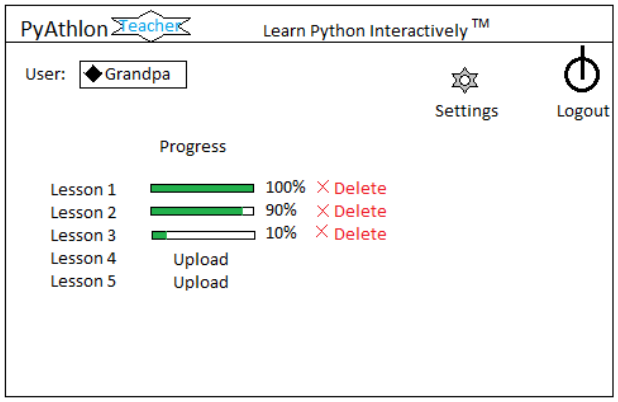

Figure 4. Teacher View

II.A.3. Backend

The backend is responsible for connecting all of the different parts of a student's front-end view, as well as connecting the student to the teacher. Eventually, the backend will also contain the server information, so that teachers and their respective students are all hosted from the same server, which removes inconsistencies from teachers using different versions of the same app. Adding the server information will allow specific version rollouts and bug fixes.

II.B. Product Sketch and Description

The flowchart for the student User Interface (UI) (Figure 5) provides an easily navigable web framework. The design and layout is meant to be user friendly and interactive. The student UI is meant to be recycled, because the teacher can continue to provide new lessons plans, but the student's UI will never change based on that. The flow of the website is kept relatively short so that the student can easily master the navigation of the website and focus on learning how to program. The flowchart for the teacher UI (Figure 6) reflects the teacher's main job to upload the course. The primary purpose of the flowchart is to upload audio and monitor the student's progress.

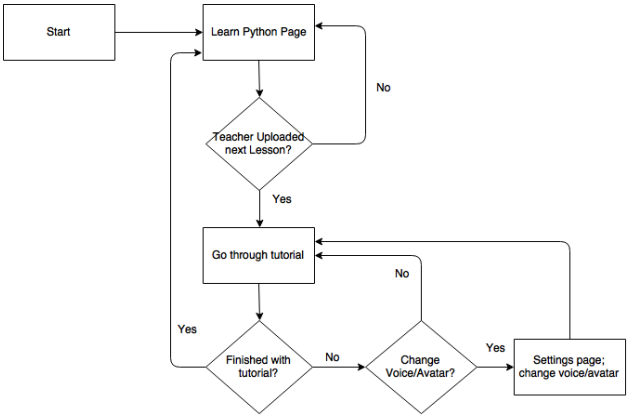

Figure 5. Flowchart for Student Interface

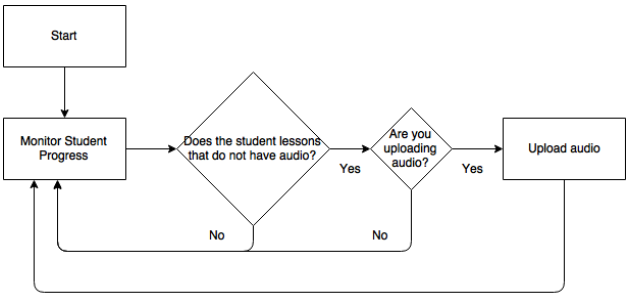

Figure 6. Flowchart for Teacher Interface

III. CONCLUSIONS

From the interview with the target demographic, “PyAthlon would give me the ability to learn about rising technology with the added personalization of hearing my grandkids; I feel like I’m connecting while I’m learning”, meaning this product and product idea are viable [6]. PyAthlon provides users with an interactive, informative method of learning Python, while simultaneously allowing the student to choose a teacher dynamically.

With a rising elderly population, the technology industry cannot afford to ignore the issue. It is estimated that, by 2030, 19% of the US population will be over 65 - roughly the same proportion that currently own iPhones. By 2050, there will be one retired person for every two that are at work [7]. Since the retirement age has stayed relatively constant, the older generation is left with their slowly outdating knowledge. With the invention of PyAthlon, people will be able to learn about current technologies more interactively.

ACKNOWLEDGMENTS

The authors would like to thank Professor Asish Ghosh for his support and guidance.

REFERENCES

[1] A. SMITH, "Older Adults and Technology Use," Pew Research Center, 2014.

[2] Ken Bryson, Lynne M.Casper, "Census Bureau," 5 1999. [Online]. Available: https://www.census.gov/prod/99pubs/p23-198.pdf. [Accessed 30 10 2016].

[3] R. Rendon, "Census Bureau," 22 10 2014. [Online]. Available: http://www.census.gov/newsroom/press-releases/2014/cb14-194.html. [Accessed 30 10 2016].

[4] J. Lee, "Makeuseof," 16 6 2015. [Online]. Available: http://www.makeuseof.com/tag/3-myth-busting-reasons-start-coding-even-older-age/. [Accessed 10 10 2016].

[5] S. Lohr, "The New York Times," 4 4 2017. [Online]. Available: https://www.nytimes.com/2017/04/04/education/edlife/where-non-techies-computer-programming-coding.html?_r=0. [Accessed 22 4 2017].

[6] I. Aswath, Interviewee, *Opinions Towards PyAthlon.* [Interview]. 17 9 2016.

[7] J. Wakefield, "The generation that tech forgot," BBC News, 2015.

Methodology to Reduce Automobile CO_2 Emissions

Malcolm Porterfield
Rensselaer Polytechnic Institute
Department of Mechanical, Aerospace, and Nuclear Engineering
portem4@rpi.edu

Carbon dioxide emissions from automobiles and other combustion processes have contributed to global warming and pollution. The goal is to reduce these carbon dioxide emissions by a significant amount (an exact percentage is not available at this time). My project (called CO_2NO*) would be an attachment that could be placed in the exhaust path of a carbon dioxide producing activity. The plan is to use a catalyst developed by Oak Ridge National Laboratory to carry out the filtration process. The catalyst in question has been shown to convert carbon dioxide into ethanol. Since ethanol can be used as a fuel source, hopefully* CO_2NO *can increase fuel economy if employed by any vehicles that use combustion as a means of power.*

I. INTRODUCTION

Within the United States and other developed countries, automobiles are a common mode of vehicular transportation. In many cases automobiles are a necessity due to how spread out certain infrastructures are (e.g., grocery stores, places of employment, schools, etc.). Automobiles that use internal combustion engines in the United States must use catalytic converters, as mandated by the Environmental Protection Agency (EPA) [1]. Catalytic converters work to decrease the output of carbon monoxide from the car's exhaust by oxidizing it into carbon dioxide. Carbon dioxide is a greenhouse gas which has been linked to respiratory problems and global warming [2]. Figure 1 shows how greenhouse gas emissions are divided by economic sector globally.

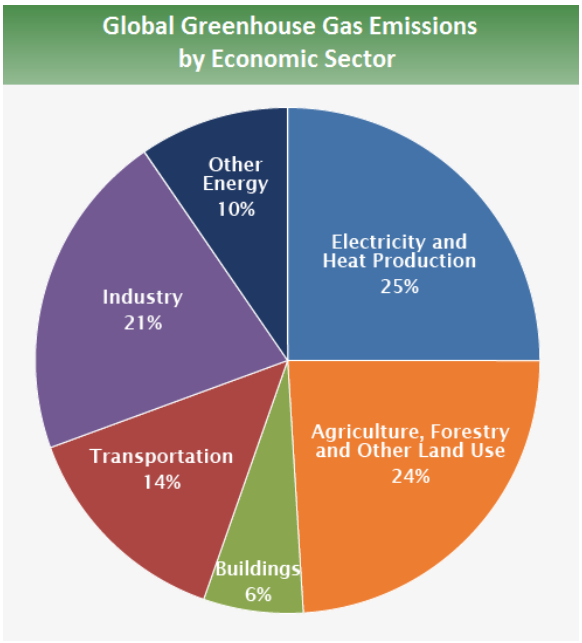

Figure 1: Greenhouse Gas Emissions by Sector, reproduced from [3].

The transportation sector is the fourth largest emitter of greenhouse gas, therefore a reduction in automobile carbon dioxide emissions would have a significant impact in mitigating global warming. Yet it would appear to make more sense to go after the largest carbon dioxide sector first instead of the fourth largest. However, the transportation sector is more flexible than the sectors that produce greater amounts of carbon dioxide. There is a new fleet of makes and models for cars in the automobile industry every year but the engines that power industry and produce electricity are made to last for up to half a century [4]. Therefore it may be fruitful to attack the automobile industry (which is part of the transportation sector) first as that could be the fastest avenue to get CO_2NO to a product market and demonstrate its value. Then CO_2NO can be adapted to the other economic sectors.

II. DESIGN DESCRIPTION

In an effort to deploy CO_2NO in the automotive industry it seems that an attachment to the exhaust pipe of an automobile to filter out the emitted carbon dioxide seems like the most straight forward way to solve the problem at hand. Why an automobile exhaust attachment seems like a feasible solution is because that there is a history of exhaust pipe filters as evidenced in US patents 3406501 A [5], 3869267 A [6] and 7523605 B2 [7]. What sets the proposed automobile filter apart from the prior patents is that this filter will be primarily tasked with eliminating carbon dioxide as an exhaust gas through use of the still currently in development Oak Ridge National Laboratory catalyst. This Nano-spiked catalyst composed of nitrogen, carbon and copper is not only able to reduce the amount of carbon dioxide that it comes into contact with, it converts the carbon dioxide into ethanol with as high as a 70 percent yield [8]. What this means is that not only is there a gain in reduced carbon dioxide emissions, the extracted ethanol could quite possibly be used to increase the automobile's fuel economy, yet another reason to attack the transportation sector first. Though, some sort of pumping mechanism would most likely be necessary in order to put the extracted ethanol back into the fuel tank. However that design feature is further down the road in CO_2NO's product development. For now a collection well may be integrated in CO_2NO as not to waste the ethanol produced. An important note on the physical shape of the filter attachment is that the filter should be small enough to fit mostly inside of the automobile's exhaust pipe in order to ensure that the vehicle's body envelop is not grossly compromised (i.e. the filter should not increase the vehicle's length, width or height substantially such that clearance issues begin to surmount). The basic tapered shape for the filter is shown in Figure 2.

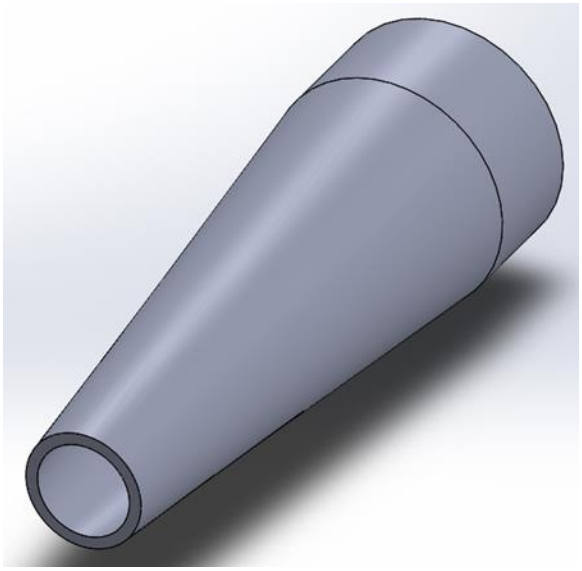

Figure 2: Automobile Filter Basic Design

III. CONCLUSIONS

The primary benefit of CO_2NO is to decrease the amount of carbon dioxide emissions from combustion processes. The catalyst in development by Oak Ridge National Laboratory appears to accomplish this task and produce the useful product of ethanol. Unfortunately this catalyst is still in its infancy so it will be some time before it is available for testing and use in CO_2NO. Hopefully once available, the catalyst will prove to be of use for automobile carbon dioxide filtration and eventually carbon dioxide filtration in general. As this technology becomes more widespread, the level of carbon dioxide emitted into the atmosphere should decrease which should mitigate the effects of global warming and pollution.

ACKNOWLEDGMENTS

The author would like to thank Professor Asish Ghosh for making possible the opportunity to gain experience by writing for an academic journal. Also the author would like to

thank fellow student Cole Funk for providing insight into the chemical nature of combustion reactions along with demonstrating possible carbon fixing techniques. Finally, the author would like to thank James Olson for his input regarding current research being developed to convert carbon dioxide into less harmful and potentially useful products.

REFERENCES

[1] C. A. Hassell, "Catalytic Converters," Salem Press Encyclopedia of Science, 2015.

[2] Jason West, J., et al. "What We Breathe Impacts Our Health: Improving Understanding Of The Link Between Air Pollution And Health." Environmental Science & Technology 50.10 (2016): 4895-4904. Business Source Premier. Web. 18 Sept. 2016.

[3] United States Environmental Protection Agency, "Global Greenhouse Gas Emissions Data," 9 August 2016. [Online]. [Accessed 18 September 2016].

[4] Riley, Colin Personal Interview. 23 September 2016

[5] D. R. Watkins, "Automobile Engine Exhaust Filter". United States of America Patent 3406501 A, 22 October 1968.

[6] J. Gaylor, "Exhaust gas filter". United States Patent 3869267 A, 4 March 1975.

[7] C. D. Whitaker, "Air Filter for Tailpipe". United States Patent 7523605 B2, 28 April 2009.

[8] Oak Ridge National Laboratory. “Nano-Spike catalysts convert carbon dioxide directly into ethanol” 12 Oct. 2016. Accessed 12 Oct. 2016.<https://www.ornl.gov> path; https://www.ornl.gov/news/nano-spike-catalysts-convert-carbon-dioxide-directly-ethanol

The Insole Generator

Yinan Ji, Yue Yu
Rensselaer Polytechnic Institute
Department of Mechanical, Aerospace, and Nuclear Engineering
jiy4@rpi.edu, yuy7@rpi.edu

As an increasing number of portable electrical devices take a part of people's life, the problem that these devices cannot be easily charged anywhere arise. The Insole Generator is a shoe pad which incorporates an electric generator and would lie in a shoe. It captures and converts kinetic energy into electrical energy with every step the user takes. The stored energy can provide power to multiple devices depending on user's needs.

I. INTRODUCTION

Every day, people consume food energy to sustain life and about 75% of food calories are used to sustain basic body function[1]. Another large use of energy is used to do work, such as walking and running, which is also called useful work. During these activities, normal force is applied against force of weight on body. These activities happened every day. But person's stepping action is hardly to utilized because it is an interaction happened between feet and ground. If there is a way to exploit these stepping actions and apply them to generate and store the energy, the electricity can be generated in a relatively user-friendly way to power small electrical devices. Insole Generator is the product designed to store this energy in the form of electricity. The details of the device are discussed in the next section.

II. PRODUCT DESCRIPTION

Insole Generator contains two main subsets of parts, mechanical parts and electrical parts, to realize its function. The Figure 1 presents the CAD design of Insole Generator. As the user presses the pad down, the powertrain drives the magnet to rotate. As the magnet rotates around the coils, electricity can be generated according to Faraday's Law.

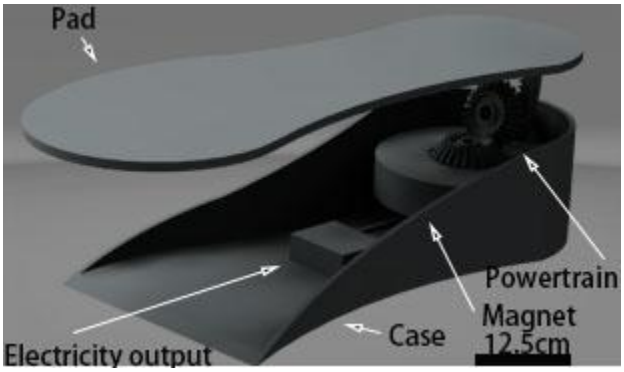

Figure 1: CAD design of Insole Generator.

II.A. Mechanical Parts - Pad and Gears

The main components of mechanical part is the housing and gear powertrain that transfer the vertical linear motion of user's foot to rotational motion of the electromagnetic generator. Two bevel gears with a unidirectional trigger gear are used to achieve the approach. From the test, a normal weight man can step down the insole pad 20mm during a 0.25 second. The process passes 11 teeth on each gear which is 360 degree revolution on a 13-teeth bevel gear.

$$11 \square\square\square\square h = 20\square\square \quad (1)$$

$$\frac{11}{13} = \frac{\square\square\square\square\square}{360^{\circ}} \quad (2)$$

$$\square\square\square\square\square = 308.8^{\circ} \quad (3)$$

$$\frac{308.8^{\circ}}{0.25\square} = 1235.2\frac{\square\square\square\square\square\square}{\square} = 3.43\ \square\square\square/\square \quad (4)$$

The above equations shows that this action can at least drive the generator initially 3.43 rev/s. The seeping action is utilized as the source of Insole Generator. And the generator must rotate fast enough to make the generator work. The data calculated here would be used in the verification/discussion part to show the feasibility of Insole Generator.

II.B. Electrical Parts - Circuits and Components

As the magnet rotates around the coils, alternating current is generated because of Faraday's Law. To make the best use of the electrical energy, the two end of coils connect with a diode bridge[3] to convert the AC into DC current without losing half of the electricity. The following figure represents the structure of a diode bridge.

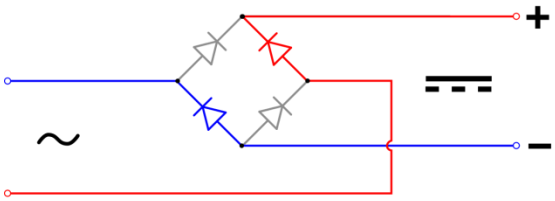

Figure 2: Diode bridge.

As Figure 3 shown below, this full wave rectifier circuit accept different polarized current[4] and output them in the same polarity.

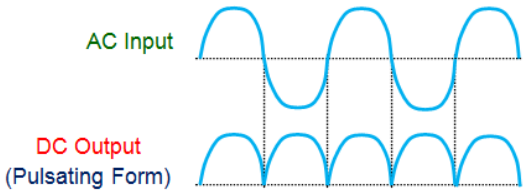

Figure 3: AC input and DC output of diode bridge.

Then, a capacitor would be used to store the energy. With the desired output, pulsed DC, connecting to the appropriate capacitor, current would flow through and charge the capacitor. Even when the capacitor is not being charging, it would not discharge because the diode limit the direction of current. The system containing a set of coils wound about a magnet, a rectifier bridge, and a capacitor would be a highly non-linear dynamic system, the analysis of the dynamic system will not be discussed in this paper because of the limitation of resources.

The last part is connecting the electrical devices and a switch to the capacitor. Due to the physical limitation of the capacitor, the electricity can not be provided as stable as regular electrical source which means current design is not suitable for charging the devices like phones. But the Insole Generator is suitable for powering small devices like LED which only needs small amount of energy to work.

III. Verification/discussion

To validate the output voltage from Insole Generator is sufficient enough to power small devices like LED, calculations approximate to the physics of the system are shown as Eq. (5). Two ½ inch dia. x ½ inch thick nickel plated magnets with N52 grade are used to for the approximation of the end system. According to the characteristics of the chosen nickel plated magnets, with the 1.6 inch gap size, magnetic field strength at the center would be 1960 gauss[5]. The figure 4 presents the characteristics of the chosen nickel plated magnets, with the 1.6 inch gap size. The red dot in the figure represents the greatest field strength which is 1960 gauss.

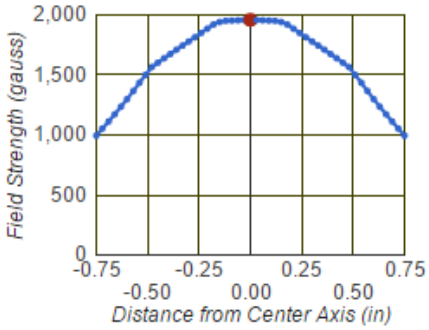

Figure 4: Characteristics of the chosen nickel plated magnets, with the 1.6 inch gap size.

To make the area enclosed by the coils as large as possible, 1.5 inch is chosen to be the diameter of the area enclosed by the coil. With the speed of rotating magnet calculated above, we can use the first order approximation of Faraday's Law to calculate the output voltage. The approximation is reasonable to use here, since it calculated the voltage generated when the direction of the magnet field is 90° with the area formed by the coils. The actual situation would generate more electricity since the area enclosed can cross the magnetic field in other angles.

$$\square_{\square\square\square} = -\square \frac{\square(\square\square)}{\square(\square)} = \square\square\square\square \quad (5)$$

$$= 0.196\square * 0.00456\square^2 * 300 * 21.55 \frac{\square\square\square\square\square\square}{\square}$$

$$= 5.7785\square$$

Eq. (5) shows that the approximated output voltage would be 5.7785v which would be enough for a flashlight LED and other devices.

The future plan for Insole Generator is finding

customized magnet vender to construct the magnet in the required shape and size for the best performance. Also, the interface between the user's feet and electrical and mechanical devices will be further developed.

II. CONCLUSIONS

To solve the problem that electricity is not easily accessed in some situations, the Insole Generator is invented to convert the kinetic energy electrical energy stored in the capacitor. The electricity it produced and stored can be used in multiple ways, for instance, install LED flashlight with the insole to light up the road ahead or distribute heat in outdoor winter. It also encourages people to walk with technologies embedded in daily wearable shoes.

ACKNOWLEDGMENTS

Special thanks to Professors Asish Ghosh for all of the guidance in the class of Inventor Studio II.

REFERENCES

[1] W. D. McArdle, F. I. Katch, and V. L. Katch, Essentials of exercise physiology, 2nd ed. Philadelphia: Lippincott Williams and Wilkins, 2005.

[2] Boundless, "Humans: Work, energy, and power," Boundless, 2016. [Online]. Available: https://www.boundless.com/physics/textbooks/boundless-physics-textbook/work-and-energy-6/power-65/humans-work-energy-and-power-287-6037/. [Accessed: Nov. 14, 2016].

[3] COLMAN, "Full wave rectifier and bridge rectifier theory," Basic Electronics Tutorials, 2013. [Online]. Available: http://www.electronics-tutorials.ws/diode/diode_6.html. [Accessed: Nov. 13, 2016].

[4] Electrical4u, "Full Wave Rectifiers". [Online]. Available: https://www.electrical4u.com/full-wave-rectifiers/. [Accessed: Mar. 13, 2017].

[5] "K&J magnetics - magnetic gap calculator,". [Online]. Available: https://www.kjmagnetics.com/gap.calculator.asp [Accessed: Nov. 3, 2016].

Systems Integration Platform for the Delivery of Inexpensive, Rapid, Point-of-Care Diagnostics

Vincent Arena
Rensselaer Polytechnic Institute
Department of Mechanical, Aerospace, and Nuclear Engineering
vincent.l.arena@gmail.com

Without a diagnosis, a doctor or clinician does not have the information needed to make decisions at the point-of-care (POC). For fast-acting, low-cost, and POC diagnostics to be implemented in time and resource constrained settings, a systems integration and delivery platform is needed to bring inexpensive diagnostics technology to areas which currently lack testing infrastructure, incur time delays, transfusion transmitted infectious, and a lack of information. A three-step solution, comprised of a disposable finger stick device with embedded paper diagnostics tests, a portable and low cost incubator and results reader, and a telehealth data analytics platform, shows promise in its ability to enable the next generation of low-cost paper diagnostics to be applied/implemented in clinical and real-world settings.

I. INTRODUCTION

An emerging class of diagnostic tests based on patterned paper shows great potential for low-cost, rapid, and accurate diagnostics, yet this potential remains to be realized. In modern global healthcare systems, there is an increasing demand for low-cost and high throughput diagnostics that can overcome the inefficiencies and shortcomings of centralized testing centers. In rich and poor countries alike, it still takes days to get results from blood donations, and treatments such as antibiotics are unnecessarily prescribed due to a lack of fast, on-the-spot diagnostics [3]. Many of the technical problems associated with microfluidics and diagnostics and have been solved by thousands of researchers around the world, but there is still no fully-integrated, market ready diagnostics platform.

This need has been poorly addressed by most diagnostics innovations which require complex infrastructure, are expensive to deploy, and have yet to be implemented in low-resource settings. This report will cover a systems analysis of the current barriers to the advancement of global health, and offer a potential three-step solution.

II. BARRIERS TO ADVANCEMENT OF GLOBAL HEALTH

In 2015, the National Academy of Medicine reported that "at least 5 percent of U.S. outpatients experience a diagnostic error, 6 to 17 percent of adverse events in hospitals result from diagnostic errors, and diagnostic errors contribute to 10 percent of all patient deaths [2]." A lack of financial incentive, simplicity of use, and systems integration for diagnostics make blind treatment often a preferred option by healthcare professionals. McDonald adds, "The current health-care system is shaped more for treatment than for diagnosis, more for action than for thinking [2]." These problems are exacerbated outside of the US, as the World Health organization reports that "the availability and safety of blood supplies for transfusion remain issues of concern in multiple settings, especially in low-income countries [1]."

In Brazil and many other emerging markets, there is an overall lack of access to diagnostics. Poor infrastructure causes unacceptable delays and therefore uninformed healthcare decisions, a high level of transfusion transmitted infections, wastage of blood products, high overheads with processing, and higher levels of mother-to-child transmission of HIV transmission in these poorer areas. The technology exists to solve these problems, however, that technology is currently not being taken from the labs and applied in real world contexts.

According to the WHO: 16 Countries are not currently able to screen all donated blood for one or more of the required infections: HIV, HepC, HepB, and Syphilis [4]. Testing is not reliable in many countries because of an irregular supply of testing kits, staff shortages, poor quality tests kits or lack of basic quality in laboratories.

Currently, there are no robust diagnostics platforms that can provide inexpensive, rapid, point-of-care diagnostics. This makes large scale testing an expensive and time-intensive process. As a result, health organizations opt to distribute antibiotics, and

other medical treatments en-masse. This scattershot technique, has led to 27 million people prescribed antibiotics unnecessarily in 2015, and creates huge problems such as antibiotic resistance, wasted resources, and ineffective medical care [3].

Sanguine Diagnostics aims to provide a system which provides for accurate diagnosis so that treatment can be used efficiently, safely, and effectively.

III. A POTENTIAL THREE-STEP SOLUTION

The proposed solution includes three fully integrated components: 1) an inexpensive delivery system, 2) a reusable, high-throughput nucleic acid amplification testing (NAAT) incubation device with built in data collection, and 3) remote analytics for providing (actionable) population health metrics for use by NGOs and National Health Systems. These steps will be outline in the subsections III.A – III.C.

III.A. Microfluidics Fingerstick Delivery Device

In order to be applied in low-resource settings, a portable, small, and low-cost device is needed to collect a patient's blood, ideally by finger stick or method not requiring trained professionals. In sub-Saharan Africa, South Asia, and Southeast Asia, more than 70% of all births in the lowest two wealth quintiles occurred at home, and therefore the device would need to be intuitive and simple [5]. This device is designed to incorporate a customizable panel of paper diagnostics tests which can be applied in diverse settings such as blood donation, childbirth, or understanding the cause of flu-like symptoms.

This device acts as a curvette, drawing blood from a fingerstick using capillary action and distributing it to a series of paper diagnostics test. The device expands the functionality of the paper tests as a standalone entity in three ways outlined below. The device acts as an enclosure which projects the paper diagnostics tests from damage by humidity or other particles. Additionally, the device offers protection to the user by containing the fluids in the device and eliminating the biohazard in handling the device. The device offers compatibility with further systems components such as enabling heat flow and alignment with the smart incubator for heating and results capturing, as discussed in Section III.B. The device is designed for manufacture to be as low cost as possible while still maintaining the features and functions as described above. The components of the device were designed to be injection molded with precision medical grade acrylic to achieve the lowest costs possible.

III.A.1. Theoretical Calculations

Capillary action occurs as the adhesive forces between the fluid and the sides of the wall become greater than the external force of gravity, driving the fluid forward, providing the diameter of the tubing or distance between the surfaces are sufficiently small. The described device uses capillary action for the delivery of blood from a pipette through plastic microfluidic channels to the paper tests, and the timed transport of blood on and through the actual paper diagnostics.

Since this mode of transport is driven by the inherent properties of the plastic and paper materials, the cost associated with manufacturing the device is low given simplicity of components required in the design.

As a theoretical model, Jurin's Formula (Equation 1) was selected as an approximation to anticipate the performance of the flow within capillary channels.

Jurin's Formula is derived from a simple force balance between the liquid within the capillary tube and the surface tension force between the liquid and the tube's surface:

$$[Weight\ Of\ Liquid] = [Surface\ Tension\ Force]$$

$$[mg = (\rho\,\forall)g = \rho(\pi r^2 h)g] = [2\pi r\sigma_s cos\varphi]$$

$$h = \frac{2\sigma_s}{\rho g r} cos\varphi \qquad (1)$$

III.B. Incubation and Data Capture

The Smart Incubator is a low cost, portable device which allows for multiple finger stick devices to be inserted into. The Smart Incubator enables simultaneous multi-sample heating and processing for the Nucleic Acid Amplification Test (NAAT) development. Placed alongside each other, collection devices are aligned and developed, and a readable result is obtained. Once results are read, the Smart Incubator functions as a mHealth device, logging

and transmitting samples whose data can subsequently be used for population analytics, disease tracking, financial reimbursement to clinics, etc.

III.C. Data Analytics

In a world where commercial airlines can carry passengers anywhere in under 16 hours, a lack of fast access to medical information can result in spread of disease and epidemics. In order to effectively allow for the advancement of global health, healthcare information needs to be available for analytics of population/patient data to determine disease trajectory, pandemic characteristics, and appropriate responses.

A data analytics system provides population health metrics for NGOs and governments, aiding disease management and healthcare system operation. Where today field teams embark on lengthy and expensive data collection campaigns, this platform would bypass these labor-intensive efforts through disruptive innovation. While individual results will be recorded by qualified personnel via colorimetric readouts of the paper diagnostics, information regarding the personnel-recorded results, device ID, use location, etc. are collected and processed remotely.

Using this data, a system could be created to provide information for strategic decision making and allocation of organizational resources by governments and NGOs in order to get ahead of disease and address pandemics and chronic ailments alike. Additionally, assured reimbursement enabled through the same data management system provides peace-of-mind for clinics struggling with tight resources and stringent bookkeeping requirements from insurance and government healthcare agencies.

IV. CONCLUSIONS

Patterned paper diagnostics promise to initiate a new class of medical devices, where chemical diagnostics on a paper substrate enable actionable, rapid, low-cost and ubiquitous access to information within the medical field and beyond. By incorporating paper diagnostics into a fully integrated deployment system, Sanguine Diagnostics provides a realizable path for rapid, systematic application of paper testing technology. In order for these tests to be implemented, outlined above is a three-step ready-to-use implementation platform for future development of the paper diagnostics field.

REFERENCES

[1] WORLD HEALTH ORGANIZATION, *Global HIV Aids Response,* pg. 67 (2011).

[2] D. JENNIE, “Diagnose this: A health-care revolution in the making,” Stanford Medicine, (2016). Accessed April 2017. https://stanmed.stanford.edu/2016fall/the-future-of-health-care-diagnostics.html#

[3] J. O’NIEL, “Rapid Diagnostics: Stopping unnecessary use of antibiotics,” *Review on Antimicrobial Resistance,* (2015).

[4] WORLD HEALTH ORGANIOZATION, “Blood Safety and Availability Fact Sheet,” (2016). Accessed April 2017. http://www.who.int/mediacentre/factsheets/fs279/en/

[5] D. MONTAGUE, G. YAMEV, A. VISCONTI, A. HARDING, and J. YOONG, “Where Do Poor Women in Developing Countries Give Birth? A Multi-Country Analysis of Demographic and Health Survey Data,” *PLOS* (2011).

Power N' Go: Portable Energy Converter

Mariana Basilio, Patrick Lopez, Elizabeth Selkis
Department of Mechanical, Aerospace, & Nuclear Engineering
basilm2@rpi.edu, lopezp2@rpi.edu, selkie@rpi.edu

In today's world, people are dependent on electricity and electronic devices. According a study in 2015, the average American residential customer uses 10,812 kWh of electricity per year, which is 29.62 kWh per day. Electricity cannot be accessed everywhere. For people camping, victims of a power outage, or people living in a third world country, electricity may not be a viable power source. The presented design is a portable energy converter that converts thermal, solar, and mechanical energy into electrical voltage to create power. Power N' Go incorporates thermoelectric generating tiles, solar cells and a mechanical hand crank, all of which are already on the market independently, into one device as a means of energy conversion. The product design produces 196.8 W of electrical energy. It is portable as it has thermal tiles only 26 cm x 26 cm in size, with a detachable solar panel, foldable hand crank and collapsible handles.

I. INTRODUCTION

In a world that is growing more dependent on electrical energy, people need to have continuous access to electrical power. Whether for business, school, travel, communication, recreation or other tasks in everyday life, electricity consumers take for granted the accessibility of electricity until it no longer is available. However, for 1.2 billion people in the world, the reality is that electricity is not accessible. [1] The target groups of people affected by this problem can fall into three main categories:

1) People who do not live on the electrical power grid
2) People who are off the electrical power grid by choice
3) People who live on the electrical power grid but are experiencing an event whereby electricity is temporarily inaccessible

The problem of inaccessible electricity is solved with a device that generates electricity and can be used anywhere. The device, Power N' Go, is a portable device that converts nonelectrical energy into electricity. This device uses three different sources of energy that are transformed into electrical power. Power N' Go differs from other energy devices already on the market because it has a three-in-one capability where the user can use accessible thermal, solar and mechanical energy interchangeably when the other sources of energy are not available. Products currently on the market utilize one or two types of energy conversion to charge or power one specific device such as a solar power phone charger or a hand crank/solar powered flashlight. [2, 3] With Power N' Go, the user can use any one of the three energy sources mentioned to supply power to a device as long as the power required is less or equal to the specified output power that Power N' Go produces.

II. PRODUCT DESCRIPTION

The initial step for the energy conversion is to harvest the energy. In the thermal energy case, the Seebeck effect of the thermoelectric tiles is used to transform the temperature gradient across the tiles into a voltage. Electrons diffuse from one high temperature end to the other low temperature end of a wire. The diffusing electrons create a thermoelectric ElectroMotive Force (EMF). The rate at which the electrons flow from the hot end to the cold end of the wire was determined by the Seebeck coefficient, known as thermopower [4].

For the thermal component of the product, the maximum power output achievable is 196.8 W using the sixteen thermoelectric tiles. To achieve this power output, the temperature gradient created across the tiles is 750°C. The temperature of the hot side of the tiles is 800°C while the cold side remains at 50°C. [5] In order to create the required temperature gradient, a heat source and a heat sink must be introduced to each the hot side and cold side of the tile, respectively. At this temperature gradient, the tile has an internal resistance of 3.38 Ω and a current passing through of 1.92 A. This generates a voltage output of 6.4 V per tile, producing the 196.8 W total power output mentioned above. The thermally conductive material chosen to conduct heat from the heat source to the hot side of the tiles

is copper due to its thermal conductivity of 385 W/(m*K) and its melting temperature of 1085℃. A heat sink is used on the opposite side of the tiles to create the lower temperature. The thermoelectric generating tiles chosen for the Power N' Go design are CMO-32-62S tiles. They use calcium manganese oxide ($CaMgO_2$) as the hot side material that can withstand 850℃ and bismuth telluride (Bi_2Te_3) for the cold side material. [5] $CaMgO_2$ is a semiconductor material with a second layer of Bi_2Te_3 on the cold side with a combined efficiency of 6%. [5] These thermoelectric generating tiles are used due to the temperature threshold of 850℃, which is greater than the temperature the hot side of the tiles will undergo if exposed to different heat sources. Masonry chimneys, fireplaces, and campfires can reach temperatures ranging from 855℃–900℃. [6] A thermally conductive adhesive compound attaches the copper to the hot side of the tiles and the heatsink to the cold side of the tiles. [7] It is an epoxy with a thermal conductivity of 3.17 W/(m*K). Once dry, it seals the copper and heat sink to the tiles. The thermoelectric module produces DC power. In order to generate AC power, an inverter is integrated into the design. [8] The maximum power output specification of 196.8 W is determined from user input and analysis of the wattage of common devices used by consumers that need electricity. Table I contains devices with a power usage of less than 200 W. [9] Power N' Go supplies enough electricity to charge and use all the devices listed in the table. Some devices in Table I may be powered concurrently, as long as total wattage is within the design specification threshold.

Table I. Common Electronic Devices under 200 [W] and Power Usage [9]

Electronic Device	Estimated Wattage
Lightbulb[10]	5 W - >200 W
Cell Phone Charger	10 W
iPad	10 W - 20 W
Blu-ray/DVD Player	15 W
Clock Radio	10 W - 50 W
Satellite Dish/Receiver	20 W - 30 W
TV 32" LED/LCD	50 W
Household Fan	50 W - 120 W
Inkjet Printer	15 W - 75 W
Stereo	30 W - 100 W
Laptop Computer	20 W - 75 W
MacBook Pro	85 W
Video Game Console	40 W - 140 W

The solar component of Power N' Go are composed of a 26cm x 26cm panel. The solar cells used will be made of Copper, Indium, Gallium, and Selenium (CIGS) materials that allow it to generate 12 W of power under 800 W/m^2 of incident light. [13] The approach used to create renewable and accessible electricity uses Photovoltaic (PV) solar cells to harness energy. In conjunction with the thermoelectric power-generating device, the solar design is such that photovoltaic cells are oriented together on a foldable, thin mat. This allows the user to store and transport the device easily. These PV solar panels are foldable and mounted on the handle of the prototype. The solar panel must not be used concurrently with the thermoelectric tiles; the solar panel will fail under the temperatures required for the thermoelectric tiles. While the solar subsystem is less powerful than the thermal subsystem, it provides enough electrical power to operate some of the devices shown in Table 1 and store power by charging a battery for later usage.

The mechanical component of the product consists of a hand crank that generates a target specification of 20 V. It has a foldable design so that it collapses into the device when not in use. The hand crank will require no more than 20 minutes of manual cranking reaching 20 V. This puts it in line with other hand crank radios and flashlights. [2, 3] Additional hand cranking results in a surplus of voltage. This will charge a battery. A step down voltage transformer protects the device to be powered from excess voltage, and allows for Power N' Go to be used without constant manual power.

The solar cells, mechanical hand crank, and thermoelectric tiles charge a battery so that Power N' Go may be used without constant need of heat, sunlight, or manual cranking power. The user will be able to access to the electrical power in real time or choose to store it for a later time. Power N' Go uses a step down voltage transformer to supply the appropriate amount of power for the corresponding device. [14]

Figure 1 shows an initial design hand sketch including all three modules: solar, thermal and mechanical.

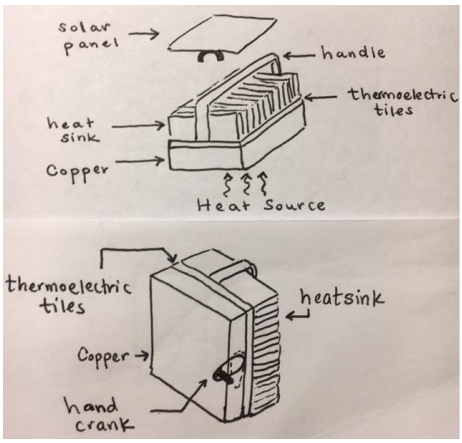

Figure 1: Hand Sketch of Power N' Go featuring Solar, Mechanical and Thermal Modules

Figure 2 shows the Computer Aided Design (CAD) model of the thermal and solar modules of the product. The orange plate represents thermally conductive copper. This is the hot side of the device; exposed to the heat source. The sixteen thermoelectric tiles are the four by four grid shown in blue. The handle (shown in yellow) is supporting the solar panel (shown in green) when the solar module is in use. When the thermoelectric tiles are in use, the solar panel is removed and the handle is collapsed around the heat sink. The heat sink, shown by the transparent wireframe, serves to keep the cold side of the tiles at a temperature that will create a temperature difference great enough to generate 196.8 W of power.

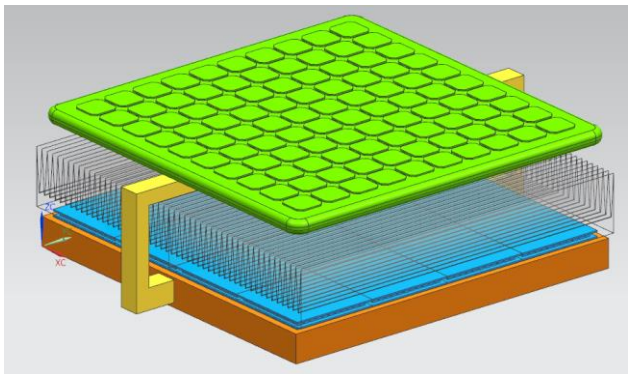

Figure 2: Power N' Go CAD Model

III. PROTOTYPE

The prototype Power N' Go is a working model for the thermal energy conversion subsystem only. The prototype consists of four 30mm by 30mm thermoelectric generating tiles made from a Bismuth-Telluride alloy (Bi_2Te_3). The tiles have a Seebeck power factor of 3.96 x 10^{-2} V/K. [15] The tiles can withstand temperatures ranging from -40℃ to 300℃. The designed prototype outputs 10W of power with a controlled temperature difference of 250℃. Thermocouples attached to the hot and cold sides of the tiles measured temperature during testing. A voltmeter measured voltage output across the tile as the temperature of the heat source was increased. During testing, a voltmeter output reading of 10V was generated from the four tiles connected in series.

In order to create the necessary temperature gradient, a hot plate serves as the heat source and a cooling container filled with ice maintains a constant cold side temperature at 0℃. The ice operates as a heat sink for testing the prototype in a controlled environment for the thermoelectric tiles. A highly conductive thermal paste with thermal conductivity of 3.17 W/(mK) fills microporous air gaps between the aluminum sheet attached to the bottom of the thermoelectric tiles and the aluminum sheet attached to the top of the tiles. To ensure contact for the paste, eight bolts hold the two plates together with the tiles in between. A picture of the working prototype is shown in Figure 3. The output voltage supplies power to the measurement instrument, and a breadboard connects the tiles in series.

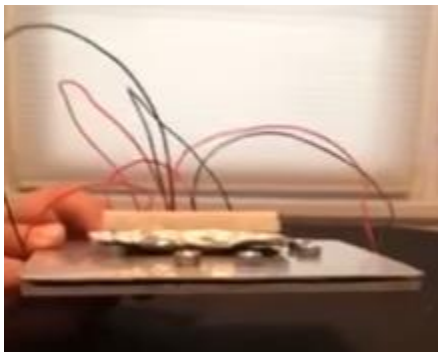

Figure 3: The working prototype for Power N' Go features four thermoelectric generating tiles compressed between two aluminum plates. Bolts and thermal paste ensure no microporous air gaps exist between the layers so that optimum conductive heat transfer can take place. A breadboard connects the four tiles in series.

The final component of the prototype was a step down voltage transformer [14] that drops a voltage

that is greater than or equal to 6 V down to 5 V, the standard voltage for a cell phone charger.

V. CONCLUSION

Access to electronic devices provides people with information, utility, and a mode of communication. The current design of the Power N' Go prototype is able to convert thermal energy into electricity. In particular, by using thermal heat as an input for the thermal module, Power N' Go has the ability to produce a voltage that is powerful enough to charge small electronic devices. According to the specifications of the tiles and thermal paste used, the output voltage was within the expected range of 9 V – 12 V.

In continuing to develop a fully functional prototype, more work will be done in developing a more compact and efficient thermal subsystem focusing in the heat sink design to be able to create a greater temperature difference across the tiles. Then, the solar and mechanical components may be incorporated physically and electronically to provide power to the same outlet ports.

REFERENCES

[1] "Energy access database," *WEO - Energy access database*. [Online]. Available: http://www.worldenergyoutlook.org/resources/energydevelopment/energyaccessdatabase/. [Accessed: 15-May-2017].

[2] 2017. [Online]. Available: https://www.amazon.com/iRonsnow-Emergency-Powered-Weather-Flashlight/dp/B00WIF2T7C/ref=sr_1_2?ie=UTF8&qid=1488485588&sr=8-2&keywords=battery+hand+crank+radio. [Accessed: 19- Apr- 2017].

[3] 2017. [Online]. Available: https://www.amazon.com/Kaito-KA500IP-RED-Voyager-Weather-Charger/dp/B007VTVDZY/ref=sr_1_16?s=aht&ie=UTF8&qid=1488486298&sr=1-16&keywords=solar+hand+crank. [Accessed: 19- Apr- 2017].

[4] 2017. [Online]. Available: http://www.scienceeducationreview.com/open_access/molki-seebeck.pdf. [Accessed: 19- Apr- 2017].

[5] "CMO-32-62S - Thermoelectric Generator", *Thermoelectric Generator*, 2017. [Online]. Available: http://thermoelectric-generator.com/product/cmo-32-62s/. [Accessed: 19- Apr- 2017].

[6] "How hot does a typical campfire get? Is it hot enough to melt silver? | Rebuilding Civilization", *Rebuildingcivilization.com*, 2017. [Online]. Available: http://rebuildingcivilization.com/content/how-hot-does-typical-campfire-get-it-hot-enough-melt-silver. [Accessed: 19- Apr- 2017].

[7] "Amazon.com: (5g) Thermal Conductive Heatsink Plaster Viscous Adhesive Compound Glue for PC GPU IC: Computers & Accessories", *Amazon.com*, 2017. [Online]. Available: https://www.amazon.com/Thermal-Conductive-Heatsink-Adhesive-Compound/dp/B00KAOP4SY/ref=sr_1_3?ie=UTF8&qid=1492618277&sr=8-3&keywords=Thermal+Adhesive+Glue. [Accessed: 19- Apr- 2017].

[8] "How Thermoelectric Generators Work - Alphabet Energy", *Alphabet Energy*, 2017. [Online]. Available: https://www.alphabetenergy.com/how-thermoelectrics-work/. [Accessed: 20- Apr- 2017].

[9] "Usage Chart: How Many Watts Do You Need?" *Donrowe.com*, 2017. [Online]. Available: https://www.donrowe.com/usage-chart-a/259.htm. [Accessed: 19- Apr- 2017].

[10] "Low Wattage Light Bulbs - 3 to 15 Watts | Lamps Plus", *Lamps Plus - The Nation's Largest Lighting Retailer*, 2017. [Online]. Available: http://www.lampsplus.com/products/light-bulbs/wattage_3w-@-15w/. [Accessed: 19- Apr- 2017].

[11] "SP3 | SoloPower®", *Solopower.com*, 2017. [Online]. Available: http://solopower.com/products/solopower-sp3/. [Accessed: 19- Apr- 2017].

[12] "Metals - Melting Temperatures", *Engineeringtoolbox.com*, 2017. [Online]. Available: http://www.engineeringtoolbox.com/melting-temperature-metals-d_860.html. [Accessed: 19- Apr- 2017].

[13] "Wrought Iron - Properties, Applications", *AZoM.com*, 2017. [Online]. Available:

http://www.azom.com/article.aspx?ArticleID=9555. [Accessed: 19- Apr- 2017].
[14] "Amazon.com: Yeeco DC-DC Buck Voltage Converter 4.5-40V 12V to 5V/2A Step-down Volt Transformer Stabilizer Voltage Regulator Module Power Supply Switch Inverter Board with LED Voltmeter 5V USB Charger: Electronics", *Amazon.com*, 2017. [Online]. Available: https://www.amazon.com/Yeeco-Converter-Step-down-Transformer-Stabilizer/dp/B00MZOJR8A/ref=sr_1_2?ie=UTF8&qid=1492620492&sr=8-2&keywords=Buck+Voltage+Converter+4.5-40V+12V+To+5V%2F2A+Step-down. [Accessed: 19- Apr- 2017].
[15] H. Goldsmid, "Bismuth Telluride and Its Alloys as Materials for Thermoelectric Generation", *Materials*, vol. 7, no. 4, pp. 2577-2592, 2014.

E-Blox and Eclipse:
Electronic Building Blocks and STEM Gaming Platform

Shaylin Collins, Margaret Eva Mungai, Daisy Rojas
Rensselaer Polytechnic Institute
Department of Mechanical, Aerospace, and Nuclear Engineering
collis7@rpi.edu, rojasd3@rpi.edu, mungam@rpi.edu

Science, Technology, Engineering, and Mathematics (STEM) fields lack racial and gender diversity. This is assumed to be due to lack of exposure to STEM fields at young ages. To increase STEM exposure and change perceptions, a toy was developed that stimulates interest in STEM among elementary school children in a non-intimidating and interesting way. The toy consists of a video gaming network that teaches STEM concepts in conjunction with a set of building blocks containing circuit components. In the game, children are given a "mission" that involves building a circuit using the block components. Children then take a picture of the blocks and the game, using color recognition software, recognizes if the mission was successfully completed.

I.A. Introduction

Many children do not grow up with the opportunities or resources to learn about Science, Technology, Mathematics, and Engineering (STEM). As a result, there is a lack of diversity in the field with respect to race, gender and socio-economic status. Racial minorities, African-Americans and Latinos, make up 6-7% of the STEM workforce while women make up 26% [1]. The lack of diversity in the STEM workforce is traced to the lack of exposure to STEM and a lack of recognition among minorities, which is assumed to be due to a lack of educational resources and a perception of who is best suited for STEM fields [2]. Minorities, in this context, refer to racial minorities and females. The lack of diversity decreases the perspectives used to create current scientific processes and revolutionary products, thereby hindering innovation.

The objective of this design was to develop a system that introduces STEM to children ages 8 through 12 in a non-intimidating way while showing no preference towards gender or race.

I.B. General Description

In order to increase exposure of STEM related principles to children, an electronic building blocks toy in conjunction with a video game was developed. Each building block, an E-Blox, contains an electronic circuit that is linked to other blocks to create more complex circuits. To ensure the safety of the user when playing with E-Blox, it was necessary to maintain a voltage below 12V and an edge angle greater than or equal to 90^0 based on existing toys such as Legos. The video gaming network, Eclipse, teaches students about STEM fields using story-based missions that require the students to solve problems. The gaming platform was chosen due to the fact that 99% of boys and 94% of girls in the US, regardless of ethnic groups or economic status play video games [3].

To combat the perception of individuals in STEM fields and the lack of recognition, Eclipse integrates information about diverse famous STEM professionals such as Katherine Johnson, an African-American physicist and mathematician who calculated trajectories for early NASA missions. Furthermore, it enables players to create avatars representative of themselves and includes a reward system. The most unique feature is the interaction of the two components, which gives students the chance of understanding and being engaged in the information presented. The gaming aspect provides challenges that involve the physical blocks while the feedback from the blocks is used to determine if the challenge was successfully completed.

II. Prototype Description

For prototyping, one of the missions that the players would encounter was demonstrated. The goal of the mission was to dim the lights of the spaceship to ensure safe arrival on a strange planet. This was achieved by building a series circuit, which dims the incandescent bulbs in the building blocks.

II.A. E-Blox

Two main block types are currently being designed for E-Blox: a battery block and a light block (Figure 1). For both blocks, all circuit components are completely enclosed within the block and are not accessible to the user.

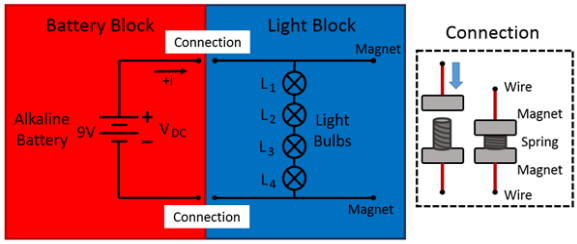

Figure 1: Side View of Block Circuit Diagram.

For the prototype, the blocks were 3D printed using PLA. The battery block contains a 9V alkaline battery and provides the power for the circuit. A future battery block design would be a power source that controls the voltage output to apply the proper voltage to circuit components and minimize the risk of being shocked. The power source would come from a wall outlet or an electronic device such as a computer or tablet.

The light block contains 4 incandescent light bulbs; each have a voltage rating of 2.5 V and operating power of 0.25 W [4]. LEDs were considered instead of incandescents, but were rejected because LEDs are not reversible (diode) and have a minimum voltage requirement to work. The four 2.5 V light bulbs are used in series so that each block will be rated for 10 V, making it safe to power using the 9 V battery. The incandescent bulbs work like resistors (R) in this circuit. A voltage (V) across a single bulb creates an electric current based on Ohm's Law, shown in Equation 1. A current (I) greater than the bulb is rated for causes the bulb to heat up, which could cause the bulb to burn out or burn the user.

$$I = \frac{V}{R} \quad (1)$$

The two blocks (battery and light) are connected to make a complete circuit, as shown in Figure 1. The connection points for each block contain a magnet and the connections on the bottom of each block contain a spring. The magnets are oriented so the top of one block and the bottom of another block are attracted to one another, making stacking the blocks easier. When two blocks are put together, the magnets are attracted and the springs compress so that it touches each of the magnets, closing the circuit.

Each block has four connection points for a positive, V+, and a negative, V-, voltage source (two on top and two on bottom); these are represented by circles in Figure 2. The positive voltage source connects to the positive side of the battery and the negative voltage source connects to the negative side of the battery. Having connections on both the right and left side of the block allows the block to be rotated without affecting the circuit. The positions of the positive voltage source and the negative voltage source connections also allows a block to be stacked off-center.

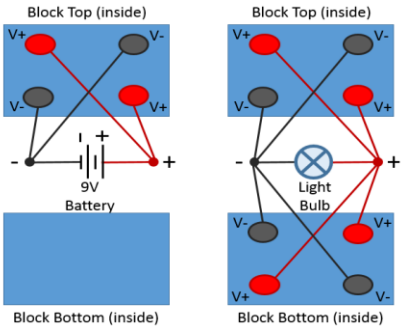

Figure 2: Inner Connections for Battery and Light Block.

Different configurations of the light blocks on top of a battery block allows for different types of circuits to be built. There are several different configurations that form both series and parallel circuits. A sample configuration of a parallel circuit is given in Figure 3. For E-Blox, a light block is in parallel if it shares at least 2 connection points with any block it is in contact

with. This means a minimum of two light blocks is required. In a parallel circuit, each light block receives the same input voltage directly from the battery (9V). Therefore, the brightness and voltage of each bulb are ideally not affected by adding extra light blocks in a parallel circuit.

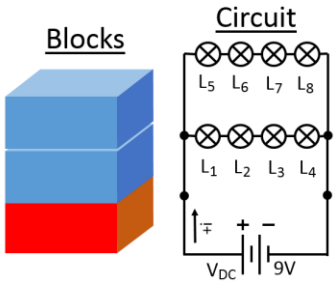

Figure 3: Parallel Circuit Diagram

A sample configuration of a series circuit is given in Figure 4. For E-Blox, a light block is in series if it shares a single connection point with each block it touches and the circuit remains continuous. Continuous refers to two connections to the power supply that are bridged by an additional block. In a series circuit, the input voltage of the battery (9V) is split across each block in the series. This causes the voltage and brightness of each block to decrease with each block added in a series circuit.

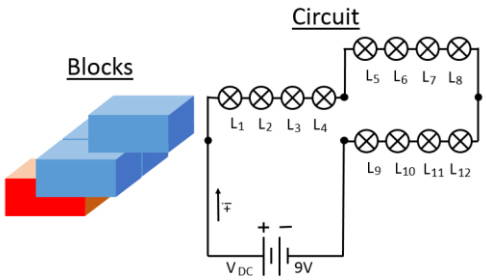

Figure 4: Series Circuit Diagram

The difference between parallel and series circuits is described by Equations 2 and 3 for equivalent resistance.

$$\frac{1}{R_{parallel}} = \sum \frac{1}{R_n} \quad (2)$$

$$R_{series} = \sum R_n \quad (3)$$

Since the incandescent bulbs act as resistors, these equations used to create an equivalent resistance represent all the resistors within the circuit. For equivalent resistors in series, the input voltage is divided among the resistors so that each one has the same current across it. This means that finding the equivalent resistance requires summing all of the resistances (Equation 3). For resistors in parallel, the input voltage is the same for each resistor so the total current is the sum of the currents across each individual resistor (Equation 2). As a result, the equivalent resistance smaller than any of the resistors in the original circuit (Equation 2).

II.B. Eclipse

For the proof of concept, a communication method between Eclipse and E-Blox was built. Once the player has built the circuit using E-Blox, they take a picture of the block using the Eclipse app and the picture is analyzed using Open Computer Vision. The Eclipse app will ideally be accessible both through the video game and as a separate downloadable app. The player then either receives a "Congratulations" screen or a "Please Try Again" screen. The flowchart in Figure 5 outlines the code that was implemented. The prototype code was ran on a PC.

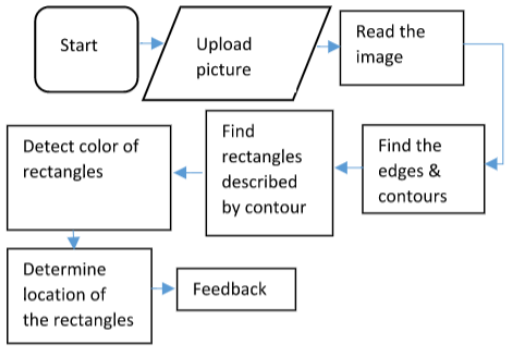

Figure 5: Open Computer Vision Flowchart

To ensure accurate edge detection, the image was first converted to grayscale, and noise was removed. The left side of Figure 6 shows the image that was loaded into the program. The right side shows the contours that were detected by the program. Legos were used in the initial design stages to debug the program because the E-Blox were not yet 3D printed.

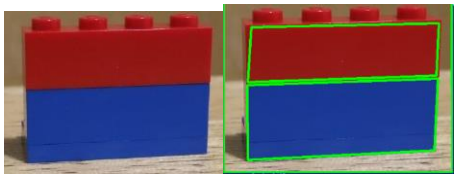

Figure 6: Picture Loaded into Program

Once the contours were determined, the program isolates the rectangle defined by the contours and detects the color of the rectangle as shown in Figure 7 and 8. The lower and upper thresholds that were used to detect color were determined using a range-detector script [5]. In both Figure 7 and 8, the leftmost image is the cropped picture analyzed by the program while the rightmost picture is the program's detection of the color red. Since Figure 7 has the red block, the color red was detected and replicated.

Figure 7: Detecting the Color Red

Figure 8: Cropped Picture and Detection of Red

While detecting the color of the rectangles, the locations were determined as well. These locations and colors were then compared to the correct solution. To ensure that the correct solution is detected regardless of the photo's orientation, the Eclipse program will be modified to detect the location of the battery block in relation to the other blocks.

III. Future Plans

The future of E-Blox includes the development of blocks with different electrical components and capabilities. Ideally, there would be blocks with motors, switches, relays, speakers, and amplifiers. These blocks would allow children to tinker with more complex circuits. Missions would be added to Eclipse to learn more about these complex circuits. The Eclipse platform would also be modified in order to create more of a collaborative gaming environment. Furthermore, donors will be collaborated with to reduce the cost of these products so that they can be used by lower-income families. There are also many engineering challenges (software, electrical, and mechanical) that need to be addressed as the product continues to develop.

REFERENCES

[1] L. Landivar, *Disparities in STEM Employment by Sex, Race, and Hispanic Origin*, 1st ed. https://www.census.gov/prod/2013pubs/acs-24.pdf, 2013, pp. 5,15.

[2] E. Pollack, "Why Are There Still So Few Women in Science?", *Nytimes.com*, 2013. [Online]. Available: http://www.nytimes.com/2013/10/06/magazine/why-are-there-still-so-few-women-in-science.html.

[3] A. Lenhart, J. Kahne, E. Middaugh, A. Macgill, C. Evans and J. Vitak, "Part 1.1: Who Is Playing Games?", *Pew Research Center: Internet, Science & Tech*, 2008. [Online]. Available: http://www.pewinternet.org/2008/09/16/part-1-1-who-is-playing-games/.

[4] "2.5V ES Mini Replacement Bulbs - Clear - For HD Light Sets", *Hard to find items.com*. [Online]. Available: https://www.hardtofinditems.com/2.5v-es-mini-replacement-bulbs-clear-for-hd-light-sets.html

[5] A. Duran and Antocuni "jrosebr1/imutils", *GitHub*. [Online]. Available: https://github.com/jrosebr1/imutils/blob/master/bin/range-detector.

Nail Removal Drill Bit Design for Reclaimed Lumber

Weston Lozier*, Catherine Mancuso
Rensselaer Polytechnic Institute
Department of Mechanical, Aerospace, and Nuclear Engineering
loziew@rpi.edu, mancuc@rpi.edu
Winner of the 2017 Inventor's Studio Innovator Award
**Winner of the2017 Mechanical Engineering Ricketts Prize*

Reclaimed lumber beams are often milled in order to increase the value of the wood or to suit specific needs of a customer. The current process for removing nails from reclaimed lumber is a slow, tedious and therefore costly process. Some of the wood cannot be processed efficiently enough to still be valuable. This design reduces the time spent on nail removal. The concept combines multiple drill bit designs to create one that would allow for faster removal of nails from these beams. This combination of designs has led to a drill bit which bores a cylindrical channel around nails allowing them to be removed.

I. INTRODUCTION

The reclaimed lumber industry in the United States takes lumber from old buildings such as barns and houses to use in new constructions. An estimated 1.2 billion board feet of lumber can be salvaged from existing structures in the United States per year [3]. The wood from these old buildings needs milling and finishing before it can be used again. Nails left in the wood cause damage to saw mill machinery; for this reason, they must be removed in order to process the lumber[6].

A current practice to remove a nail is to chisel down to the top of the nail, drill 1/16" diameter holes along the side of the nail to relieve pressure from the wood. Then using the Crescent 56 nail puller, the nail is removed from the wood. The final process of pulling the nail from the wood often results in broken nails, which then causes the process to restart. This issue of removing the nail is found when attempting to remove nails from structural beams of wood. These beams limit the method previously discussed, due to the nail only being accessible from one side[8].

A solution to this process would allow reclaimed lumber companies to save on labor costs and economically process lumber that would otherwise be waste material. Up until now, the reclaimed lumber industry has used tools of other trades, such as construction and forestry to accomplish its tasks. The tools have not been tailor made for processing reclaimed lumber[4]. Because of this, a tool that is custom-made for the process could improve on the current methods within the reclaimed lumber industry.

The developed solution is a drill bit design that bores a cylindrical channel surrounding the nail embedded in the wood. The drill bit leaves a plug that contains the nail that is then removed. One potential method of removal would use a modified pair of pliers that can reach to the bottom of the channel. Here, it can grip the bottom of the plug and break it off at this point. Once the cylindrical piece of wood and nail has been removed, the hole can be plugged with a wooden dowel. The outer diameter of the drill bit was designed to correspond to a standard wooden dowel size of 3/4".

II. CONCEPT DEVELOPMENT

To create a solution to the existing problem, the new method must be faster, easier, more consistent, and a cost-effective choice for the business over time. These restrictions led to the concept of using a drill bit style solution. To create a design that was an improvement on the current method, a new set of requirements were used. The drill bit:

- would minimize the amount of material removed from the wood.
- fit in any standard adjustable-chuck drill.
- allow for the drilled hole to be plugged easily.
- drill at least 2.5" into the wood.
- allow for the nail to be removed completely.

The drill bit cuts a channel wide enough to allow for the cylinder of wood and nail to be removed completely. The outer diameter of the drill bit should be 3/4", the same size as a standard dowel size, to allow for plugs to fit in the holes.

Once the drilling is finished, a plug of wood with a surrounding channel will remain. A concept for removing this plug is shown in Figure 1. The concept shown illustrates a modified set of pliers with cutting edges at the end and near the beginning of the arms.

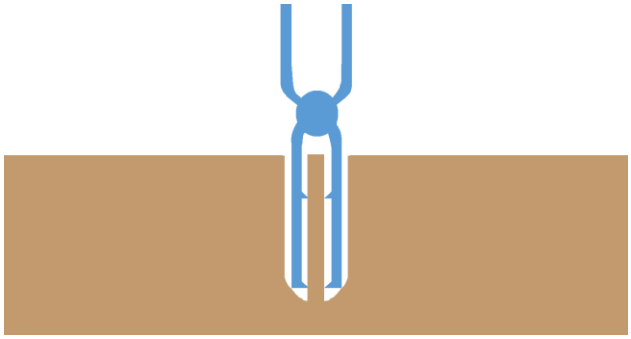

Figure 1. An initial concept for removing the plug after drilling.

This set of pliers would cut the plug near the bottom and grip the plug near the top, allowing for removal of the plug.

II.A Similar Solutions and Novelty

Currently, there are drill bit types that are similar to the invention concept. The closest drill bit types to the concept are variations of plug cutters. Plug cutters are a specialized woodworking tool designed to cut a channel around a cylindrical plug ½" into a piece of wood. This plug is removed and then placed into a countersunk hole. Plug cutters come in styles shown in Figure 2.

Figure 2. Three styles of plug cutters available to consumers [5,4,7].

The primary differences between the design and these plug cutters are the application and geometry specifications of the drill bits. Components of the plug cutter design were used to enhance the design of the invention. Based on product testing, the cutting teeth of the middle plug cutter in Figure 2 allow the bit to dig into wood twice as fast as the two plug cutters on the sides. The plug cutter on the left is better at creating an initial starting channel for the bit that allows it to stay square to the workpiece. Features of these plug cutters were incorporated and the geometry was changed so that the plug can be at least 2" long to allow the drill bit to reach the bottom of the embedded nails.

III. PRODUCT DEVELOPMENT

The drill bit solution went through three iterations to reach the final product. Initially the design had 16 teeth to create an initial cut and 2 steps to increase to the final diameter. The cutting edges and channels were straight as shown in Figure 3.

Figure 3. The initial design of the drill bit. The drill bit body was 2.5" long with a maximum diameter of 3/4".

After some research and investigation, it was determined that the step portion of the drill bit was not necessary and the cutting edges needed to be more aggressive. This is shown in Figure 4.

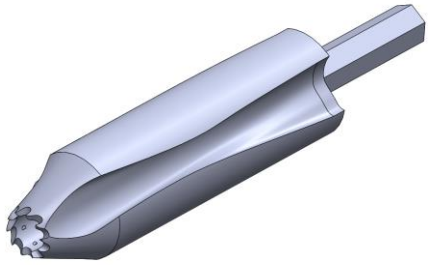

Figure 4. The second iterative design of the drill bit.

The third and final iteration reduced the amount of teeth, altered the cutting edges, and introduced an open window that was observed in plug cutters as shown in Figure 2. The third iteration of the design

is shown in Figure 5.

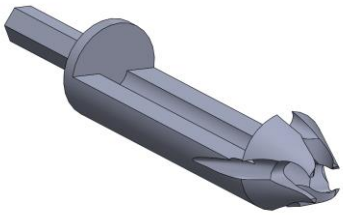

Figure 5. The third iterative design of the drill bit.

An engineering drawing of this final design is included in the appendix. A finite element analysis was performed on this third iterative design to analyze the displacements and stresses of the cutting teeth. The results of this analysis are shown in Figures 6 and 7.

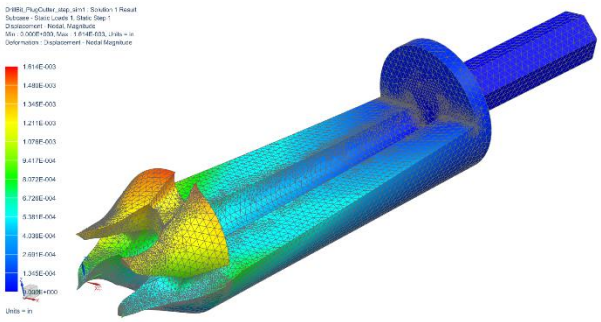

Figure 6. Displacement results of finite element analysis.

The maximum displacement was found at the top of the cutting channels on the side with the open section of the drill bit. The maximum displacement was 1.614E-4 inches.

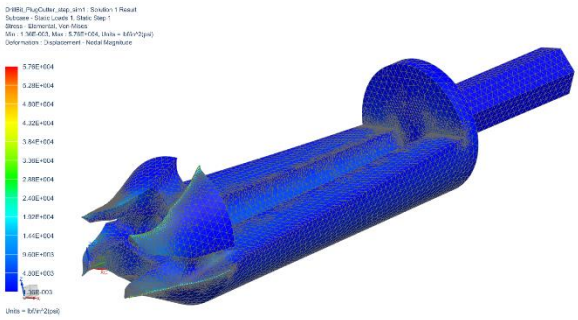

Figure 7. Stress results of finite element analysis.

The stresses were concentrated along the cutting edges and along the edge where the drill chuck met the drill body. The stress reached a maximum of 57.6 ksi near the drill chuck and 28.8 ksi along the cutting edges.

III.A Testing & Results

In order to test the design, an SLA 3D printed model of the prototype was used on a block of wet flower foam. This was done to observe the effectiveness of the teeth and cutting channels. Using the design shown in Figure 4, the drill bit bored into the foam, but the center plug broke off inside of the hollow center and was difficult to remove. Once the design changed to what is shown in Figure 5, the cylinder was drilled and was removed from the drill bit.

Following testing of the 3D printed models, a prototype was fabricated out of 1” mild steel rod. All cylindrical sections were made using a manual lathe. The open window section was made using a manual milling machine. The cutting teeth and channels were created using a Dremel and metal cutting wheels. This method was used so that variations of cutting edges could be tested with a single prototype. The final prototype is shown in Figure 8.

Figure 8. Final prototype made of mild steel.

The prototype was tested on both spruce and pine lumber with embedded nails. When tested, the drill bit bored a hole around the nail, leaving the nail exposed. This is shown in Figure 9.

Figure 9. The hole and nail left in the wood from testing with the drill bit.

A pair of pliers was used to remove the nail shown in Figure 9. The entire process took an average of 20 seconds to complete.

IV. PRACTICAL USE

The following are some potential circumstances users may find when using this product.

IV.A Nails of Various Sizes

The geometry of the drill bit designed is based off of a 2" length nail with a diameter of 1/8". A set of drill bits will come in a variety of sizes to account for different size nails.

IV.B Angled Nails

In the case that a nail has been driven into the wood at an angle, an adjustable jig can be used to guide the drill bit to follow the same angle as the nail. An example of this type of jig is shown in Figure 10.

Figure 10. Drill Master angled drill jig [1].

The jig would also prevent the drill bit from walking along the surface of the wood.

V. CONCLUSIONS

At this point in time the drill bit has been 3D printed and machined out of mild steel. The method of production for the steel prototype is similar to other standard drill bits. This will allow for this product to be priced competitively in the reclaimed lumber industry. With the current design the drill bit decreases the nail removal time to 20 seconds. The new drill bit will cause an increase in lumber that can be economically processed and therefore an increase in the revenue of the reclaimed lumber business. The benefits previously mentioned cover the requirements for this solution to be an improvement for the customer.

The next steps in developing this invention focus on optimizing the drill bit, learning more about the problem and potentially expanding the solution based on further results. A setback of the current drill bit design is that the cutting teeth and channels in the 3D CAD model were only developed as a visual aid and were not created with dimensional accuracy. The cutting channels in the CAD model could not be easily manufactured and would increase the cost. Further designs will require the manufacturing to be taken into account to remain

cost efficient. In order to properly understand the problem that faces the reclaimed lumber industry, more testing must be completed to learn the issues that will arise when removing nails from harder and older lumber. The testing should also be conducted with a more ideal version of the drill bit that has been heat treated or coated.

ACKNOWLEDGMENTS

The authors would like to thank Professor Asish Ghosh, Sam Chiappone, Larry Oligny, Erik Lozier, Natasha Sanford, and Rensselaer Polytechnic Institute for the support, guidance, and technical help with the project.

REFERENCES

[1] "Angle Drill Guide", *Harbor Freight Tools*, 2017. [Online]. Available: https://www.harborfreight.com/angle-drill-guide-95622.html. [Accessed: 08- May- 2017].

[2] S. Bratkovich. *Reclaiming Lumber Products From Waste Wood*. 1st ed. 2009. Web. 18 Apr. 2017.

[3] B. Falk, "Wood-Framed Building Deconstruction A Source Of Lumber For Construction?". *Forest Products Journal* 52.3 (2002): n. pag. Web. 18 Apr. 2017.

[4] Fuller, *Fuller Plug Cutter 7/16" 355-3070*. .

[5] Grizzly, *Grizzly Plug Cutter*. .

[6] R. LeBlanc, "What Is Reclaimed Lumber, What Are The Benefits, And How To Find It". *The Balance*. N.p., 2016. Web. 18 Apr. 2017.

[7] Letterman Hand Tools and Air Tools, *Tenon Dowel and Plug Cutter*. .

[8] E. Lozier, "Reclaimed Lumber Industry Knowledge", 2017.

[9] "Machining Wood", *Woodtools.nov.ru*, 2017. [Online]. Available: http://woodtools.nov.ru/mag/understanding_wood/understanding_wood_id2.htm. [Accessed: 21- Apr- 2017].

APPENDIX

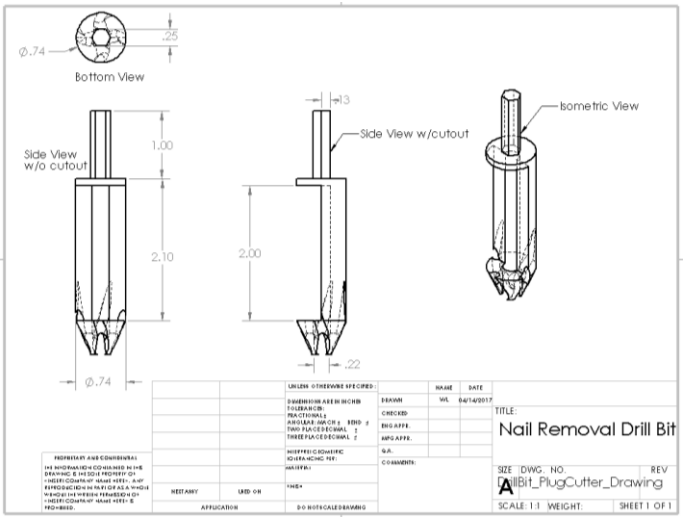

Figure A1. Engineering drawing of drill bit.

Solar Powered Automatic Composter

Andrew Muenkel
Rensselaer Polytechnic Institute
Department of Mechanical, Aerospace, and Nuclear Engineering
Muenka@rpi.edu

Organic waste such as food scraps are often thrown away by residential homes and restaurants, ending up in landfills where they slowly degrade and produce methane. Composting is a way to keep this organic waste out of landfills. However, the act of composting is inconvenient to the average person. The compost is produced in a big pile stored in the back of a yard taking up valuable square footage, or it is done in a rotating drum that is often difficult or impossible to rotate. This innovation, targeted to residential housing, attempts to make composting more efficient and convenient by providing a double barreled, 55-gallon total capacity, solar powered automated composter, that will always have a bay available for fresh organic waste to be deposited as it produces compost in a timely manner.

I. INTRODUCTION

With the rise of the green movement, there is a push towards recycling and repurposing items that were previously thrown away into landfills. Composting reduces the amount of total trash going into landfills because it recycles all non-animal fat based organic waste. Composting can be done on location, which means that it can provide nutrient rich dirt to people who require it for their planting needs, and does not need to be transported, reducing the logistics costs of trash in locations where composting becomes prevalent.

II. THE ECOLOGY MOVEMENT

There is a large push in the United States, and to a larger effect the world, towards environmentally stable and renewable practices. With the threat of rising water and increasingly severe storms, people are becoming more informed about the dangers of climate change. Many governments around the world are pushing for legislation that will make industry and agriculture more sustainable. On a more local level, people want more organic food, and often grow some food themselves in rural and suburban areas. This practice is migrating into cities with the rise of urban gardens, which are plots of land specifically used for farming located within small urban environments.

II.A. Organic Waste and Landfills

Moving and storing trash is a major cost to suburbs and cities alike. Money needs to be spent on reallocating land for landfills, hiring people to pick up trash, paying for vehicles to move the trash, and paying for maintenance of the whole process.

Any significant decrease in the amount of trash being transported from locations will significantly decrease logistics costs as well as reduce the filling rate of the landfills. Recycling at the location of trash generation is a possible way to accomplish this. If some portion of the trash could be instantly recycled into a new product on location, both the trash generators and the trash removing bodies would benefit. At the current time, recycling plastic, glasses, and metals would be too difficult to recycle using this method. Because of the large energy required to recycle these materials, and the difficulty with reforming the materials into something useful, it would be a ridiculous endeavor to try to do so at many small-scale locations instead of a larger focused facility. However, non-animal fat based organic waste can be recycled at the location of waste generation without these cons.

II.B. The Composting Process

Composting is a process in which organic waste can be broken down into a nutrient rich dirt called compost with the aid of aerobic bacteria. The process requires certain conditions to take place, but can be accomplished with a large pile of organic waste placed in a pile somewhere in a back yard. One can expect the compost at the center of the pile to be ready every spring if organic waste is placed on it year-round. To compost in an efficient manner, a pile needs to be created in a specific ratio of nitrogen rich organic waste to carbon rich organic

waste of 1:30, and to be cycled on a bi-daily schedule. The carbon provides a structure for the compost, while the nitrogen provides nutrients for plants after being broken down. This is further explained later in the section describing the Berkley method [1].

This process is only useful if there is a need for the compost on location of waste generation. Without that demand, the dirt would be simply moved, and logistics of suburbs and urban areas would be unaffected, and consequently there would be no benefit to producing the compost on location, instead of on a large-scale basis. Fortunately, with the ecological movement, urban farming and permaculture are becoming more mainstream, providing the demand for nutrient rich compost.

II.C. The Rise of Permaculture

Urban farming is farming done within a city location with a focus on efficiently producing as many crops as possible within a small available growing area. It is becoming extremely popular in the United States as people grow their own organic crops to reduce the amount of pesticides in their food and to reduce their food bills. In urban areas, plots of land can begin on rooftops of apartment buildings or in abandoned parking lots, for example.

Urban farming is not limited to the U.S. however. In Africa, rapid urbanization has caused a reduction in food security for many individuals because of higher food prices in the city, and small yields from local areas. To counter this, many individuals have turned to urban farming to provide some food security for themselves and their families [2].

These activities are part of a greater movement towards permaculture, or sustainable agriculture. This means that it is agriculture that will constantly reapply nutrients to soil so that crops can be grown year after year in the same plots. Permaculture applies to suburban and rural households as well, and has caused an increase in gardens in both regions as well, increasing demand for compost.

II.D. No Time to Farm

Unfortunately, individuals who might be interested in permaculture are as busy as ever, especially in city environments. They do not have the time or the space to care for their permaculture between responsibilities such as jobs, caring for children, and recreational activities. Also, for most people living in urban areas, and many living in suburban areas, there is a premium for space. There is neither the necessary space nor a desire to have a huge pile of compost in the backyard. On top of that, there is a lack of time to do the proper maintenance and cycling to properly have a compost pile quickly and efficiently turn into compost.

There are devices that are compact composters, consisting of a horizontally mounted steel drum placed on a support structure, with a handle attached to the main axle of the drum. The device is meant to be rotated every few day. The issue with these devices is that they can be hard to turn, and don’t provide a way for storage of new organic waste. If something is turning into compost, adding new organic waste will only lengthen the process.

III. MAKING COMPOSTING CONVENIANT

Composting is in a higher demand now more than ever. However, it is an inconvenient process. When space is at a premium such as when urban farming, a device that has a quick turnaround is a necessity so that unprocessed organic waste is not taking up valuable space. Devices that do speed up the composting process by allowing the user to turn a rotating drum are often difficult to turn when at fuller capacities, and don’t provide storage for new organic waste as old organic waste is being processed. These devices are also unsightly. Metal barrels do not fare well against Home Owner’s Associations (HOA), nor do they fit the aesthetic styles of much of American architecture. This innovation will make final aesthetics an important part of the finished product, such that the device can be used in yards where people value aesthetics or must deal with harsh HOA regulations

III.A. Efficiency: Automating the Berkley Method

The Berkley method is an aerobic composting cycle that promises a complete breakdown of organic waste into compost in eighteen days. As aforementioned, the process requires a mixture of carbon to nitrogen of approximately 30 to 1. The process uses this ratio to make conditions optimal for the bacteria responsible for breaking down organic waste into compost. Too much nitrogen and the material will rot. Too little, and the organic

waste will not break down. In the process, the material is thoroughly mixed, then let to sit for four days. After four days, the material is mixed thoroughly every two days.

This may not be doable for some individuals, and not desirable to do by others. In response, this device will be automated to follow the exact procedure for the Berkley method. Once the process is started, a microcontroller will wait four days before beginning the cycle, rotating the drum until the organic waste is thoroughly turned. The process will repeat for another six cycles with two day rests, at which point the organic waste should be fully broken down into compost.

To monitor the soil and to make sure that the ratio of nitrogen to carbon is correct, temperature monitors will be present in the streel drum. As the composting occurs, it creates heat. An optimal temperature range is 55-65 degrees Celsius. Going above this range indicates that there is too much nitrogen in the organic waste, which will cause the device to rotate to drop the temperature, and prompt the user to provide more carbon. Likewise, a temperature below the range will prompt the user to provide more nitrogen and will hold off rotating the device until there is some certainty that bacteria have begun the composting process [1].

III.B. Two is Better than One

An important part of the Berkley method is that the material needs to complete an eighteen-day cycle at which point the compost will be prime for composting. If new organic waste is added during the process, then the product will have mixed bits of organic waste after eighteen days. This is not ideal. Instead, the device will consist of two separated drums. While one is going through the Berkley method and producing compost, organic waste can be placed in the other drum. When the first drum finishes producing compost, it can be emptied, and the roles of the drums will reverse. The first drum will collect waste while the second completes its cycle.

III.C. Sustainability and Solar

This device will be produced with the ideals of the ecology movement in mind. Therefore, it is important that the device produce zero emissions. For now, the device will be powered using solar energy, thus restricting the device to areas with four hours or more of access to the sun. This simplifies the circuity because there is no device required to convert AC current to DC current, as solar panels produce a DC current. The solar panels will power a battery, which will power the microcontroller and motors of the device.

Replacing the solar power source with wind power may be possible in the future to reduce possible electronics failure. A wind mill will be added to the design in place of a solar panel, and will turn a small alternator connected to a battery which will power the Arduino and other connected electronics. However, the motors turning the two compost containers will be replaced with a Arduino controlled differential between the windmill and either barrel. This may be beneficial by providing a way to power the device in areas that don't get enough sun.

III.D. Pleasing the Home Owner's Association

Lastly, aesthetics of current unpowered models on the market are an issue. The selection of exterior rotary composters that the Solar Powered Automatic Composter is targeted to replace are majorly black plastic containers with a shiny metal frame [3]. This does not fit with the architecture of many houses located in the United States, nor does it fit the décor of most American yards, though it may mix well with the qualities of an urban garden located on a roof top. This causes an issue for many Americans who have yards under the watch of a Home Owner's Association. Composting in their yards is almost impossible due to strict regulations on what is not allowed in a yard [4].

To counter this and provide a way for HOA yards to compost, the innovation will have an option to have a cover to disguise its purpose. A possible solution will be to cover the steel barrels with an aesthetic wood barrel, such as a wine or beer barrel. The two halves of the barrel will rotate independently as part of the design, as described above, but will seemingly remain as one barrel to onlookers. The support structure, normally just steel rods, will be replaced with a more ornate wood frame, that will be able to support the device in a way that seems normal for a wine barrel, similar to how they are situated when being drained.

IV. CONCLUSION

This innovation is being developed with the intention of removing organic waste from landfills by providing an easy and convenient method for people to recycle their organic waste into nutrient rich compost. This solar powered device consists of two individually rotating barrels. The two barrels are motorized, and alternate running through cycles of the Berkley method, which is a technique used to quickly produce quality compost. While one barrel is running the cycle, the other is used as a place to deposit compost in the meantime.

ACKNOWLEDGEMENTS

Thank you to Professor Asish Ghosh and the students of Inventor's Studio II for helping me brainstorm and develop my idea. Also thank you to Professor Ron Eglash for your interesting insight into urban farming and the problems faced by individuals living in Ghana and South Africa.

REFERENCES

[1] Deep Green Permaculture, "Hot Compost - Composting in 18 Days," Deep Green Permaculture, 5 May 2014. [Online]. Available: https://deepgreenpermaculture.com/diy-instructions/hot-compost-composting-in-18-days/. [Accessed 18 April 2017].

[2] BBC, "African soil crisis threatens food security, says study," 4 December 2014. [Online]. Available: http://www.bbc.com/news/science-environment-30277514.

[3] Home Depot, "Results for "Composter"," Home Depot, [Online]. Available: http://www.homedepot.com/s/composter?NCNI-5. [Accessed 27 April 2017].

[4] B. Evans, "HOAs: What You Need to Know About Rules," REALTORS, [Online]. Available: https://www.houselogic.com/home-thoughts/hoas-what-you-need-to-know-about-

Synthesizing Ideation Tools and Technical Analysis to Design a Spring-Mass System

David Schwenker*, Michael Smith, Dan Goodman
Rensselaer Polytechnic Institute
Department of Mechanical, Aerospace, and Nuclear Engineering
In association with the RAMS lab at RPI
david.j.c.schwenker@gmail.com, smithm.mech@gmail.com, goodmd@rpi.edu
Winner of the 2017 Mechanical Engineering Weiss Award
*Winner of the 2017 Arthur M. Greene Prize

The general design framework for a spring-mass system which reduces the root bending fatigue of a wind turbine blade is outlined. Ideation tools were first implemented to define the problem and initial solution. Technical analysis was then performed which further refined the solution. Finally, design techniques were used to process the results from the technical analysis to make informed design choices. This two-step process – technical analysis followed by processing through design techniques – was iterated until a sensible solution was achieved.

I. INTRODUCTION

Within supplementary articles, the general theoretical framework for a spring-mass system was outlined [1] along with the results of the technical analysis used to model the aerodynamic loading [2], wind turbine behavior [2], spring-mass tuning [3], and physical response of the overall system [4], all of which are necessary to effectively design the apparatus to address the root bending fatigue within the wind turbine blade.

However, much of this technical analysis is contingent upon properly defining the problem, design parameters, and technical metrics which is only achievable through the application of design processes. Additionally, one must interpret the technical results in terms of their physical design elements to make informed design choices.

II. PROBLEM DEFINEMENT

II.A. Interviews

iOne of the most basic design tools is the interview process where the designer has dialogue with both users and experts in a given field of interest to discover a need and identify a potential solution.

For this project, the designers engaged in discussion with experts in the fields of rotorcraft and wind energy – including Dr. Farhan Gandhi, Dr. Etana Ferede, and Dr. Bharat Bagepalli – to collaborate on identifying a need and potential solution. Information from these interviews were categorized through diagrams to compare the gathered information between the conversations [5].

II.B. Quality Function Deployment

Quality Function Deployment (QFD) is a useful tool in quantifying these discussions with industry experts into definable design parameters, beginning with the definition of functional requirements and ending with the definition of manufacturing processes [5]. In addition, the QFD is accompanied with a weighting system which helps the designer prioritize the design elements which need to be immediately addressed within the technical analysis versus those which can be set aside for later analysis.

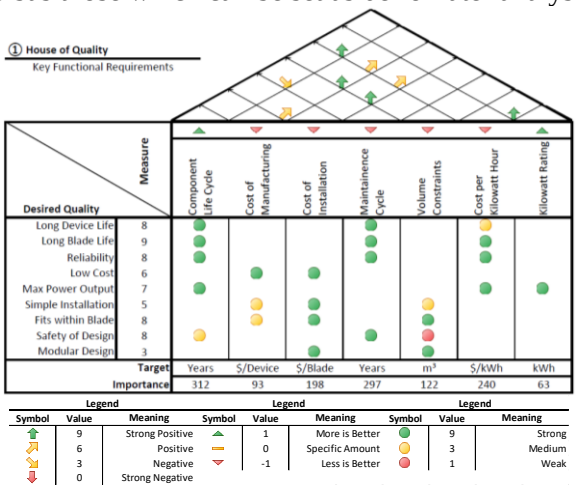

Figure 1. The first phase for quality function deployment analysis – technical metrics.

Figure 1 demonstrates the formatting one would use within QFD analysis. The left column lists the desired qualities a user would state within the

interview process while the top row lists the technical metrics in which these qualities can be measured. The colored symbols demonstrate the type of interaction which exists between the qualities and technical metrics (positive, neutral, or negative). A measure of importance – listed at the bottom – is calculated through algorithms and informs the designer as to which metrics are priorities.

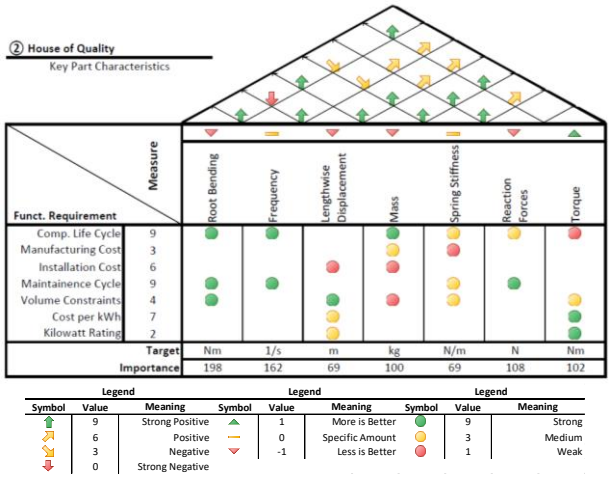

Figure 2. The second phase for quality function deployment analysis – part characteristics.

Figure 2 demonstrates the second phase for the QFD analysis which considers the results from the first phase – the technical metrics – and quantifies it further in terms of part characteristics using the same methodology discussed. Results showed that the top priorities for the technical analysis was to address root bending reduction and the frequency of the spring-mass system, while lengthwise displacement and spring stiffness weren't seen as major concerns.

However, after performing technical analysis, the spring stiffness proved to be directly correlated with both the frequency response and magnitude of the Coriolis force being generated and therefore was a greater concern than the QFD analysis initially suggested. This was a common occurrence throughout the design process – an ideation tool may have predicted the importance of an element, but technical results may have yielded a very different response. Regardless, these tools were invaluable in ensuring one was focused in their analytics.

II.C. Failure Mode Effects Analysis

Failure Mode Effects Analysis (FMEA) is a useful tool which allows the engineer to anticipate possible failure modes within their design. For the analysis of the spring-mass system, the overall design was divided in two – (1) the spring-mass element and (2) the mounting support for the device – in order to effectively address failures within both subsystems. These subsystems were then further subdivided by failure modes and effects, which in turn were subdivided once again into potential causes for these failures. Lastly, these potential causes were individually examined and ideas for controls to resolve these issues were explored.

Figure A1 within the appendix shows the results of this analysis, which generated a list of design features or actions needed that would effectively anticipate potential problems. For this project, the FMEA expressed a concern for fracture within both the spring-mass system and the mounting support, therefore finite element analysis was performed [4] to address this concern as listed in the figure.

III. DECISION REFINEMENT

Once the problem, design parameters, and technical metrics had been defined using information from customer interviews, rigorous technical analysis could then be performed [2,3,4]. After results were collected, decisions had to be made concerning the design of the system. The PUGH matrix was used extensively in order to evaluate the different design options against the design criteria determined through technical analysis and customer interviews.

III.A. Weight Matrices

Prior to using the PUGH matrix, however, weighting matrices were used in order to evaluate the importance of the different design criteria. The weight matrix evaluates each individual criteria against the other, assigning "1" if the criteria in the first column is more important than the criteria in the first row and "0" elsewise [5]. *Figure 3* and *Figure 4* are the weight matrices for the mounting and spring-mass compensator designs.

Weight Matrix: Mounting

Design Criteria	Minimally Invasive	Lightweight	Compatible	Geometric Fit	Tunable	Durability	Cost	Weight
Minimally Invasive		0	1	1	0	1	0	3
Lightweight	1		1	1	0	0	1	4
Compatible	1	0		1	1	0	0	3
Geometric Fit	1	1	1		1	0	0	4
Tunable	1	1	0	0		0	1	3
Durability	0	1	1	1	1		0	4
Cost	1	0	1	1	0	1		4

Figure 3. Weight matrix of mounting design.

Weight Matrix: Spring-Mass Design

Design Criteria	Minimally Invasive	Region I & II Passive	Region III Active	Design Tolerance	Tunable	Durability	Cost	Weight
Minimally Invasive		1	0	1	0	0	0	2
Region I & II Passive	0		0	1	0	0	1	2
Region III Active	1	1		1	1	0	0	4
Design Tolerance	0	0	1		1	0	0	2
Tunable	1	1	0	0		0	1	3
Durability	1	1	1	1	1		0	5
Cost	1	0	1	1	0	1		4

Figure 4. Weight matrix of spring-mass design.

The weights determined through *Figure 3* and *Figure 4* could then be transposed into the corresponding PUGH matrices.

III.B. PUGH Matrices

The PUGH matrix evaluates each potential design against the relevant criteria on a scale from -2 to 2, where -2 means the design has a very negative effect on the criteria and 2 conversely means that the design has a very positive effect on the criteria. The rated value is then multiplied by the previously determined weights. The PUGH matrices used in the design of spring-mass device are provided in *Figure 5* and *Figure 6*. The customized PUGH matrix outputs the weight of the design against the maximum possible value, percent optimization, and the standard deviation of that statistic.

Mounting

Criteria \ Option		Bolted	Glued	Molded
Minimally Invasive	3			
Lightweight	4			
Compatible	3			
Geometric Fit	4			
Tunable	3			
Durability	4			
Cost	4			
Percent Optimization		31.50%	78.25%	**87.00%**
Deviation		2.0%	1.3%	1.0%

Legend: 2 1 0 -1 -2

Figure 5. PUGH matrix of mounting design.

Spring-Mass Design

Criteria \ Option		Nonlinear Chord-wise Spring	Nonlinear Width-wise Spring	Precompressed Spring
Minimally Invasive	2			
Region I & II Passive	2			
Region III Active	4			
Design Tolerance	2			
Tunable	3			
Durability	5			
Cost	4			
Percent Optimization		64.77%	56.76%	**81.82%**
Deviation		1.3%	1.5%	1.6%

Legend: 2 1 0 -1 -2

Figure 6. PUGH matrix of spring-mass system.

Utilizing the PUGH matrices in *Figure 5* and *Figure 6*, the team could then evaluate which design was most feasible for the determined design criteria. As shown in the aforementioned figures, the molded mounting design and pre-compressed spring designs best fit the design criteria determined through research and customer interviews [1,4].

IV. DESIGN EMBODIMENT

After defining the problem, performing technical analysis, and making design choices, what remains is to implement these decisions. This implementation occurs in the conceptual model for the device as well as in its corresponding embodiments of the CAD and physical models.

IV. A. Conceptual Modeling

The design choices resulting from the PUGH matrices directly alter the conceptual model for the spring-mass system. A thorough exploration of this model and its operation has already been given [1], but its relationship to the design process wasn't highlighted. From *Figure 6*, the concept of the pre-compressed spring was chosen as it ensured no activity within Region I & II – a design parameter defined during interviews. This design choice then affected the technical analysis from MATLAB and Simulink as one could then assume no activity during the system startup until Region III operation was achieved. However, this would then affect the results which, in turn, could alter the outcome of the decision matrices. This again illustrates the iterative process that inherently exists within the design process.

IV.B. Computer-Aided Modeling

Computer-aided-design (CAD) modeling is a useful tool which allows for the production of geometrically accurate visual designs, thereby allowing for intuitive interaction and rapid modification. Furthermore, such modeling requires less time and capital investment than a physical prototype would require.

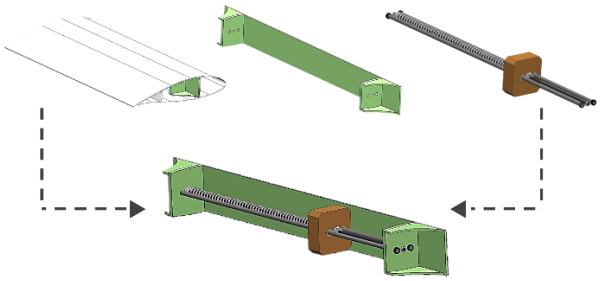

Figure 8. CAD modeling.

The PUGH matrices were utilized to determine the design parameters for the CAD models, including material, geometry, and mechanical constraints that are explored more comprehensively in a preceding article [4]. For example, from the PUGH matrix in *Figure 6*, the minimum stroke length of the device was interpreted which, in turn, determined the overall required geometry of the device. From this, the material thickness and component sizes were inferred and drawn within CAD as a sense of scale and placement are easily understood within a CAD model. As shown in *Figure 8*, assemblies can be made which allowed components to be analyzed (through such methods as finite element analysis) in isolation or within a system. Such analysis typically led to new or updated design iterations.

IV.C. Physical Prototyping

Another important stage in the development of a product is the physical prototype of the device. Prototyping allows for relatively inexpensive demonstrations of concept functionality, model verification, and refinement of finite constraints [5]. Different variants of prototypes allow for different systems or functions to be analyzed. Some prototypes are purely aesthetic, while other prototypes mimic conditions or limited aspects of the device operation [5]. Scaling and limited operational prototypes are often required to prototype large scale projects such as the wind turbine spring-mass compensator discussed here and in previous articles [1,2,3,4]. The schematic for the scaled prototype designed and constructed for this project is shown in *Figure 9*.

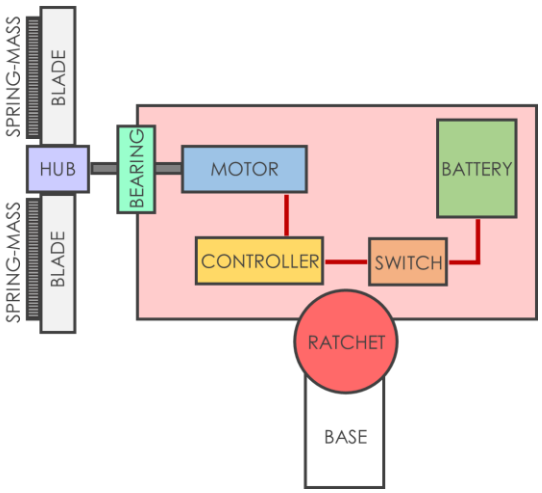

Figure 9. Simplified system prototype schematic.

Although the design focus is on the spring-mass compensator device, the additional mechanical and electrical components listed in *Figure 9* were required in order to mimic the operational conditions of the wind turbine blade. For example, the motor and controller were required to accurately simulate the rated wind turbine operational speed of approximately 1.288 rad/s. The use of such a prototype was useful to ensure that other analytical models were accurate in predicting the spring-mass system oscillation as well as functioning as a practical simulation of device operation for presentation purposes. A prototype, such as the one constructed in *Figure 10*, provides real data and live feedback on device operation in order to confirm analytical models and convey device operation and functional conditions to customers and peers for feedback. More details on the prototype's construction and performance can be seen in a preceding article [4].

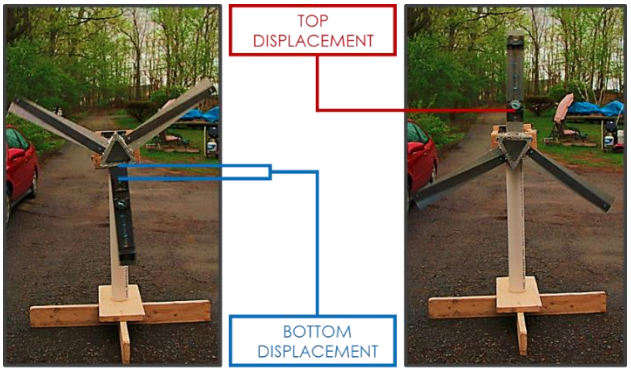

Figure 10. Physically produced prototype.

V. CONCLUSIONS

Design processes create the foundation upon which an engineer can refine a problem definition, characterize design performance, and determine the most feasible design. The problem definition can be further refined, expanded, simplified, or even pivoted through information gathered in interviews and using such tools as the QFD or the FMEA. The refined problem statement may then be juxtaposed against the results of the technical analysis generated by the team through the PUGH matrix in order to determine the minimum viable product that is the most apt at solving the issue at hand. This product can then be modeled through CAD or physically constructed through prototyping processes for further analysis, which in turn may cause the problem to be re-defined or previous design choices further refined.

The QFD, FMEA, PUGH matrices, CAD modeling, prototyping, and other design tools are thus critical methods for design teams to use in determining essential product characteristics and narrowing the field of potential solutions to a problem. However, it is vital that these tools work in tandem with rigorous technical scrutiny to ensure sound engineering judgement is permeated throughout the entire design process.

ACKNOWLEDGMENTS

The authors thank Dr. Farhan Gandhi (PhD) for his many contributions to the design of the spring-mass system including the definition of the pre-compressed spring and the general design procedure, Dr. Etana Ferede (PhD) for his contributions to the effective modeling of the wind turbine system to accurately anticipate loading conditions, Dr. Bharat Bagepalli (PhD) for his knowledge on the materials and manufacturing of wind turbine blades, Dr. Asish Ghosh (PhD) for his knowledge on ideation tools and his experience of designing for industrial applications were invaluable to the project, and the many resources RPI has offered in support of this project.

REFERENCES

[1] D. SCHWENKER and M. SMITH and D. GOODMAN, “Reduction in Root Bending Fatigue of Wind Turbine Blades by a Spring-Mass System,” *The MANE Student Research and Design Journal*, pp. 19-23, Rensselaer Polytechnic Institute, Troy, NY, (2017).

[2] D. SCHWENKER and M. SMITH and D. GOODMAN, “Modeling a Simplified Wind Turbine System to Ascertain Parameters for a Spring-Mass System,” *The MANE Student Research and Design Journal*, pp. 3-8, Rensselaer Polytechnic Institute, Troy, NY, (2017).

[3] M. SMITH and D. SCHWENKER and D. GOODMAN, “Modeling of a Spring-Mass Compensator System for a Wind Turbine Blade,” *The MANE Student Research and Design Journal*, pp. 9-14, Rensselaer Polytechnic Institute, Troy, NY, (2017).

[4] D. GOODMAN and D. SCHWENKER and M. SMITH, “Designing a Simplified Wind Turbine Mounting System to Ascertain Device Performance,” *The MANE Student Research and Design Journal*, pp. 15-18, Rensselaer Polytechnic Institute, Troy, NY, (2017).

[5] Y. HAIK and S. SIVALOGANATHAN and T. SHAHIN, *Engineering Design Process*, pp. 147, 211, 262, Cengage Learning, Boston, MA (2018).

APPENDIX

Failure Modes and Effects Analysis (FMEA)																				
Process Step/Part Number	Potential Failure Mode	Potential Failure Effects	SEV	Potential Causes	OCC	Current Controls	DET	RPN	Actions Recommended	Responsible	Actions Taken	SEV	OCC	DET	RPN
Mass-Spring System	Deformation of the Spring	Unintended Periodic Loading	7	Improper Material Selection of the Spring	3	None	2	42	Laboratory material testing under cyclical loading	Material Engineers	Incorporate strain gauges in design	7	1	1	7
				Improper Mass-Spring Calibration	6	Proper Calibration	6	252	System modeling	Control Systems Engineers	Simulation model in MATLAB		3	6	126
	Breaking of the Spring	Impact Loading	9	Manufacturing Defects	3	Inspection Procedures	2	54	Six-Sigma Tolerance Procedures	Blade Manufacturers	Recommend protocol and tolerances to manufacturers	9	1	1	9
				Brittle Fracture due to Temperature Fluctuations	2	Proper Material Selection, Insulation	3	54	Modeling based upon temperature data and material	Material and Design Engineers	Recommend protocol and tolerances to manufacturers		1	3	27
				Ductile Fracture	5	Finite Element Simulation	3	135	Laboratory material testing under cyclical loading	Material and Design Engineers	FEA in progress		2	3	54
Device Mounting	Stress Concentration at the Point of Mounting	Impact Loading	8	Manufacturing Defects	2	Inspection Procedures	2	32	Six-Sigma Tolerance Procedures	Blade Manufacturers	Recommend protocol and tolerances to manufacturers	8	1	2	16
				Slackening of Mounting Points	6	Design Minimalism and Proper Material Selection	3	144	Tight tolerances; Material Selection	Material and Design Engineers	Consider tolerances within design process		4	3	96
				Brittle Fracture due to Temperature Fluctuations	2	Proper Material Selection, Insulation	3	48	Modeling based upon temperature data and material	Material and Controls Engineers	FEA and Thermal analysis in progress		1	3	24
				Unintended External and Opperational Loadings	3	Maximum Critical Loading Analysis	2	48	Consider critical loading models and performance	Structural Analyst	Consider extreme conditions within design process		1	2	16
	Tribology of the Mounting System	Periodic and Sustained Loading	6	Creep or Fatigue within the Leading Edge Shear Web	8	Material Selection of the Leading Edge Shear Web	7	336	Non-invasive mounting, balanced reaction forces	Design Engineers	Dual mounting on either side of the Shear Web	6	5	7	210
				Cumulative Damage in Adhesive and Bonding Agents	7	None	5	210	Laboratory material testing under cyclical loading	Material Engineers	Research bonding agents		5	5	150

Figure A1. FMEA chart.

Solar-Powered Building Envelope

Duncan Smith, Cassandra Castillo
Department of Mechanical, Aerospace, and Nuclear Engineering
smithd24@rpi.edu

"Solar siding" is a proposed building envelope utilizing photovoltaic (PV) solar cells to generate electricity while maintaining the simplicity and function of typical siding materials. Utilizing luminescent solar concentrators (LSC), solar siding performs optimally when the sun is lowest in the sky, while panels produce the most energy when the sun is highest, making this product the perfect complement to solar panels. Furthermore, many states in the US have implemented plans to approach "Net Zero" energy generation (consumption of energy is equal to production) for all new buildings, which could make the application of solar siding quite necessary. An initial prototype has been developed in an effort to demonstrate the potential that such a product could have.

I. INTRODUCTION

Photovoltaic systems are an increasingly effective method of producing electricity. In fact, solar electricity generation is projected to grow by a factor of eight by 2040, from 50 billion kilowatt hours to 400 billion kilowatt hours[1]. In 2016 alone, the solar market grew 119%, reaching one million total solar installations[2]. Looking towards the future of solar, there is certainly reason to be optimistic.

Current fossil fuel alternatives to electricity generation bear a heavy cost on the environment. Coal, the leader in electric generation until recently, has a terrible environmental impact. Burning and mining of coal has been shown to produce a variety of pollutants leading to acid rain, smog, and many other harmful effects. Additionally, coal has been shown to produce carbon dioxide, the leading contributor to global warming[3]. Some have pointed to natural gas as the solution, as the "lesser of two evils", and natural gas use is expected to rise significantly. Natural gas already constitutes a large share of GHG emissions and has been shown to have irreversible effects on the fresh water supply[4]. It is clear that the growth of solar energy could help mitigate these problems and greatly reduce the environmental cost associated with electricity generation in the United States. However, Solar energy is not without its own problems. Manufacturing solar cells takes a vast amount of resources, including the use of a number of hazardous materials. Additionally, large areas of land must be leveled in order for PV arrays to produce a significant amount of electricity[5].

Building-integrated photovoltaics (BIPV) are already an emerging market due to their aesthetic value and ability to eliminate hard and soft costs[6]. One of the biggest disadvantages of most current PV systems is that potential customers do not like their appearance. More than this, their appearance actually stops people who are interested in solar from getting panels due to the opinions of others who live nearby[7]. In fact, many states currently have building ordinance laws that prohibit solar installation due to sightline issues[8]. Current building-integrated PV systems do broaden the aesthetic appeal of solar systems, but, in many cases, cost becomes a limiting factor. Regular PV panels do not produce effectively at high tilt angles[9] and options, such as solar windows, have shown very low efficiency[10]. Building-integrated roof top installations have shown the potential to be cost-effective[6], and, here, solar siding will be a complementary technology.

II. PRODUCT JUSTIFICATION

A solar powered building envelope, referred to as "solar siding" in this paper, is presented as an alternative method of solar energy production capable of diversifying the solar portfolio.

Solar siding is not meant to replace traditional solar installations. While initial payback period has been calculated to be lower than traditional systems, the proposed benefit does not hinge upon a complete revolution within the solar industry. Solar siding provides an additional option alongside solar panels and presents huge advantages due to added flexibility within solar design, uniform energy production, and increased overall solar capacity. Additional surfaces usable for solar increases a solar designer's ability to optimize a solar system for particular residential/commercial buildings. Shade

plays a large role in the performance of individual solar systems and the additional capacity/surface area would allow a designer to have more flexibility to avoid this constraint. Furthermore, many properties are not compatible with typical rooftop or ground-mounted solar, but may be able to utilize solar siding instead. The additional benefit of solar siding amongst solar panels, is the advantage of consistent energy production. Solar panels produce most effectively in the summer, and during the middle of the day. Conversely, solar siding produces most effectively in the winter, and during the morning and afternoon. Additionally, snow (which is inherently difficult to model/predict) is a huge inhibitor to rooftop installations but would likely increase the production of solar siding due to ground reflection. Solar siding is the perfect complement to solar. More uniform production is more valuable to the grid, increases inverter efficiency, and would a great step forward for home energy independence. However, likely the best justification for solar siding is the simplest. More surface area usable by PV means more energy production. Not all buildings can account for their load requirements with rooftop solar alone. Solar siding can add to overall solar capacity, and the capability of solar as a whole. All new residential buildings in California will be "Net Zero" by 2020, with commercial following in 2030. Oregon, Massachusetts, and many other states are attempting similarly aggressive renewable energy plans[11]. In order for California, and other states nationwide to accomplish their goals, additional solar capacity could prove exceptionally valuable. Architects in California already have to plan for solar installations on their buildings. Aligning with customer needs, energy requirements, and cost restrictions will only prove to be a more enormous task as time progresses. Here, solar siding could have an immediate impact, and should not be dismissed due to the presence of current photovoltaic technology.

Furthermore, by boosting the power output of individual solar cells, less silicon is required for equivalent energy gain, yielding both environmental and cost benefits. Every building needs some form of siding (vinyl, aluminum, etc), and solar siding would be a replacement for these products. These benefits diminish the overall cost of solar siding, and demonstrate its unique environmental benefit when compared with other photovoltaic systems.

Solar siding works by employing wedge-shaped luminescent solar concentrators (LSC). Wedge-shaped LSCs focus light upon a solar cell (located at the base of the wedge) using a layer of phosphor deposited above a reflective surface within a clear matrix (see Figure 1). Incident light that enters the LSC can be focused towards the solar cell simply due to shape of the wedge with the mirror along the long-side perpendicular to the solar cell. Light may also be absorbed and re-emitted by the phosphor layer at a longer wavelength capable of exciting electrons within the solar cell more effectively. An increased power output per unit area of 1.8x has been demonstrated with this technology. Conveniently, the cross-section of a wedge-shaped LSC appears quite similar to the cross-section of typical siding materials[12].

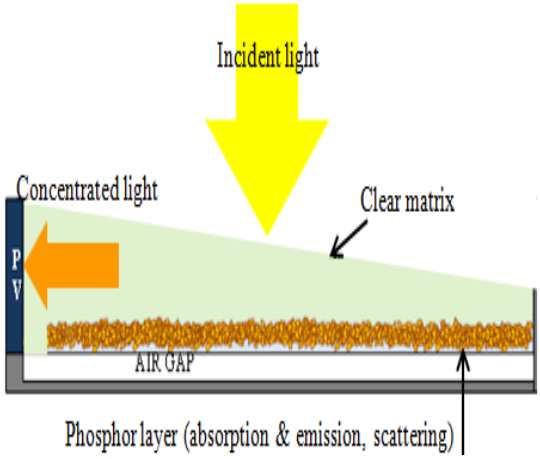

Figure 1. Schematic of wedge-shaped LSC[12].

III. PROTOTYPE DESCRIPTION

In order to develop an effective product, a number of design constraints must be met. After reaching out to a variety of potential customers, it was determined that the design must remain cost-effective, aesthetically pleasing, reliable, and should seek to ensure that installation does not become too labor intensive. To meet these requirements, the rendering shown in Figure 2 has been proposed to accomplish these goals. This product includes a dark red phosphor, the most optically efficient phosphor[12], deposited on top of a mirror layer, with 22 x 7x 1.5mm solar cells soldered in series. To serve as the outer surface of the siding, a transparent, cleanable, and durable cover is used. Lastly, lengths of roll-formed aluminum clasp together vertically in

a similar method to vinyl/aluminum siding, making up the siding frame. To minimize the impact of self-shading the bottom of the frame bends back in towards itself to minimize the shadow cast on the phosphor layer below. In order to determine the spacing between each row, Google SketchUp[13] was used to model shading on the southern face of a building throughout the year (see Figure 3). Striking a balance between differing seasons and the time of day, a distance of ten inches was determined to be effective for Troy, NY. With this in mind, initial siding prototypes were developed to reflect the design shown above as seen in Figure 4.

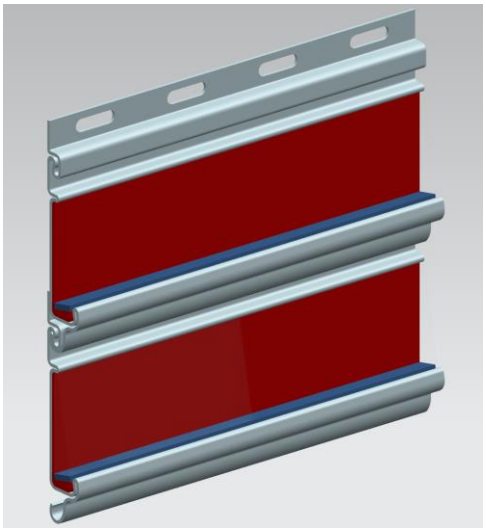

Figure 2. Solar siding proposed prototype

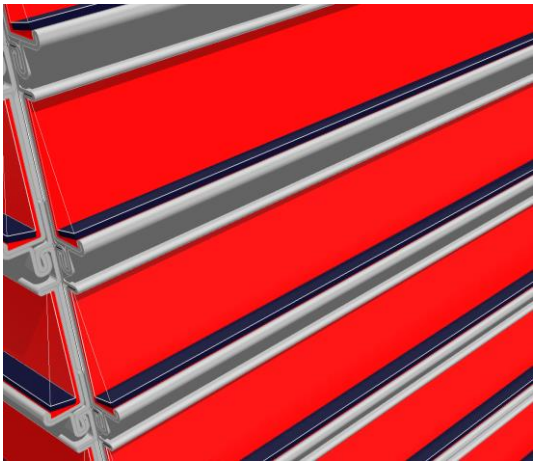

Figure 3. Self-shading at noontime in April on a south-facing wall. The gap imposed between siding modules allows the phosphor layer to avoid most of the shadow cast from the row above it.

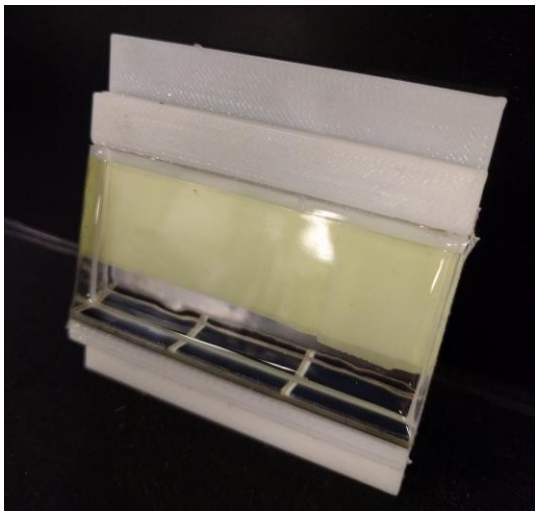

Figure 4. Initial siding prototype

Using a fused deposition modeler (FDM), the frames of each prototype were 3D printed. The FDM presented an easy method of representing some of the intricacies of the design. First, to enhance incident light on the solar cells the base was placed at a slight angle as shown in Figure 5. Small slots were also placed flush with the back of the solar cells to ensure that solder between cells did not interfere with overall alignment (Figure 6). Additionally, clasping mechanisms were tested for effectiveness to enable future printing of a larger prototype. These clasps are found in Figure 7.

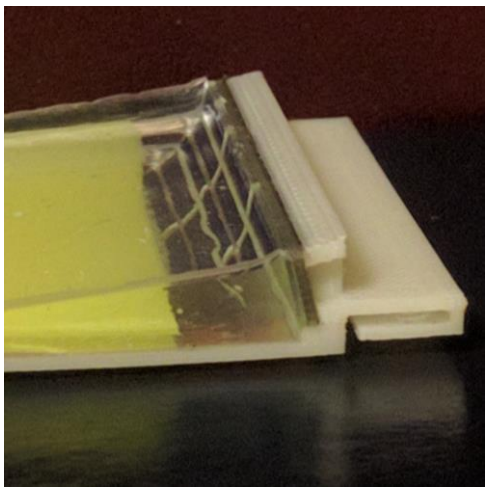

Figure 5. Inclination of wedge base to increase reflection of light toward solar cells.

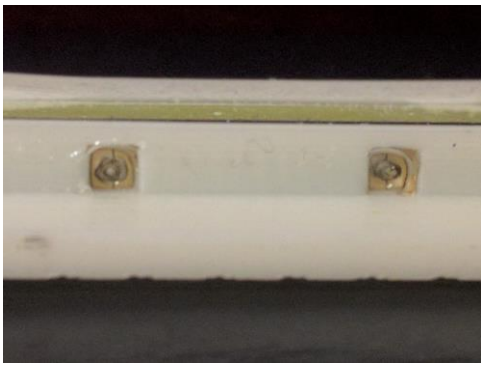

Figure 6. Small slots shown where soldered connections could be placed.

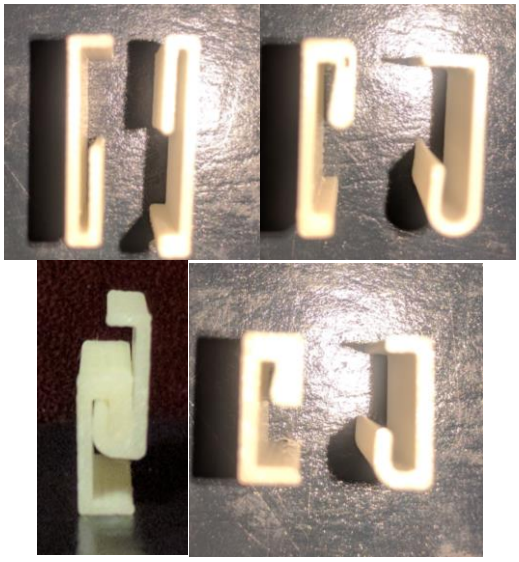

Figure 7. Various clasping designs shown above. Bottom right/left design proved to be the best fit and such a compact design offered the greatest modularity to account for self-shading.

V. CONCLUSIONS

While solar siding presents an economical and environmentally-friendly alternative to typical photovoltaic systems, its true benefit may lie in its ability to complement rooftop photovoltaic systems. Solar siding performs greatest during the morning and afternoon, throughout the winter, and maintains a high level of efficiency on a vertical surface. These traits allow solar siding to fit perfectly alongside traditional PV, enhancing overall solar capacity and creating the potential for uniform energy generation throughout the year. While this initial prototype demonstrates the potential simplicity of solar siding, future work must be done to fully define how some of the complexities associated with a large scale PV system will be addressed.

ACKNOWLEDGMENTS

Diana Borca-Tasciuc, Ph.D.
Michael D. Hughes, Ph.D.
Ryan Quinn
Asish Ghosh, Ph.D.

REFERENCES

[1] "Annual Energy Outlook 2017," *U.S. Energy Information Administration*, 5 Jan. 2017. Web.
[2] “U.S. Solar Market Set to Grow 119% in 2016” *Solar Energy Industries Association*, 9 Mar. 2016. Web.
[3] "Coal and the Environment." *Coal and the Environment*. Energy Information Administration, 1 Feb. 2017. Web.
[4] Souther, Sara. "Drawbacks to Natural Gas." *Science*. American Association for the Advancement of Science, 12 Apr. 2013. Web.
[5] "Environmental Impacts of Solar Power." *Union of Concerned Scientists*. 5 Mar. 2013. Web.
[6] James, Ted, Alan Goodrich, and Michael Woodhouse. "Building Integrated Photovoltaics in the Residential Sector." *National Renewable Energy Laboratory*. 11 Nov. 2011. Web.
[7] Johnson, Lacey, and ClimateWire. "Solar Panel Boom Pits Neighbor against Neighbor."*Scientific American*. 24 Jan. 2012. Web.
[8] "Getting Solar Installed: Solar Access Laws in Your State." *A Guide to Solar Access Laws*. SolarResourceGuide.org, 2017. Web.
[9] "How Does the Tilt Angle And/or Orientation of the PV Panel Affect System Performance?" *Lighting Research Center*. Rensselaer Polytechnic Institute. Web.
[10] Stauffer, Nancy W. "Transparent Solar Cells." *MIT Energy Initiative*. Massachusetts Institute of Technology, 20 June 2013. Web.
[11] Hewitt, Dave, and Stacey Hobart. "Net Zero by 2030." *ACEEE* (2011). Web.
[12] Hughes, M. “Monte Carlo Simulations of Luminescent Solar Concentrators: A study towards improved performance,” PhD Thesis, Rensselaer Polytechnic Institute, December 2015.

[13] *Google Sketchup*. Trimble Navigation, 11 Nov. 2017. Web.

Using Bioimpedance as a Method to Detect Blood Alcohol Content

Steven Sperazza
Electrical, Computer, and Systems Engineering Department
sperazza.steven.a@gmail.com

Across the United States, overconsumption of alcohol is a serious issue that has lasting emotional and physical effects on a many Americans. Currently, there is no viable way to continuously and non-invasively monitor the amount of alcohol in one's system in real time. This article discusses the possibility of using a developing technology, bioimpedance, to detect blood alcohol content in order to this need.

I. Background

Bioimpedance is a revolutionary new technology with many applications that is currently being developed. One of the potential uses for this technology is the estimation of blood alcohol content (BAC). Several studies have been conducted in this area, but there have not yet been any major implementations.

I.A. Motivation

Alcohol can be an incredibly dangerous substance when consumed uncontrollably or in large amounts. While it's a popular drug for many Americans, it can cause serious damage when it is all too often involved in relationships, everyday life, and driving. People who develop or have serious issues with alcohol use have a core problem with a lack of control once they've started drinking. The idea that an alcohol user can handle one more drink, or that they are ok to drive, has been the source of concern, ranging in scale from interpersonal to worldwide. Alcohol use affects all Americans, and there needs to be a better way to help those who drink control themselves and their actions.

I.A.1. Alcohol Abuse Statistics

Americans over the age of 18 report staggeringly high alcohol usage; 86.4% engage in the use of alcohol to some degree. Beyond that, 26.9% engage in binge drinking, or consumption of 5 or more drinks in a sitting. Finally, 6.2 percent of this same age group have alcohol use disorder, or a serious medical/emotional problem directly caused by excessive alcohol use or dependency (2). Outside this age group, alcohol maintains a strong presence in America's high schools, with underage drinking a difficult enough problem to track on its own. All of this same alcohol consumption, in varying degrees, by a massive segment of the population has resulted the thousands of alcohol related deaths every year. A solution to an alcohol users level of control under the influence has the potential to have intense, wide ranging effects on nearly all Americans.

I.B. Bioimpedance as a Method to Detect Blood Alcohol Content

The most revolutionary and critical aspect of this product is the use of bioimpedance spectroscopy to detect blood alcohol content. As shown in the paper Estimation of Blood Alcohol Content with Bioimpedance Spectroscopy, by Mark Ulbrich et al., this is difficult but possible. In their study they were able to produce estimations of BAC that were 88.7% accurate (1), which is comparable to DUI Breathalyzer accuracy levels (3).

I.B.1. How Bioimpedance Detects BAC

Bioimpedance works by measuring the impedance, of a biological system, in this case human cells. Real resistance is the electrical resistance you see when running a current through a resistor, and complex resistance is the electrical current and voltage fluxuations produced by running a current through a capacitor or inductor. When you combine the real and imaginary elements of resistance, you get impedance. The below figure shows the cell as an electrical circuit. Millions of different kinds put together creates a circuit, and analyzing that circuit allows for bioimpedance measurement. The membrane of the cell adds a capacitive element in parallel with a resistive element, while the inside of the cell and inter-cell connections add only a resistive element.

Adding alcohol to the system produces a significant effect on the real, resistance of the cell, so frequency would not have to be greatly modified in order to read the necessary aspects of bioimpedance. The chart in Figure 1 shows a graph of results from the paper Estimation of Blood Alcohol Content with Bioimpedance Spectroscopy. (1)

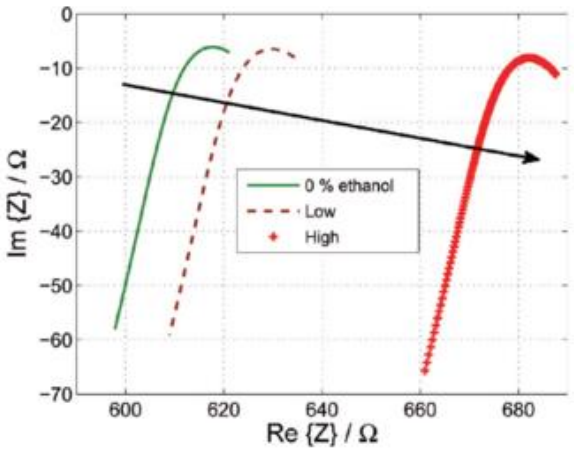

Figure 1. Result of study showing how ethanol content in the blood directly affects the real aspect of bioimpedance (1)

If this difference in real resistance can be accurately detected and recognized on a regular basis, then bioimpedance can be used as a reliable, non-invasive method for BAC testing.

II. Implementation

It is difficult to determine the exact technical feasibility of this product. A study found through experimentation found a strong similarity between alcohol's resistance effect on cells and a person's hydration level, which may make implementing an estimation algorithm difficult (1). The product revolves around the bioimpedance detection system, upon which development still needs to be done. Having access to more appropriate equipment and a team of biomedical engineers' will truly prove the feasibility of this product.

I.A. Wearable Design

The product is based on the concept of a wearable bioimpedance device, similar to a watch. Bioimpedance is used due to the fact that of all BAC testing methods, it was the most likely to succeed. A watch/bracelet design was chosen due to it being a tried and true method of measuring bioimpedance on the body. Electrodes will be attached to the band to measure bioimpedance, and a small case containing all necessary electronics will be attached to the band. A mechanism for locking the bracelet in place will be implemented in a clasp near this case as well. There will likely be multiple models for different kinds of users. Software to track data and interface with cars and mobile devices will be designed later in the process.

III. CONCLUSIONS

Alcoholism is a serious issue in the United States, resulting in the destruction of lives and livelihoods across the country. A non-invasive detection option that can be worn and constantly updated will do much to mitigate and solve this problem by offering another solution.

ACKNOWLEDGMENTS

I would like to thank the Severino Center for Technological Entrepreneurship for running the Change the World Challenge competition, where this concept was a winning entrant during the Spring 2016 semester. I would also like to thank Dr. Asish Ghosh for providing assistance in the development of this project during the class Inventor's Studio 2. Finally, I would like to credit Matthew Germanowski of the Electrical, Computer, and Systems Engineering department, and Sean Waclawik of the Computer Science department, who are working with me on the project.

REFERENCES

[1] M. Ulbrich, M. Czaplik, A. Pohl, M. Zink, and S. Leonhardt, "Estimation of Blood Alcohol Content with Bioimpedance Spectroscopy," Lecture Notes on Impedance Spectroscopy, pp. 27–35, 2015.

[2] "National Institutes of Health," National Institutes of Health. [Online]. Available: https://www.niaaa.nih.gov/alcohol-health/overview-alcohol-consumption/alcohol-facts-and-statistics. [Accessed: 25-Apr-2017].

[3]“Breathalyzer Accuracy,” Breathalyzer Accuracy. [Online]. Available: https://www.duicentral.com/evidence/breathalyzer-accuracy/.

The Double-Layer Armrest

Jiequan Zhang
Rensselaer Polytechnic Institute
Department of Mechanical, Aerospace, and Nuclear Engineering
zhangj28@rpi.edu

When people fly in a plane, one issue they have to tackle is how to share the armrest. There is only one armrest between two passengers. Some people even argue amongst each other for the armrest. In order to solve this problem, an armrest that has two layers, called double-layer armrest, was designed. With this double-layer armrest, some passengers can have more arm space by taking advantages of the vertical space above a regular armrest. This will not cause too much trouble even for people whose arms cannot fit into this double-layer armrest, because it can be pivoted up to hide between seats.

I. The Problem that we Face

Airline travel is a becoming more accessible to everyday people is becoming a more common means of transportation. Usually, in order to save space, there is only one armrest between two seats. This is inconvenient because most people want to put their hands on their own armrest.

I.A. The Solution

In order to solve this problem, a double-layer armrest, which is adjustable, comfortable, and most importantly able to accommodate two arms, was designed.

II. The Double-Layer Armrest

By utilizing the vertical space above the armrest, this design is able to contain two arms. One layer is below another and there is a slider that can be moved along slots on each layer so that passengers can discuss with the person sitting next to them about which layer they want. Some figures below depict the armrest and its function. In Figure 1, the red and yellow sliders can be moved to the left or right, which increases the adjustability of the armrest. Figure 2 shows where the armrest will be located between the seats. Figure 3 shows the length of the armrest, which are only a preliminary dimension.

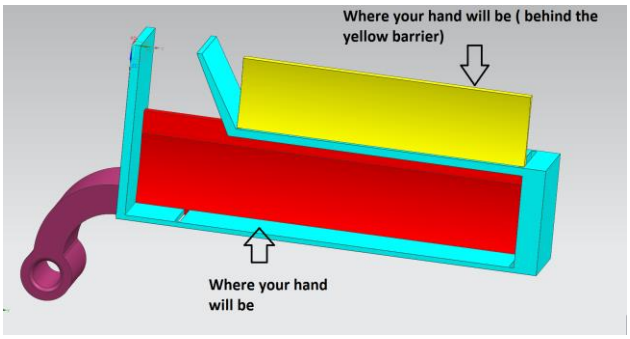

Figure 1. The double-layer armrest with arrows showing where the arms should be.

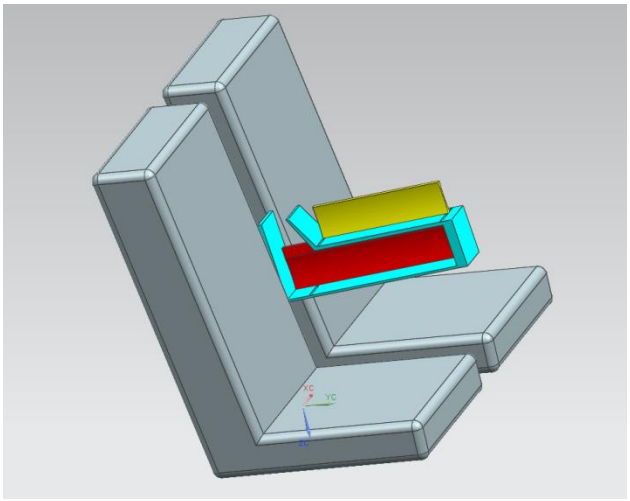

Figure 2. The double-layer armrest and its position.

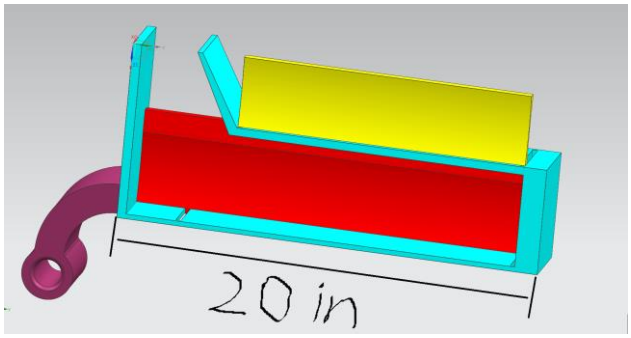

Figure 3. The double-layer armrest and one of the preliminary dimensions

Figure 4 and 5 below shows how the armrest will be pivoted and hid between the seats if the armrest does not fit the passengers' requirements. In this case, a regular armrest will be used.

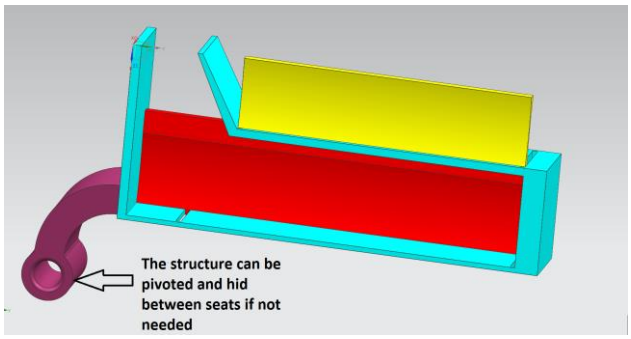

Figure 4. The double-layer armrest with an arrow pointing where it will be pivoted

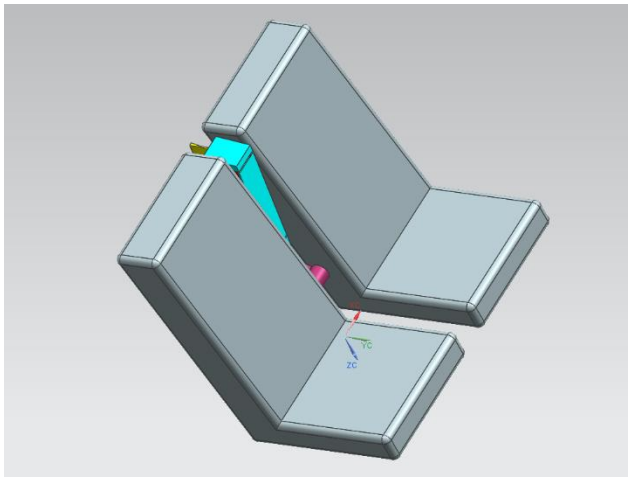

Figure 5. The double-layer armrest and its position after it is pivoted

III. CONCLUSIONS

In summary, the double-layer armrest is designed to ease the problem of limited arm space between passengers on a plane. With the double-layer feature, this new armrest is able to accommodate two arms and therefore provides more space. For people whose arms cannot fit into the armrest, the armrest can be pivoted and hidden between the seats so that it will not be a disturbance to passengers. This double-layer armrest can improve the experience of the increasing numbers of airline travelers.

An Optimized Multi-Robot Disaster Response Solution

Christina Paolicelli
Rensselaer Polytechnic Institute
Department of Electrical, Computer & Systems Engineering
c.paolicelli@ieee.org

In the event of a disaster, search and rescue operations must be delayed until it is reasonably safe for human operators to enter the area. This delay, however, must be balanced with the fact that delays reduce the probability of victim survival. Current techniques for robotic exploration of post disaster environments are designed for specific circumstances, by employing a specific path planning methodology, or by developing for a single platform, and therefore are of limited use in general application. In this paper, a methodology for integrating multiple path planning approaches into a single, seamless application is discussed. This is done by developing predictive models for several path planning approaches which can be improved as more results are entered into the system and therefore being able to determine the best method for searching a post disaster environment using prior known information about the scene and available agents.

I. INTRODUCTION

Autonomous exploration for post disaster environments has improved over the last several years, however, the solutions which have been explored are typically limited to a single path planning approach or a single platform, and therefore these methods are unable to respond effectively to more than a fraction of disasters to which they could potentially be useful. Integrating flexibility into robotic disaster response would allow a set of resources to respond to a greater number of post-disaster circumstances. To address the limited application of current methods this paper examines a optimized distributed autonomous multi-robotic solution to scouting tasks in unknown, post-disaster environment where accuracy and speed is maximized given available resources and environmental conditions.

I.A. Analyzed Algorithms

In order to demonstrate the capabilities of this approach, two path planning algorithms for exploring an unknown space were modeled based on simulation results. The simulations – and therefore the models – were simplified to predict the time it would take to search an area based on two predictors: area to search and number of agents available to perform the search. These predictors were chosen as they were the most commonly modeled in the literature with 100% of surveyed literature indicating the number of agents used and 67% indicating the area searched; all other mentioned parameters occurred less than half of the time. Both the number of path planning method models and the number of predictors for the models are scalable for full system deployment.

I.A.1. Frontier Find

The first path planning method modeled is a frontier find method which directs the agents to the closest cell designated as a frontier, a boundary unexplored cell. The simulation was run for a range of predictors and a first iteration model was developed. The "goodness" of fit statistics for this initial model were calculated to be; SSE of 989.4, R^2 of .9987 and a RMSE of 9.947, these were better than any other model tried on the data.

I.A.2.Particle Swarm Optimization

Next Particle Swarm Optimization (PSO) method was modeled. The simulation

was developed from the work in Ref.(1). The simulation was run over a similar range of predictors and from this a first iteration model was developed.

The "goodness" of fit statistics for the initial model were calculated to be; SSE of 6.949E5, R^2 of .8966 and a RMSE of 117.9, these were better than any other model tried on the data.

II. SOLUTION

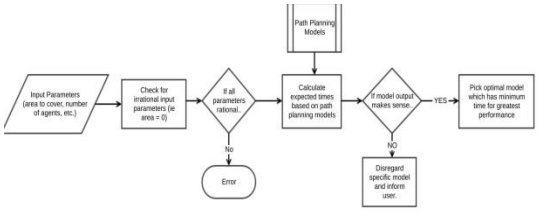

Figure 1. Overall Solution Implementation Process

Fig. 1, above is a graphical representation of the overall process. Available agents are listed in a database along with the characteristics of these agents such as operational temperature range, water resistance, etc. The agents which are available for deployment are then compared to the situational requirements that are known, Fig. 2. For example many of the robots deployed to Fukushima were unable to operate in radioactive conditions and therefore were rendered ineffective, [2]. This initial filtering process enables only the resources which may be useful in a given situation to be considered.

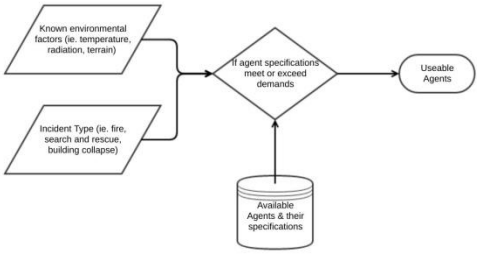

Figure 2. Determining Useful Agents

The second stage of the process determines which path planning model will be most effective given the available and useful agents, path planning models and known operating conditions such as area to search, terrain challenges or obstructions, noisy wireless environments, etc, Fig. 3.

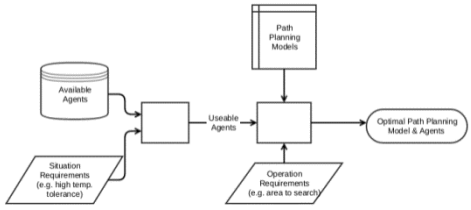

Figure 3. Determine Optimal Path Planning Model

These two processes will enable the solution to inform the user what agents and path planning method are best for the given scenario based on available knowledge.

II.A Dynamically Updated Models

One of the current issues with this approach is the imprecision of current simulation and overall lack of path planning models, however given the segmentation of this design as more and more search and mapping missions are undertaken with robotic agents the results of their missions as well as the parameters can be added to the models which will improve overall system performance. Furthermore the system has been designed such that the models may be updated dynamically as new data is available within the framework itself, see Fig. 4.

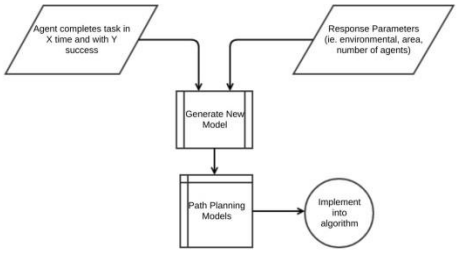

Figure 4. Dynamically Updating Models

III. RESULTS & ANALYSIS

Below in Fig.5 the number of iterations are plotted for each of the simulations and model outputs, this was done to demonstrate the correlation between which simulation performs better and which model performs better, validating the system's approach to choosing the best path planning method in this rudimentary proof of concept.

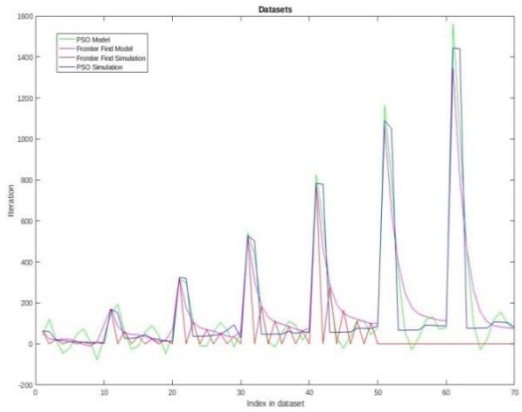

Figure 5. Simulations & Models

III.A. Edge Case Analysis

III.A.1. Null Cases

Tests were performed to validate algorithm output for null cases where a parameter is outside range (ie. range or area less than or equal to zero). The null case handling logic caught these issues and returned the appropriate text as seen below depending on the null case:

"No available agents are useful for the given incident's parameters"
"No available agents to perform search"
"Please enter an area greater than 0"

III.A.3 Model Bounds

The models were created from simulation data based on specific parameter ranges. This test evaluated the performance of the models compared to the raw simulation data at the edges of these ranges as can be seen in Fig. 6. A scoring of "Right" indicates that the model predicted the correct algorithm would finish in the shortest time. A scoring of "Wrong" indicates that the model either predicted the wrong algorithm would finish sooner or the optimal algorithm's model was not accurate enough for the data range. A scoring of "Neutral" indicates that there is no time difference among the two algorithms and therefore whichever the model selected there is no incurred harm to the user.

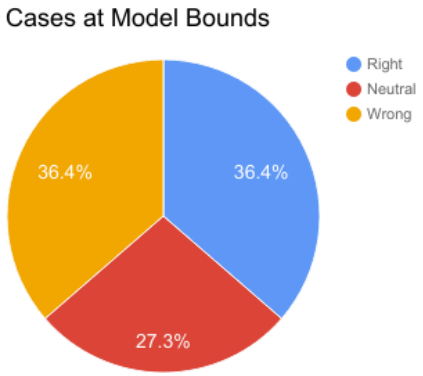

Figure 6. Percentages for Edge Cases

As Fig. 6 shows there are a large number of "Wrong" cases, these are predicted to improve as the model does and emphasis the importance of the dynamic modeling component in this system.

IV. CONCLUSION

As we seek to use technology to improve the quality of life for humans around the world a need for better disaster response mechanisms emerges. Current disaster response implementations of swarm robotics are rigid and only meet some requirements. Creating a solution for exploring and gaining information about disaster environments will help increase survival rates among victims and decrease risk for first responders. This paper presents a method for optimizing the used path planning model regardless of platform by first comparing available agents to

environmental constraints and then determining which model will result in the fastest response time given the available resources. There is much work that needs to go into a system of this nature before it would be useful in the field, however, this project demonstrates the possibility of such a system and the need for greater data collection about these incidents to better future response.

ACKNOWLEDGMENTS

The author would like to thank the Inventor's Studio II classmates, along with Professor Asish Ghosh for all their support and guidance.

REFERENCES

[1] Y. Wang, A. Liang and H. Guan, "Frontier-based Multi-Robot Map Exploration Using Particle Swarm Optimization", 2011.

[2] R. Murphy, Disaster robotics, 1st ed. Cambridge, Massachusetts: The MIT Press, 2014.

[3] J. G. Monroy, J. Blanco and J. Gonzalez-Jimenez, "Time-variant gas distribution mapping with obstacle information", Autonomous Robots, vol. 40, no. 1, pp. 1-16, 2015.

[4] M. Couceiro, P. Vargas, R. Rocha and N. Ferreira, "Benchmark of swarm robotics distributed techniques in a search task", Robotics and Autonomous Systems, vol. 62, no. 2, pp. 200-213, 2014.

[5] H. Mo and L. Xu, "Research of biogeography particle swarm optimization for robot path planning", Neurocomputing, vol. 148, pp. 91-99, 2015.

[6] M. Schwager, P. Dames, D. Rus and V. Kumar, "A Multi-Robot Control Policy for Information Gathering in the Presence of Unknown Hazards".

[7] T. Cieslewski, S. Lynen, M. Dymczyk, S. Magnenat and R. Siegwart, "Map API - Scalable Decentralized Map Building for Robots".

[8] "Distributed Robotic Mapping of Extreme Environments", Pittsburgh, PA.

[9] D. Gage, "Minimum-resource distributed navigation and mapping", SPIE Mobile Robots, vol. 4195, no., 2000.

[10] P. Sauer, T. Hausten and P. Hofstedt, "Using the Internet of Things Technology to Create a Really Platform Independent Robotics Framework".

ISBN 978-0-692-89505-4

Department of Mechanical, Aerospace & Nuclear Engineering

Rensselaer Polytechnic Institute

110 8th St Troy, NY

ISBN 978-0-692-89505-4